DIAGENESIS AND THERMAL MATURATION OF THE EUREKA SOUND FORMATION,

STRAND FIORD, AXEL HEIBERG ISLAND, ARCTIC CANADA

by

DAVID PETER BEDDOME ALLEN

A THESIS SUBMITTED IN PARTIAL FULFILMENT OF

THE REQUIREMENTS FOR THE DEGREE OF

MASTER OF SCIENCE

in

THE FACULTY OF GRADUATE STUDIES

(Department of Geological Sciences)

We accept this thesis as conforming

to the required standard

THE UNIVERSITY OF BRITISH COLUMBIA

Spring, 1986

(Department of Geological Sciences)

THE UNIVERSITY OF BRITISH COLUMBIA
2075 Wesbrook Place
Vancouver, Canada
V6T 1W5

Date: <u>Spring, 1986</u>

ABSTRACT

Nearly 3000 continuous metres of Eureka Sound Formation sandstones, shales and coals were examined in outcrop along Kanguk Peninsula, Axel Heiberg Island, N.W.T., in the present study. From these rocks, diagenetic parameters such as illite crystrallinity, 1.0 nm peak sharpness ratios, proportion of illite in illite/smectite mixed layers, and sandstone cement paragenesis have been used in combination with thermal modelling to make inferences about the thermochemical evolution of the strata and their contained pore waters.

The findings from both the thermal modelling and sandstone petrology suggest that a syn- or post-tectonic heat flow anomaly existed whereby heated Na^+-enriched waters passed from diapir cores (where halite dissolution occurred) into laterally adjacent permeable lithologies such as coals and arenites. This concept is supported by an offset in the plot of vitrinite reflectance versus depth whereby the upper segment (based primarily on coals) has higher reflectance values than the lower segment (based mainly on phytoclasts), and on the formation of the sodium rich phase dawsonite as the last authigenic phase precipitated in the pores of the sandstones. An examination of the chemical conditions under which halite dissolves and dawsonite precipitates suggests that the Na^+ concentration may have been as high as 105 g l^{-1}.

Clay mineral analyses suggest that the major part of the clay variation in the Eureka Sound Formation can be attributed to changes in detrital minerals rather than to diagenetic reactions between the clay minerals and their chemical environment.

Textural relationships between the six principal authigenic sandstone cements (calcite, ankerite, siderite, dawsonite, kaolinite and quartz overgrowths) and dissolution features in the aluminosilicates suggest that at least 7 episodes of changing pore fluid chemistry have occured since the strata were deposited.

Table of Contents

List of Tables

List of Figures

List of Plates

Acknowledgements

Note on Nomenclature

During the final stage of preparation of this thesis the formal status of the Eureka Sound Formation was changed to the Eureka Sound *Group* (Miall, *in press*). Formations within the renamed Eureka Sound Group roughly correspond to the informal zones used in this thesis. Due to the timing of the change in the Eureka Sound nomenclature it was not possible to re-organize this thesis to incorporate the new group status and, therefore, the author has retained the formation status for the Eureka Sound strata throughout.

GENERAL INTRODUCTION

GENERAL STATEMENT

Diagenetic and thermal maturation studies are important aspects of sedimentology in that they provide information about the thermal and chemical evolution of strata. A number of characteristics of the Late Cretaceous-Early Tertiary Eureka Sound Formation along Strand Fiord on western Axel Heiberg Island make strata from this location of particular interest for diagenetic analyses. First, the nearly 3000 m of continuous section provides an excellent data base with an opportunity to examine changes in diagenetic and thermal maturation parameters across a number of different paleo-environments. Second, the abundance of coal throughout the Eureka Sound Formation along Strand Fiord allows for comparisons to be made between inorganic diagenetic parameters and thermal maturation information. Finally, localized heat flow complexities in the Strand Fiord area provide an opportunity to examine the effects of high heat flow on diagenesis and thermal maturation.

The present study looks at variations in coal, sandstone and clay diagenetic parameters with depth and relates these variations to chemical and thermal changes that occurred during the evolution of the Eureka Sound Formation at Strand Fiord. The primary parameters considered include illite crystallinity, sharpness ratio of illite peaks, percentage of illite in illite-smectite mixed layer clays and vitrinite reflectance. The primary objectives of this study are to:

1) determine variations in both shale and sandstone mineralogy and diagenesis throughout the studied section;

2) determine the paragenesis of authigenic minerals;

3) estimate the geothermal gradient and maximum depth of burial of strata in the study area;

4) examine the effect that changes in paleo-environment has on diagenesis and thermal maturation; and

5) model the diagenetic pore fluids and chemical environments.

STUDY AREA

Samples from the present study were collected from approximately 3000 m of continuous section of the Eureka Sound Formation that crops out along the south shore of Kanguk Peninsula on western Axel Heiberg Island (Figure 1) The studied section was measured along the south limb of a syncline exposed along the top of a ridge extending from 79°30'N latitude, 91°30'W longitude, to 79°14'N latitude, 91°03' longitude. Relief in the area never exceeded 600 m. Figure 2 is a generalized geologic map of Kanguk Peninsula showing the location of the studied section and associated geology. Geological Survey of Canada map sheet *1301A*— Strand Fiord, District of Franklin (Thorsteinson, 1971) should be consulted for a smaller scale map of the study area.

GEOLOGIC SETTING

The Eureka Sound Formation is a Late Cretaceous to Late Eocene, predominantly non-marine and nearshore marine clastic sequence that comprises the youngest strata of the Sverdrup Basin of the Canadian Arctic Archipelago. The Sverdrup Basin is a pericratonic structural depression occurring adjacent to the northern margin of the North American craton (Balkwill, 1978; Miall, 1984, *in press*). At its depocenter, the basin succession is up to 13000 m thick. Regionally, the Sverdrup Basin extends for approximately 1300 km along the north central part of
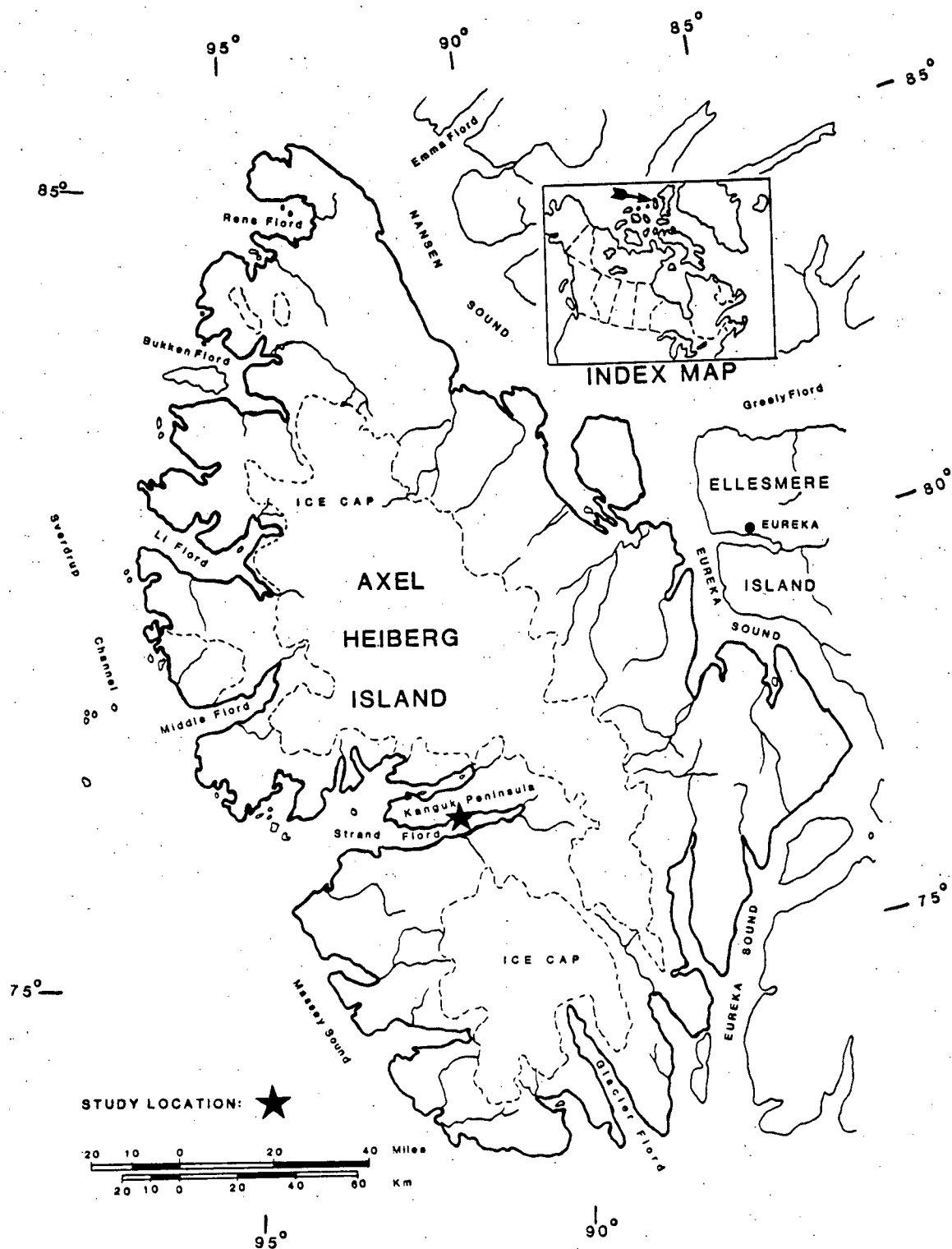
Figure 1- Location map showing study area on Kanguk Peninsula, Axel Heiberg Island, N.W.T..
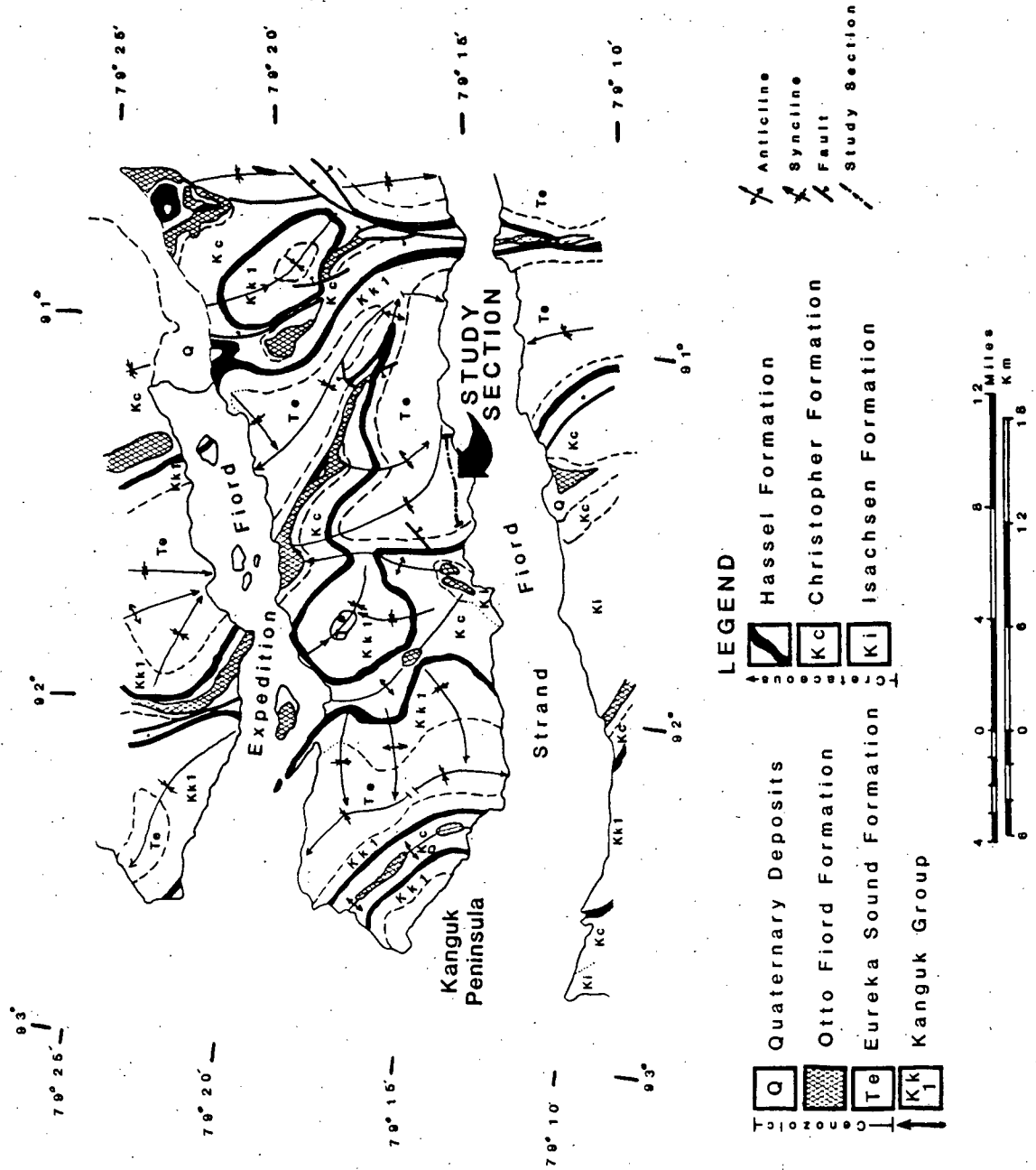
Figure 2- Simplified geologic map of Kanguk Peninsula showing the generallized structure in the study area (modified from Thorsteinson, 1971).

the Archipelago. Sediments of the Sverdrup Basin range in age from Late Paleozoic (Visean) to Early Tertiary and represent deposits derived in part from Franklinian Geosyncline strata uplifted by the Ellesmerian Orogeny (Devonian–Mississippian) and cratonic sediments derived from terrains to the south and east of the Basin (Balkwill and Bustin, 1980; Ricketts and McIntyre, *1985, written pers. comm.*) The Sverdrup Basin's southern and eastern margins correspond roughly to Ellesmerian structural belts (Balkwill, 1978). The northern margins are reported by Meneley *et al.* (1975) to have been defined by an intermittently positive tectonic ridge.

The studied section has been divided into a number of different paleo-environments by Ricketts and McIntyre (*1985, written pers. comm.*) which form the framework for the following discussion. Figure 3 outlines the general stratigraphy and corresponding paleo-environmental interpretations of the studied section. The base of the section is marked by approximately 235 m of marine shale of the Kanguk Formation. The contact between the Kanguk shales and the overlying Eureka Sound Formation has been selected at the base of the first major sandstone unit. Approximately 500 m of coarsening upwards sandstone-shale sequences characterize the basal lithofacies of the Eureka Sound Formation. Each coarsening upwards unit within the first 500 m of section is interpreted as an individual prograding lobe of a wave dominated delta strand plain. A thin iron stained unit marks a major disconformity between the top of the wave dominated delta facies and the overlying 265 m of marine shale. Approximately 1020 m of transitonal and fluvial dominated delta facies overlie the marine shale. These deltaic and transitional facies comprise sandstone-shale coarsening upward sequences which represent interdistributary bay subdelta-lobes. The entire 1020 m represents a transitional facies between the underlying wave dominated delta and overlying fluvial dominated delta

AGE	HEIGHT ABOVE BASE (Metres)	GENERAL STRATIGRAPHY	ROCK STRATIGRAPHIC UNITS[1]		INTERVAL THICKNESS (Metres)	LITHOLOGIC DISCRIPTION	PALEO-ENVIRONMENT[1]
LOWER TERTIARY	2780		SOUND FORMATION	Zone			
				5	770	Interbedded fine to medium grained quartz arenites, coal (vitrain) and dark grey, friable shale; sandstones are commonly crossbedded and contain abundant chert and organics; shales are commonly coaly; sandstone cements include dawsonite, magnesium-poor ankerite, siderite, calcite, and kaolinite; dawsonite proportion generally increases toward top of section; segment consists of approximately 30 fining- upwards sequences commonly capped with coals; fining upward packages range from 2 to 15 metres in thickness; coal seams are ≤3 metres in thickness.	FLUVIAL DOMINATED DELTA
	2020			4	1020	Fine to medium grained quartz arenites interbedded with dark grey, friable shale; sandstones are well indurated and poorly to moderately sorted; shales consist primarily of kaolinite, illite and some chlorite; major sandstone cements are magnesium-poor ankerite, calcite and kaolinite; calcite proportion decreases toward top of section; minor coal seams of predominantly vitrain are present; section consists of approximately 45 coarsening upward packages ranging from 5 to 25 metres in thickness.	TRANSITIONAL
UPPER CRETACEOUS / U. CAMPAINIAN	1000		EUREKA	3	285	Moderately friable carbonaceous shale; blue-grey on weathered surface; minor sandstone horizons occur through out zone.	MARINE
	735			2	500	Interbedded very fine to medium grained, poorly sorted quartz wackes, dark grey siltstones and carbonaceous shales; sandstones are moderately to well indurated; shales consist primarily of kaolinite and illite.	WAVE DOMINATED DELTA
				1			
	235		KAN-GUK Fm.		235	Interbedded dark- grey shale and siltstone; shale is moderately friable.	

[1] Ricketts and McIntyre (pers. comm., 1985)

Figure 3- Generallized stratigraphic section showing lithofacies interpretation (Ricketts *et al*, *pers. comm.*) and section subdivisions (zones).

systems. The final 770 m of the section are composed of a repetition of fining upward sequences commonly capped with coals and vertical accretion deposits. These lithologies represent delta plain deposits of a fluvial dominated delta. The Beaufort Formation elsewhere unconformably overlies the Eureka Sound Formation although it is not present in the study area.

Locally, in the area of Kanguk Peninsula, broad northwesterly trending doubly plunging anticlines and synclines dominate the structure (Trettin, 1972; Thorsteinson, 1971). Carboniferous evaporite diapirs occur over much of the area and are, for the most part, localized along the axes of anticlines (Gould and DeMille, 1964; Thorsteinson, 1971; Balkwill, 1978; Ricketts and McIntyre, 1985, written pers. comm.). Gravity studies by Sobczak et. al. (1963) originally suggested that the diapirs of the Sverdrup Basin may be cored with halite and, infact, later studies by Davies (1973) confirmed the presence of halite in the subsurface. Previous field investigations, however, have been unable to find direct or indirect evidence in outcrop to support the presence of halite cores in the diapirs.

PREVIOUS WORK

The stratigraphy of the Eureka Sound Formation throughout the Canadian Arctic Islands is described by Fortier et al. (1963), Fricker (1963), Tozer and Thorsteinson (1964), Stott (1969), Balkwill and Bustin (1975), Balkwill et al. (1975), Bustin (1977), Balkwill et al. (1982), Reidiger (1985), and Ricketts and McIntyre (1985, written pers. comm.). In previous studies the base of the Eureka Sound Formation at Strand Fiord has been considered Maastrichtian (Bustin, 1977). Recent palynological analyses by Ricketts and McIntyre (1985, written pers. comm.), however, have determined that the Eureka Sound sediments at Strand Fiord were deposited as

early as the Middle and possibly Early Campanian. Further east, at Fosheim Peninsula, the base of the Eureka Sound Formation may be as old as Late Santonian-Early Campanian age, based on the presence of the index fossil *Shenoceramus* cf. *patoontensiformis*.

Coalification levels of the Eureka Sound Formation have been determined from a number of localities in the Arctic Islands by Bustin (1977; *in press*) and Riediger (1985). A cursory examination of variations in coalification levels with depth was done by Bustin (*in press*) through a 2500 m thick section at Strand Fiord. Bustin's (*in press*) results indicate that no systematic increase in $R_o$max exists with depth over the interval examined. Bustin attributed this phenomenon to the abundance of evaporite diapirs in the area whose high thermal conductivities interfered with the normal thermal maturation of the coal. Regional coalification mapping of the Canadian Arctic Archipelago by Bustin (*in press*) revealed that vitrinite reflectance values vary from a low of 0.17% at Makinson Inlet to a high of 0.70% at Strand Fiord.

Diagenetic analyses of sandstones and shales have received a great deal of attention over the past few years. It has been demonstrated in numerous studies of the textural relationships between authigenic phases that it is possible to infer from rocks information about changes in porewater chemistry and physical conditions through time. Merino (1975), Boles and Franks (1979) and Hutcheon *et al.* (1980), for example, used textural relationships to predict diagenetic reactions such as the kaolinitization of chlorite, conversion of dolomite and kaolinite to chlorite and calcite, conversion of biotite to chlorite and the reaction of anorthite with sodium to produce diagenetic sodic plagioclase. Boles (1978) also predicted the fluid chemistry necessary to facilitate the ankeritization of calcite. Recent work by Surdam

(1984), Moncure *et al.* (1984), Seibert *et al.* (1984), and Crossey *et al.* (1984) have addressed the mechanics of creating secondary porosity through the dissolution of aluminosilicates. Wescott (1983) used diagenetic analyses to assess the reservoir quality of the Cotton Valley Formation of east Texas. Other recent papers on sandstone diagenesis include those of Wilson and Pittman (1977), Hurst and Irwin (1982) and Hutcheon (1983).

Thermodynamic studies of authigenic assemblages and pore fluid chemistry have previously been done on strata from other locations. Merino (1975b) used a distribution of species analysis to assess authigenic phase stabilities with respect to fluid chemistry from Tertiary sandstones of California. Hutcheon (1981) used thermodynamics, in a general sense, to examine clay and other authigenic mineral equilibria. Other papers that consider the chemistry and origin of pore fluids include those of Chave (1960), Siever *et al.* (1965), and White (1965). Problems associated with defining a "stable system" and in determining the stoichiometry of the clay phases involved in low temperature diagenetic reactions have prompted many investigators in the past to avoid similar analyses.

Papers by Sarkisyan (1972), Hower *et al.* (1976), Hancock and Taylor (1978), Foscolos and Powell (1978), Powell *et al.* (1978), Hower (1981), Bruce (1984), Foscolos (1984), and Srodon and Eberl (1984) represent just a fraction of the literature that has been written on shale diagenesis. Diagenetic changes such as the progressive illitization of smectite with depth have been discussed by Burst (1969), Foscolos and Kodama (1974) and Bruce (1984). Related studies by Reynolds and Hower (1970) and Srodon (1980) have developed relatively sophisticated ways of calculating the relative proportions of illite and smectite in mixed-layered clays based on XRD analyses. Changes in 1.0 *nm* peak shape from XRD analyses (developed by

Weaver (1961) and Kubler (1966)) are commonly used (Foscolos *et al.*, 1976) to index and predict diagenetic stages in strata. Clay diagenesis of the Eureka Sound Formation has been briefly examined by Bustin and Bayliss (1979) in the area of Fosheim Peninsula.

ORGANIC MATURATION

Traditionally, pressure and temperature information has been extracted from strata by analysing organic and inorganic maturation parameters. Clay mineral assemblages and related diagenetic parameters were once thought to reflect maximum temperature and pressure conditions attained (Burst, 1969) but it has since been shown (De Segonzac, 1970; Foscolos et al., 1976, 1978; Hower et al., 1976) and is now commonly accepted that clay minerals are equally as sensitive to their geochemical environment (pH, Eh, cation activities, etc.) as they are to their physical environmment (pressure and temperature); see following chapter. As a result, the use of stable(?) clay assemblages as geothermometers and/or geobarometers is limited unless constraints on the geochemical environment are known (Hutcheon et al., 1980).

The preferred method for calculating the maximum temperature attained in a sequence of strata is by measuring the mean maximum reflectance (R_0max) of vitrinite and performing a time—temperature maturation analysis (after Lopatin, 1971; Waples, 1980; Middleton, 1982). Unlike mineral metamorphism, vitrinite maturation does not undergo retrograde metamorphism and is, therefore, a relatively reliable indicator of the maximum attained temperature. Studies by Lopatin (1971), Dow (1977) and Middleton (1982) have shown that R_0max increases linearally and exponentially with increases, respectively, in time and temperature. Recent studies by Hutton et al. (1980), Fujii et al. (1982) and Price et al. (1985) have shown that although coalification is generally considered to be unaffected by pressure (Hutton et al. (1980)), increases in the H/C ratio of vitrinite and associated macerals may suppress the reflectance of vitrinite. As a result, if vitrinite reflectance is to be used

as a reliable paleothermometer close attention must be paid by the investigator to the variations in microlithotypes (i.e., increases in exinitic component) and vitrinite types with depth.

This chapter examines the studied section for trends in coalification, estimates the maximum depth of burial of the strata and the geothermal gradient and makes inferences about the thermal and baric evolution of the section.

EXPERIMENTAL

Sample Preparation

Forty samples were chosen for R_0max analysis from the approximately 3000 m of section. Both kerogen concentrates (phytoclasts) and coals were examined. R_0max measurements from the upper half of the studied section were taken primarily from coals that were grab—sampled at approximately 40—50 m intervals. The relative absence of true coal seams from the lower half of the section required that R_0max measurements be made on phytoclasts. Samples from the lower half of the section were collected from approximately 100—150 m intervals.

Coal Pellets

Coal pellets were prepared using methods modified from Bustin (1977). The samples were initially crushed with a mortar to reduce the coal fragment size to approximately 850 μm. The less than 850 μm fraction was then separated from the larger fraction by sieving with a 60 U.S. mesh sieve. That portion that was finer than 60 U.S. mesh was collected and used in the pellets.

A 1:3 mixture of the <850 μm coal and Transoptic® powder was then placed in a hydraulic Buehler Pneumet I® pellet press and heated for 12—15 minutes. Once a temperature of 100°C was attained a pressure of 3.5 KPa was applied and the mixture was allowed to cool under pressure for 15 minutes. Polishing was left until immediately before the operator was prepared to proceed with $R_o$max measurements in order to minimize the oxidation of the vitrinite. Once polished, the samples were left in a desiccator under helium for no longer than 48 hours prior to being analysed.

Phytoclast Pellets

Phytoclast concentrates were prepared using methods modified from Bostick and Alpern (1977). Shale samples were initially crushed in a mortar to reduce the fragment size to 1 mm^3. Samples were then placed in 1 litre buckets containing 100% hydrochloric acid and left for 24 hours in order to remove any carbonates present. The HCl bath was followed with 4 rinses with tap water separated by 24 hour settling periods. Silica was next removed by leaving the samples in 48% hydrofluoric acid for 3 days. Any residual coarse silica was removed by sieving the product and retaining the fine fraction. Pellet preparation followed the techniques outlined in the preceding paragraph on coal pellet preparation.

Analytical Techniques

All samples were analysed in accordance with ASTM procedures (ASTM D2797, 1980). Polished pellets were examined on a Leitz MPV2 microscope equipped with a 50x oil immersion objective, 10x ocular, stable voltage supply, photomultiplier, and computer assisted data collector. The size of the limiting

aperture used was 8 μm. Measurements were taken while the stage was rotated at a rate of approximately 360°/7 seconds. Immersion oil with a refractive index of 1.515 was used. Fifty measurements were taken per sample with the system being recalibrated against the standard after every 25 measurements. If the calibration was out by more than 0.02% at the end of a run, the run was discarded and redone. Most R_o max readings were taken from telocollinite with desmocollinite being measured if telocollinite proportions were low. Non—specific vitrinite was measured in the shale samples. For a detailed description of the optical properties of vitrinite, the theory behind measuring vitrinite reflectance, and the mechanics of the reflectance microscope refer to Bustin et al. (1983).

Elemental Analysis

A representative sample from both the coals and the phytoclasts was chosen for C H N elemental analysis to determine if variations exist in the H/C ratios of the two sample groups. Each sample was analysed twice from separate "masked" vials to ensure accuracy within 0.5%. The two samples chosen for elemental analyses are indicated on figure 5.

Time—Temperature Model

One of the methods used to calculate the maximum paleotemperature attained in the studied strata is Lopatin's (1971) time—temperature model (Waples, 1980). In applying Lopatin's model to the Eureka Sound Strata at Strand Fiord a number assumptions were made regarding the tectonic history and thermal properties of the strata. First, for the sake of simplicity the rates of subsidence and uplift are assumed to be uniform. Second, heat flow and thermal conductivities are assumed

to be constant (Lopatin, 1971). Third, the activation energy for the entire range of maturation is assumed to be constant. The basic premise of Lopatin's TTI model states that kerogen maturation is simply a function of time and temperature. An increase in temperature of $10\,^{\circ}C$ will result in a doubling of the maturation level, thus, defining an exponential relationship expressed by the equation:

$$\gamma = r^{n}$$

where,

γ = factor which relates the exponential dependence of maturation to temperature.

r = factor by which the rate of maturation increases for every $10\,^{\circ}C$ increase in temperature. $r=2$ if one assumes that each increase in temperature of $10\,^{\circ}C$ produces a doubling in the rate of increase in maturation level (Waples, 1980).

n = temperature interval index value.

A linear relationship exists between maturation and the length of time that a sedimentary package has been exposed to a given amount of heat. Doubling the heating time will result in a two fold increase in maturation for any given temperature. Lopatin's equation for the total maturity (TTI) of any sediment is given by:

$$TTI = \sum_{i\,=nmin}^{nmax} (\Delta T_{n})\,(r^{n})$$

where,

nmin = smallest n-index value encountered.

nmax = largest n-index value encountered.

ΔT_n = length of time spent by sediment in temperature interval i. The computer model used in this study uses the integrated form of Lopatin's (1971) model; expressed as follows:

$$TTI = \int_{t_o}^{t_p} 2^{(T(t)-105)/10} \, dt$$

where T(t) is the temperature ($^{\circ}$C) as a function of time with t_o being the time of deposition and t_p being the time at present.

RESULTS AND DISCUSSION

Coalification Gradients

Coal rank was generally found to increase with increasing depth from sub—bituminous A/high volatile bituminous C to high volatile bituminous B. At approximately 1400 m above the base of the section there is an apparent decrease in the reflectance values and change in the coalification gradient. Whether this change in the coalification gradient is real or not is discussed later.

A number of $R_o$max versus depth curves were tested to determine the 'best fitting' coalification gradient for the measured gradients. Both arithmetic (Fig. 4) and semilog (Fig. 5) plots were analysed. In each case, the data were treated as representing first a single population and second two separate populations of points; namely coals in the upper population and phytoclasts in the lower population. For both the semilog and the arithmetic treatments it was found that curve—fits were improved when the data were assumed to represent two separate populations of points. For example, the r^2 values for the data assuming a single population were 0.172 for the semilog treatment and 0.176 for the arithmetic treatment. By assuming
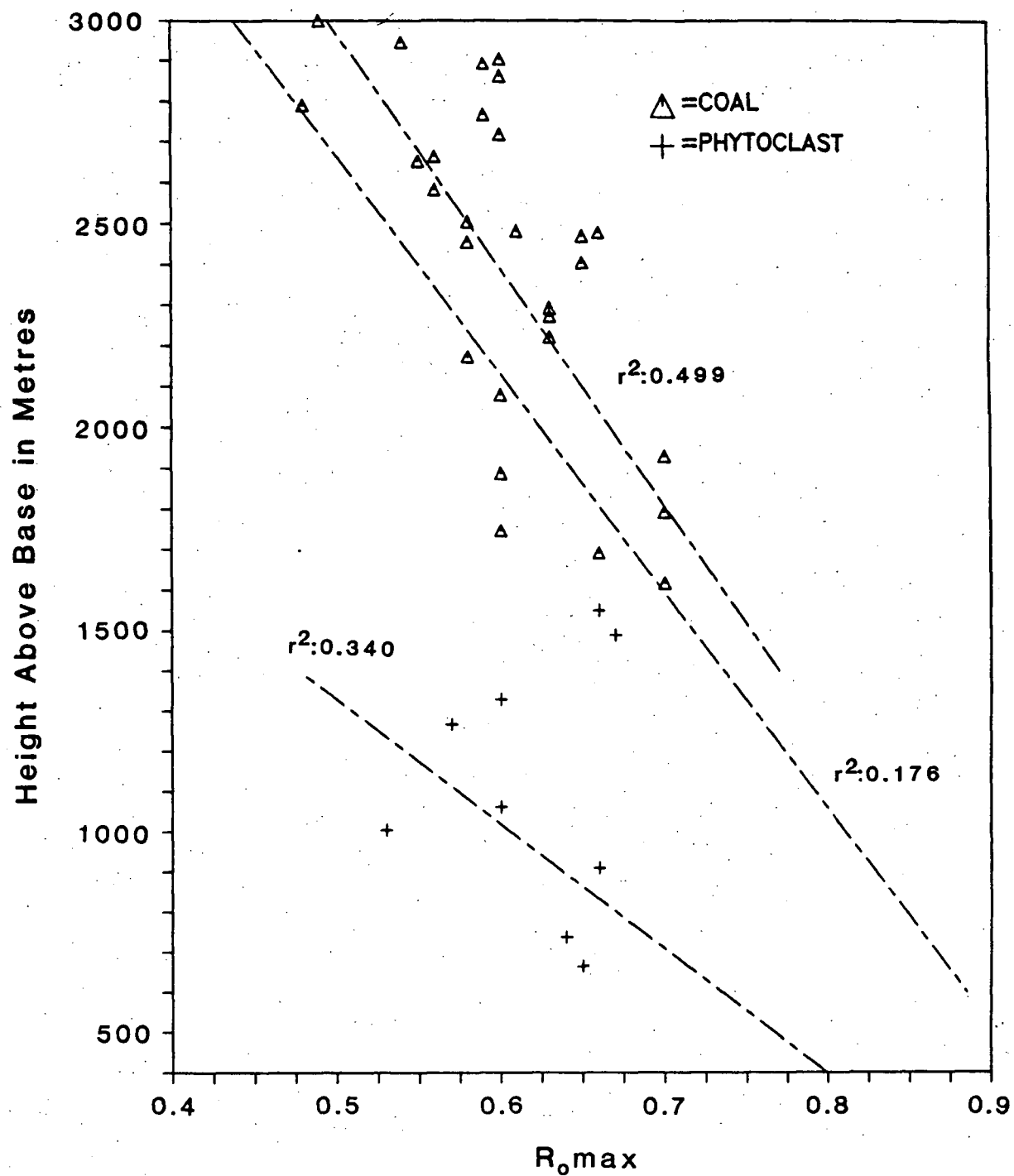
Figure 4. Arithmetic plot of mean maximum reflectance versus depth
showing regression lines and corresponding r-squared
values through the 3 possible populations (upper
population consisting primarily of coal, lower population
consisting of phytoclasts, single population consisting of
entire section).
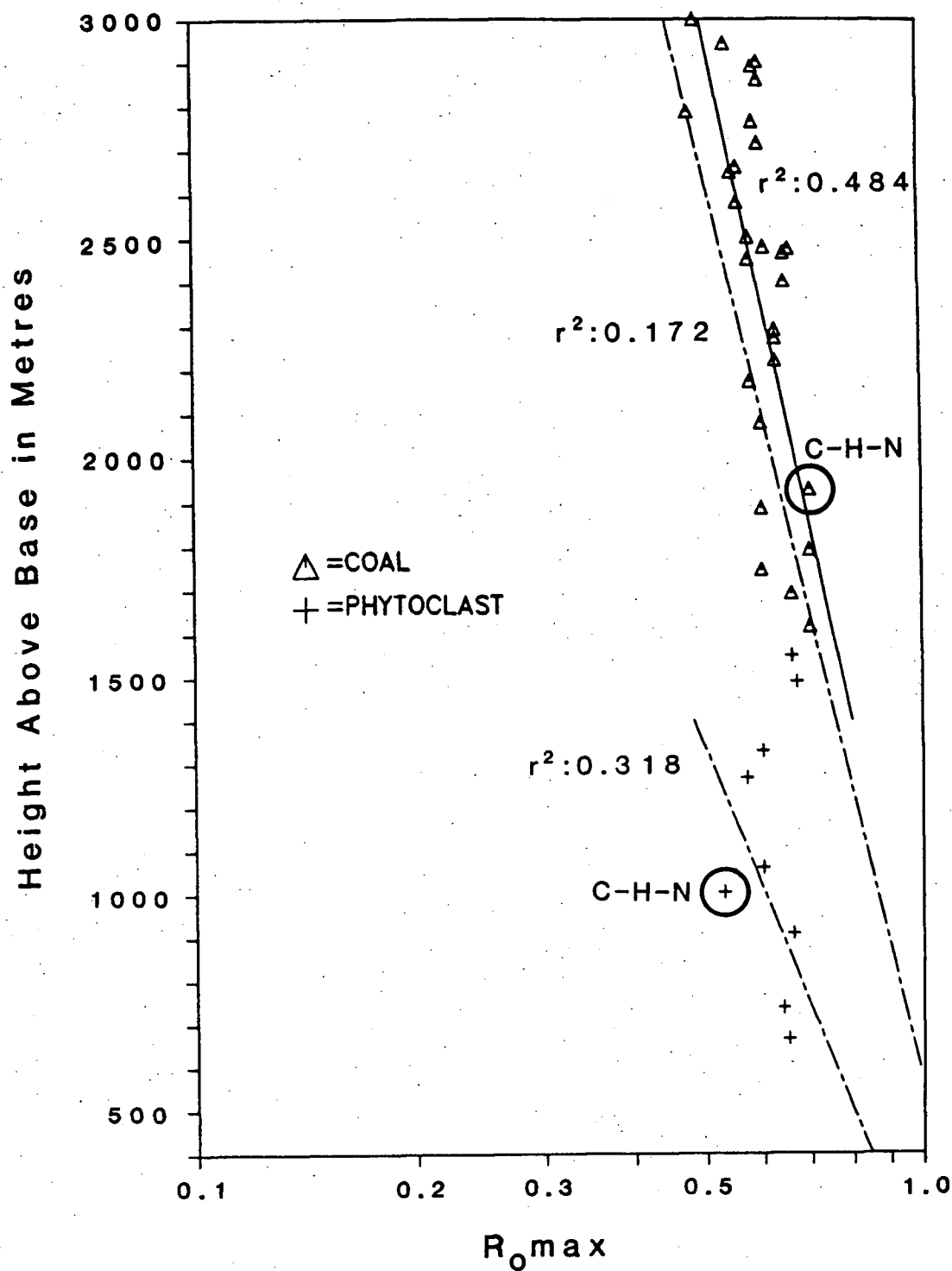
Figure 5. Semilog plot of mean maximum reflectance versus depth showing regression lines and corresponding r-squared values through the 3 possible populations (upper population consisting primarily of coal, lower population consisting of phytoclasts, single population consisting of entire section).

two separate populations the r^2 values for the semilog plot were 0.484 (upper population) and 0.318 (lower population). Corresponding arithmetic values were 0.49 and 0.34, respectively.

Statistical Considerations

Given the low coefficient—of—determination (r^2) values and relatively small sample sizes, depth and thermal modelling of the studied strata using any of the above mentioned curves yield results with a good deal of uncertainty. The following sections, therefore, attempt to minimize this uncertainty by adjusting, where necessary, the various gradients such that they are in relative agreement with published local tectonic models.

A literal interpretation of the r^2 statistic states that for an r^2 value of 0.49 (i.e., as seen in the arithmetic fit of the upper population) only 49.9% of the variability in R_0max values can be explained by the depth values. From the present study this suggests that, at best, 50% of the variability in R_0max must be explained in terms of some other variable(s). If the entire section was considered ($r^2 = 0.172$, semilog) at *least* 82% of the variability in R_0max would have to be explained in terms of some variable other than depth. The following sections discuss a number of factors which are believed to contribute to at least some of the remaining variability in observed R_0max values.

Consideration of R_0max Distribution with Depth

Arithmetic fits of the data were found to be consistently better than semilog fits for any given depth interval. Similar findings have been reported in studies by England (1984) and Moffat (1985) in areas with considerably different tectonic histories than Strand Fiord. In general, coalification gradients in these other areas were found to be arithmetic only in areas where thermal disequilibrium with basement heat flux was suspected. In addition, the arithmetic relationship between R_0max and depth did not extend over the full range of R_0max values but was restricted to values below 0.35% reflectance. Such conditions were suggested to have been created by rapid basin infilling and short sediment residence times. Thermal disequilibrium may be possible at Strand Fiord but for reasons other than rapid sediment loading and unloading as, although sediment accumulation rates were relatively high (approximately 120 m per million years), residence times were generally long (Balkwill, 1978).

Thermal disequilibrium at Strand Fiord, if it exists, is most likely related to the presence of the numerous evaporite diapirs in the study area. The concept of hot diapir intrusions affecting their surrounding sediment is not unique as indicated by Balkwill (1973) where the formation of hornfels adjacent to diapirs is attributed to such a phenomenum. At Strand Fiord, however, thermal disequilibrium between the diapirs and the coals is suspected and believed to have resulted in part from rapid emplacement and unrooting of a diapir which would, theoretically, have a similar local effect as rapid deposition and unloading of sediments. Heat derived from depth while the diapir remained rooted would be transfered through the diapir and into the surrounding rock. Upon becoming unrooted, heat conduction from the source at depth would cease and the temperature in the isolated diapir would

drop. This theory is substantiated by Selig and Wallick (1966) who find that as the separation distance of an isolated diapir from its source increases, the geothermal gradient in the sediments overlying the diapir decreases. If the process was sufficiently rapid, thermal equilibrium with the surrounding rocks may never be attained. The result would be a general deviation of the coalification gradient from the predicted log–linear distribution.

Another factor which may contribute to the deviation of the coalification gradient away from a log–linear distribution may be seen in examining the fundamental assumptions underlying the coalification process. Karweil (1956) defined coalification as a time/temperature process which could be explained in terms of first order reaction kinetics, stating that maturation $(R_0\,max)$ *rate* varies log–linearly with temperature. Lopatin (1971) also used first order reaction kinetics to predict maturation level. Recent studies by Price (1983) and Barker (1983) have suggested, however, that the maturation process is not properly explained using first order kinetics and that coalification is more likely a 'multi–order' kinetics phenomena that is a function of time only during the early stages of the reaction. Barker's (1983) findings state that the thermal maturation process is more strongly temperature dependent than previously realized and that maturation reactions may proceed to completion in as little as 1,000 to 10,000 years. In short, vitrinite reflectance is believed by these authors to be an absolute, rather than a time dependant, geothermometer. There nevertheless remains a good deal of controversy as to whether vitrinite reflectance is an absolute rather than time dependent geothermometer. If reflectance is an absolute geothermometer, a log–linear plot of $R_0\,max$ versus depth would only produce a straight line plot if each given depth increment were to correspond to a *constant* temperature increment. This would only

occur under conditions of a constant geothermal gradient and uniform heat flow throughout the section. As is discussed in the following paragraph, uniformed thermal conductivities and, therefore, a consistent geothermal gradient through the Strand Fiord section is a poor assumption and, therefore, a log—linear coalification gradient is not to be expected.

Consideration of Shifts in Coalification Gradient

An examination of the R_0max distribution with depth reveals a second enigma which must be considered— how can the apparent shift in the coalification gradient at 1400 m and apparently random distribution of R_0max values below that depth be explained? The following discussion recognises fluid migration of heated diapir—derived waters as being the primary factor in explaining the observed shift in the coalification gradient. This theory is supported by sandstone diagenesis findings which are discussed in a later section. A number of minor factors which may contribute to producing the observed offset in the coalification gradient are also included in the following discussion.

Similar shifts in coalification gradients have been explained in other study areas (Bustin, 1983; England, 1985) by the presence of thrust faults. The occurrence of a major thrust fault in the study area is highly improbable for a number of reasons. First, there is good lithostratigraphic continuity between units both above and below the R_0max break (Ricketts and McIntyre, *pers. comm.*). Second, there is no structural evidence that would suggest a thrust fault through the studied section or associated geology. Third, a thrust fault with a considerable amount of throw would be required to produce the observed shift in the R_0max gradient. No field evidence in support of such a structure was observed or has been previously

reported in the literature.

Lithology and fracture controlled migration of fluids is believed to exert the primary control on the observed shift in the coalification gradient. The present model proposes selective horizontal migration of heated pore fluids from diapirs into stratigraphically adjacent permeable lithologies. Studies by Hitchon (1984) and Nurkowski (1984) have suggested that the heat carried by ground waters has a significant effect on the maturation of vitrinite. Given that coal seams serve as better aquifers than shales (from which the phytoclasts were extracted) the maturation effect of the heated diapir—derived waters would be observed primarily in vitrinite from lithologies with the greatest permeabilities; specifically, fractured coals rather than the tight shales. Again, if thermal equilibrium was not attained, the result would be a shifting of the upper curve toward higher reflectance values and a deviation from a log—linear curve.

The present study's results from the elemental analyses (Table 1) of the coal and phytoclast sample support the idea that the offset in the coalification gradient is of a chemical, rather than compositional, nature. In the past, it has generally been regarded that there is no appreciable difference in $R_o$max values extracted from coals and $R_o$max values obtained from associated phytoclasts, however, recent studies by Price et al. (1985) and Fuji et al. (1985) have shown that this is not always true. Increased exinitic components in coal and even increased proportions of H/C in the vitrinite can result in suppression of R_o. In the present study the coal sample was found to have a *higher* H/C ratio than the phytoclast of *lower* reflectance. Although these findings do support the idea that the permeable coals have matured preferentially as a result of being in contact with heated waters they also suggest that oxidative degradation of the coals associated with the horizontal

TABLE 1

C H N Elemental Analysis of Organic Matter

(%)

Sample	C	H	N	H/C
RAK—62—25	44.09	3.51	1.39	0.079
	44.14	3.50	1.37	0.079
RAK—27—25	69.95	4.74	1.01	0.067
	70.41	4.85	1.02	0.068

migration of water may have occurred.

A final contribution to producing the offset in the coalification gradient may come from the differences in thermal conductivities of the two segments of section (Gretener, 1981). When complete sedimentary packages are considered, an average thermal conductivity may be assigned to the package based on the relative proportions of sandstone and shale (assuming, of course, that the average thermal conductivity of a package is a linear combination of the conductivities of the individual lithotypes (Moffat, 1985)). Assuming that this is the case, the section occuring below 1400 m, consisting of approximately 80—90% shale and only about 10—20% sandstone, would have a bulk thermal conductivity of 1.8—2.0 W/m°C. Above 1400 m, the section is considerably richer in coal and sandstone (approximately 60—65%) than shale (35—40%) thereby producing an average bulk thermal conductivity of approximately 2.8—2.9 W/m°C. This difference in thermal conductivities would produce difference in the geothermal gradients between the two packages of up to 20°C/km if it is assumed that heat flow is uniform

throughout the section. If the primary heat source is the diapir, which is stratigraphically adjacent to, rather than beneath, the section it is possible to envisage an offset in the coalification gradient resulting from non—uniform horizontal heat flow. The result is that the observed shift in the coalification gradient is more likely a function of the thermal conductivities and permeabilities of the two packages rather than the tectonic history of the section.

It was decided to model the coalification gradients determined from the semilog plots because the maturation model used later in this study assumes an exponential increase in maturation rate (i.e., R_0max) with increasing temperature (i.e., depth). The coalification gradient from the studied section was, therefore, found to be 0.127 %logR_0max/km ($r^2 = 0.484$) as determined from a semilog analysis of the upper population of points.

Paleo—depth of Burial

The pre—tectonic thickness of sediment from a section of strata has been calculated by extrapolating the coalification gradient to a depth which corresponds to a zero—maturity level. This zero—maturity level usually corresponds to an R_0max value of 0.15% or 0.20% (Middleton, 1982). The present study uses a zero—maturity value of 0.15% R_0max as a previous study by Bustin (*in press*) has determined that R_0max values as low as 0.15% do occur throughout the Canadian Arctic Archipelago.

Paleo—depth of burial calculations determined that as much as 4100 m of sediment may have been eroded from above the studied section at Strand Fiord (Figure 9). This would suggest a pre—tectonic thickness of the Eureka Sound

Formation at Strand Fiord of up to 6800 m.

Previously reported pretectonic thicknesses of syn— and post—Eureka Sound sediments are reported by Bustin *et al.* (1977) from Fosheim Peninsula and May Point where values of 3500 and 2500 m, respectively, were determined. Bustin (*in press*) reports Eureka Sound Formation depths of burial of up to 6000 m from Meighen Island. At Strand Fiord previous studies were unable to determine a coalification gradient and, therefore, a pre—tectonic thickness because of a general lack of data. Bustin (1977) estimated a Mid Eocene thickness of approximately 3200 meters based on his paleo—reconstruction of the area. The present study's findings, if corrected for the diapir—induced maturation, are in partial agreement with Bustin's (1977) model. The gradient was corrected for diapir—induced maturation by shifting the coalification curve to the left until an R_0max value of 0.50% corresponded to a position in the section of 1400 m above the base of the section. This was done in order to align the upper coalification gradient with the lower coalification gradient. In modelling the corrected gradient it was assumed that only the *position*, rather than the *slope*, of the gradient was affected by the diapir. Sixty eight hundred metres of burial would represent the absolute maximum possible depth of burial if the effects of high heat flow and, therefore, diapir—induced thermal maturation were absolutely minimal. A minimum, and perhaps more realistic value for the maximum depth of burial could be estimated by examining the corrected gradient which attributes the positioning of the upper coalification gradient to heat flow anomalies. The adjusted depth of burial, from which the shallowest possible depth of burial was determined, was calculated to be approximately 2500 meters, which gives a total pre—tectonic thickness of 5200 m. This adjusted value is in better agreement than the non—corrected value of 6800 m with previously published

paleo—reconstructions of the Sverdrup Basin.

Maximum Pressure Considerations

A number of assumptions regarding the density and pressure distribution of the overlying strata make it possible to estimate the pressure at the base of the section. First, because sediment accumulation rate was relatively high (Balkwill, 1978) and the modelled heat source is diapir—derived waters it was assumed that the pressure at depth was wholly hydrostatic. By modelling the pressure to be entirely hydrostatic it is assumed that there has been a relaxation of all creep related shearing stresses at depth (Hobbs *et al.*, 1976). The hydrostatic pressure at depth (h) is equal to ρgh where ρ is the density of the overlying rock and g is the acceleration due to gravity. As the lithologic proportions of the removed section are unknown the hydrostatic pressure was calculated assuming that the 5200 m of sediment consisted first of 100% sandstone with 10% porostiy ($\rho = 2.5$ cm^3 (Clark, 1967)) and second of 100% shale ($\rho = 2.25$ cm^3 at 2500 m depth, 2.38 cm^3 at 4100 m depth and 2.42 cm^3 at 5200 m depth (Clark, 1967)). Given then that the actual strata consisted of some combination of the two lithologies, the actual pressure would lie somewhere between these two values (Figure 6). The results indicate that the total hydrostatic pressure at the 1400 m mark ranges from 95 MPa for pure shale to 100 MPa for pure sandstone. Values from the top of the section are 55 MPa and 61 MPa for pure shales and sandstones, respectively. Maximum pressures at the base of the Eureka Sound Formation are 123 MPa (pure shale) and 127 MPa (pure sandstone).

Hydrostatic Pressure in Megapascals
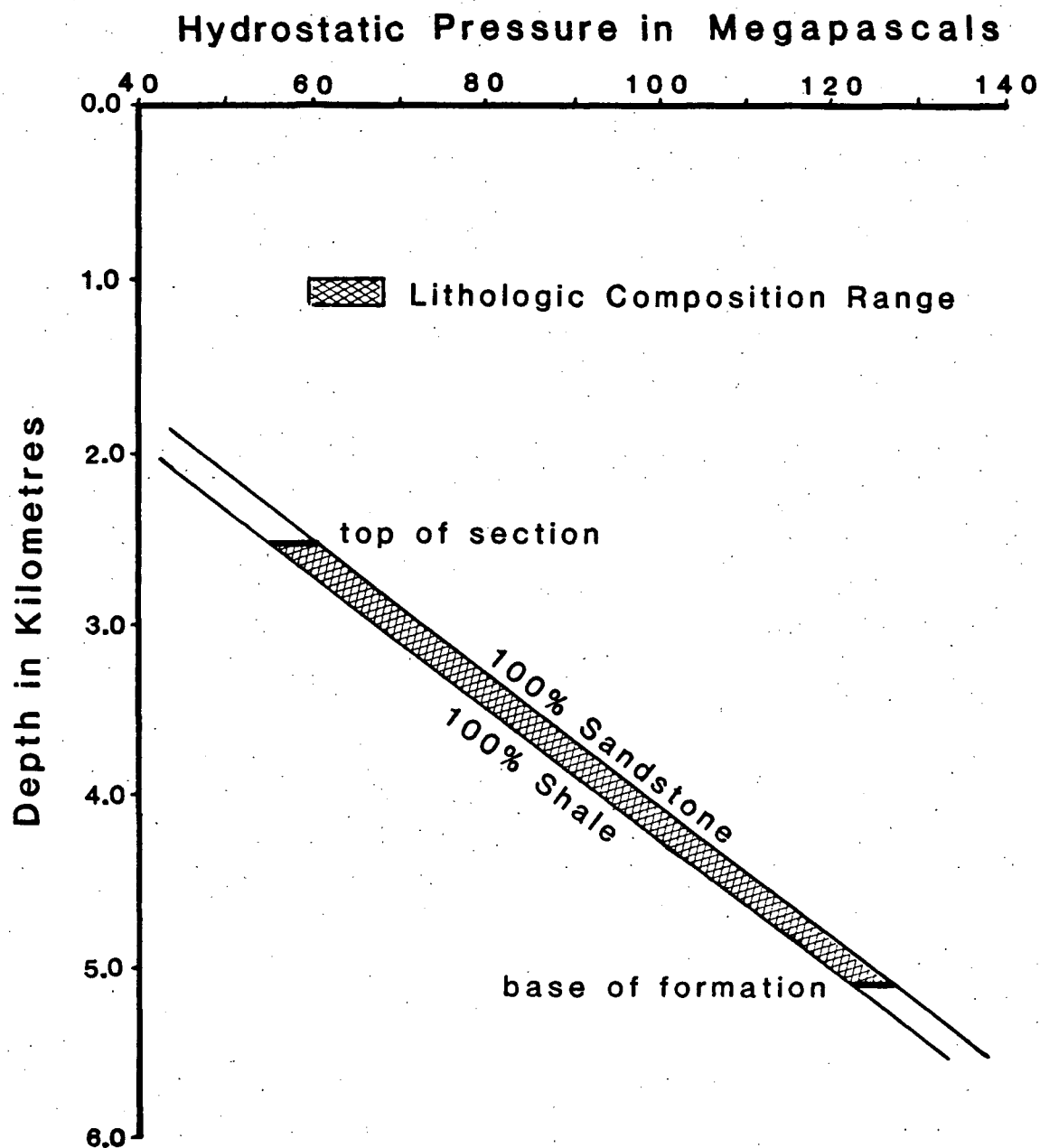
Figure 6- Hydrostatic pressure distribution through studied section assuming a maximum depth of burial of 5500 metres. Pressure brackets were calculated using saturated bulk densities for 100% pure sandstone and 100% pure shale.

Paleo—geothermal Gradient

To model the paleo-geothermal gradient using Lopatin's method the burial history of the strata must be known. At Strand Fiord the basal strata of the Eureka Sound Formation were deposited approximately 70 Ma with basin infilling and subsidence occurring up until 35 Ma. Between 62 and 66 Ma deposition ceased, as shown by the disconformity between unit 2 (the wave dominated delta strand plain) and unit 3 (the marine shale) (Ricketts and McIntyre, *pers. comm.*). Going down section at approximately 35 Ma regional uplift and erosion terminated the infilling of the Sverdrup Basin at Strand Fiord. Figure 7 outlines the tectonic history used to calculate geothermal gradients (using Lopatin's (1971) method) of the Eureka Sound Formation at Strand Fiord. Figure 8 outlines the tectonic history using the corrected depth of burial.

Predicted curves (geothermal gradients) generated from Lopatin's model based on the above mentioned depositional and tectonic history of the Eureka Sound Formation at Strand Fiord are shown in figures 9 (non—corrected) and 10 (corrected). The calculated geothermal gradient from the study area is also plotted in Figures 9 and 10. A numerical value for the calculated geothermal gradient (18.3°C/km) was determined by performing a least squares regression analysis of the geothermal gradient (GTG) versus corresponding log coalification gradients (logCG). The relationship between GTG and logCG at Strand Fiord is as follows:

$$GTG = 160.40*(logCG) - 2.0411, \quad r^2 = 0.98$$

Using the previously calculated geothermal gradient, the maximum attained paleo—temperature was 75°C at the point where the shift occurs in the coalification gradient (i.e., 1400 m from the base of the section) and 45°C at the top. The

Tectonic History

Ma BP
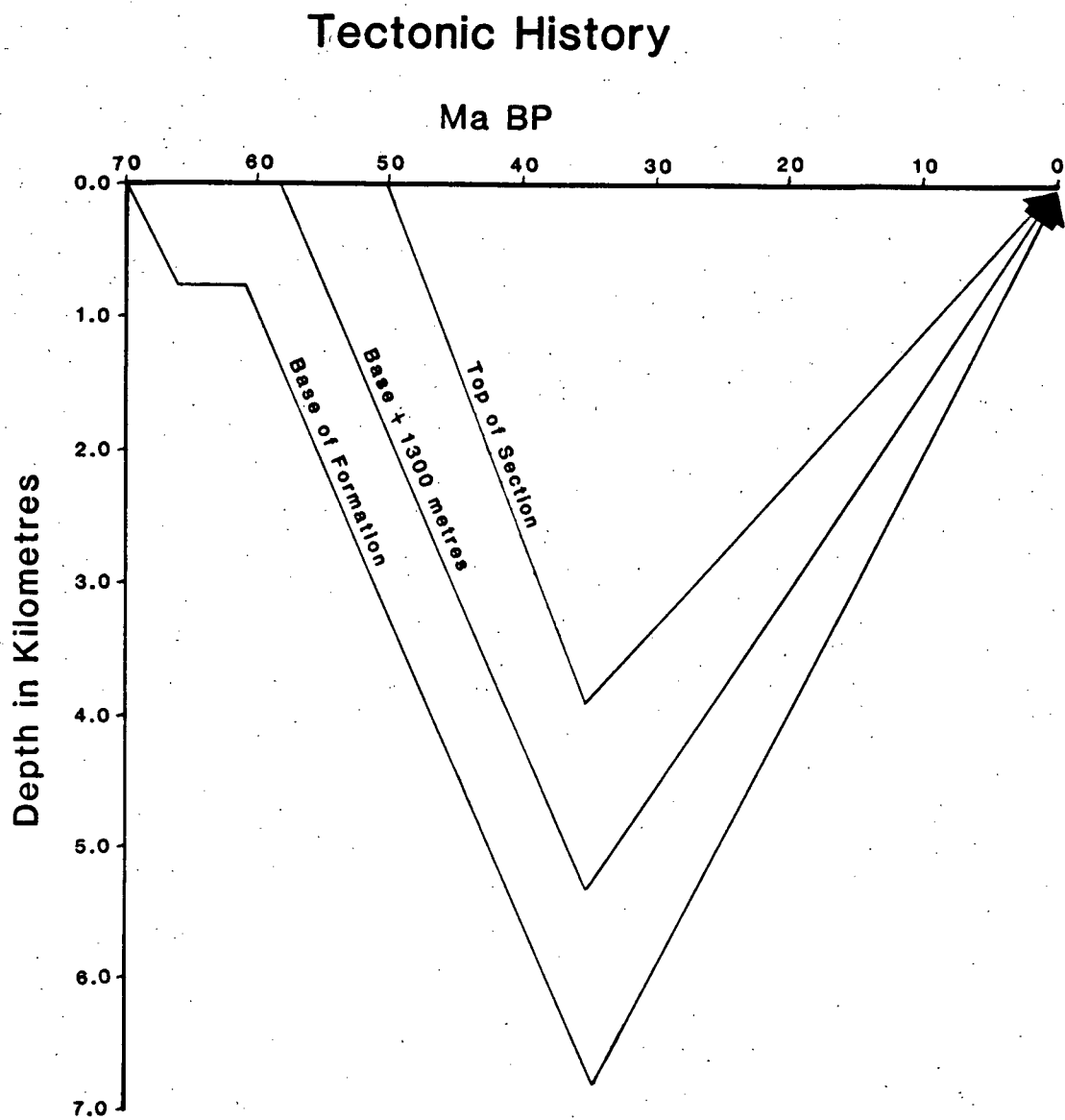
Figure 7. Representation of the tectonic evolution of Eureka Sound strata at Strand Fiord assuming a maximum depth of burial of 6800 metres.

Corrected Tectonic History
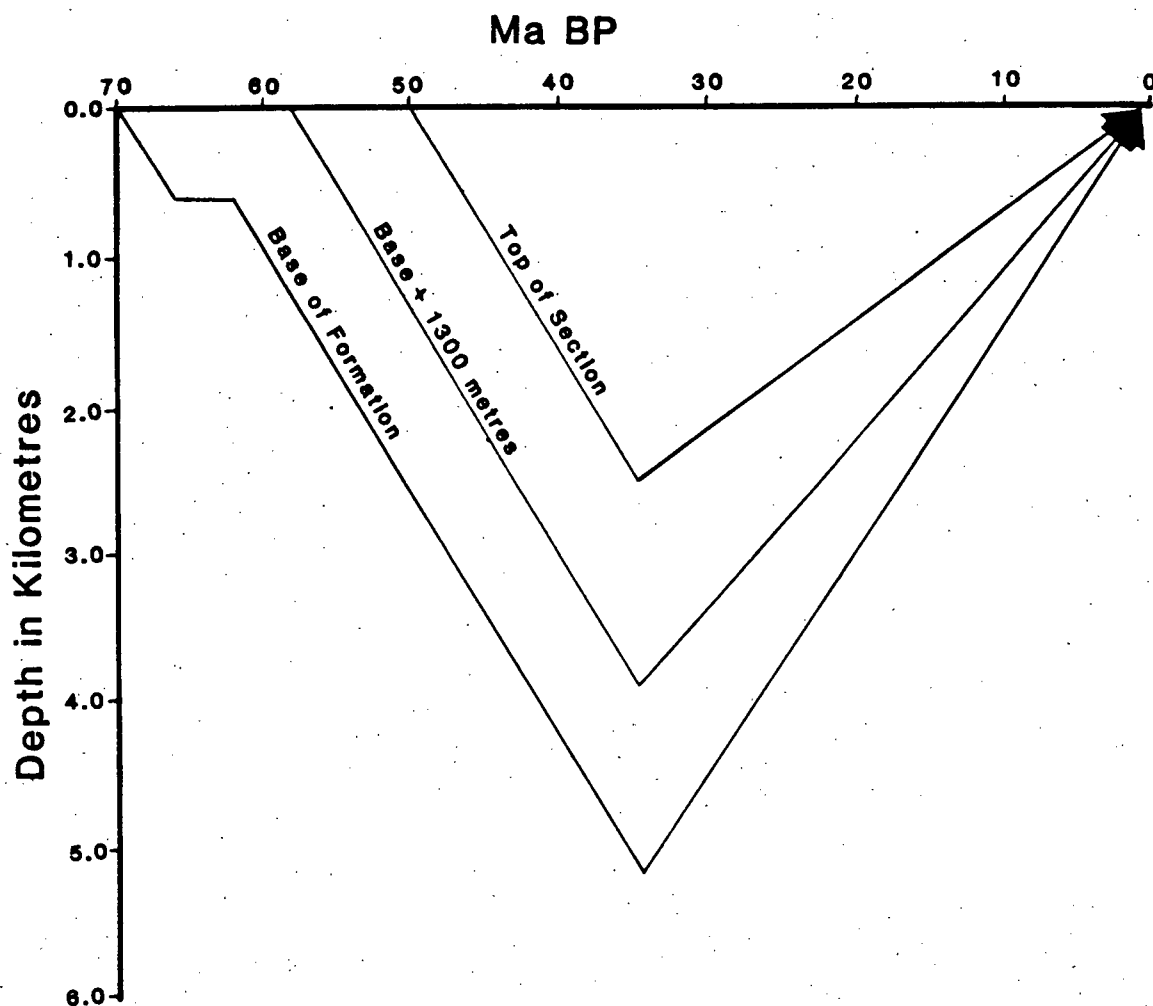
Figure 8- Representation of the tectonic evolution of Eureka Sound strata at Strand Fiord assuming a maximum depth of burial of 5500 metres.

Non-corrected Geothermal Gradients
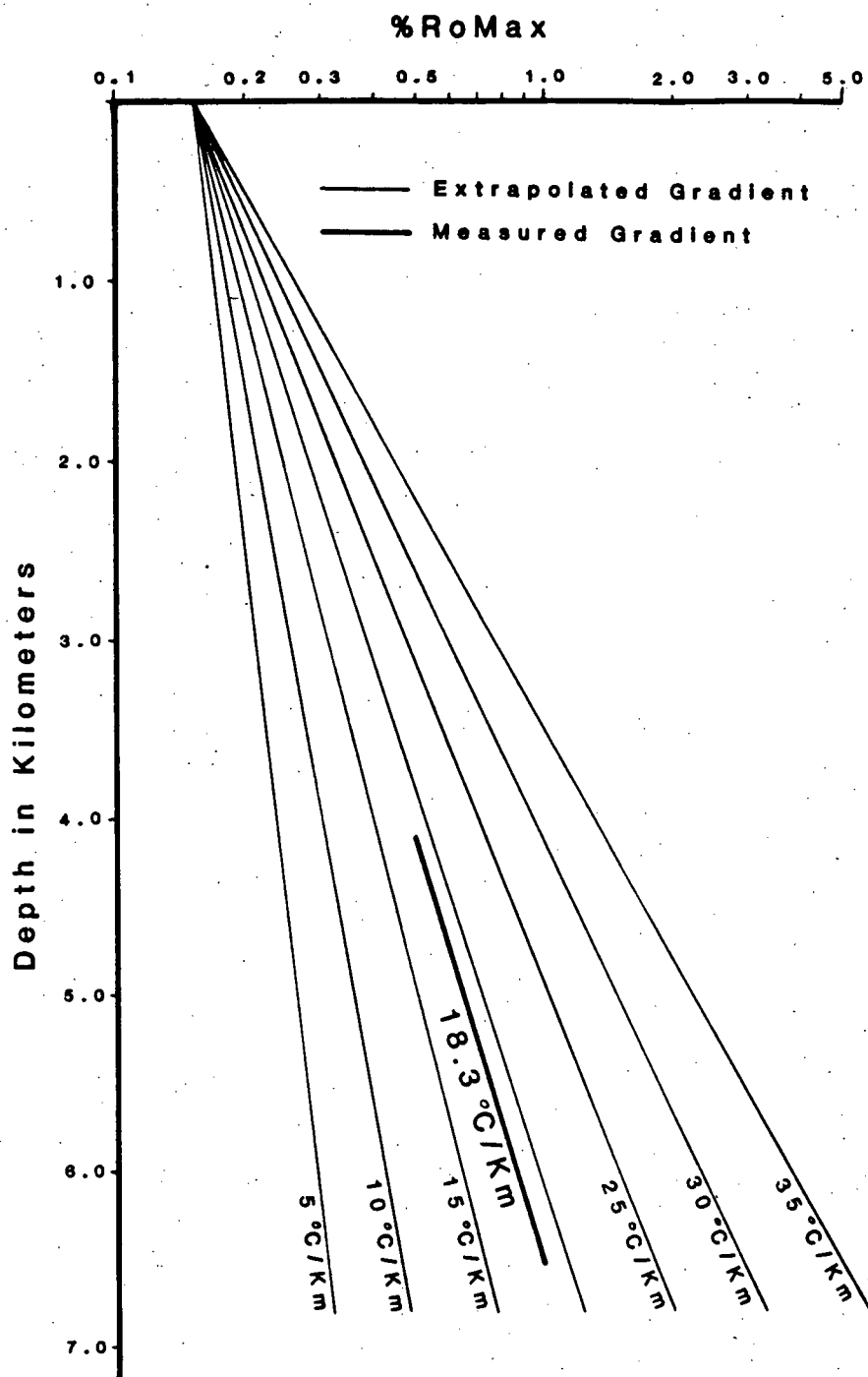
Figure 9-   Geothermal gradient determination using Lopatin's (1971) method and assuming a maximum depth of burial of 6800 metres.

Corrected Geothermal Gradients
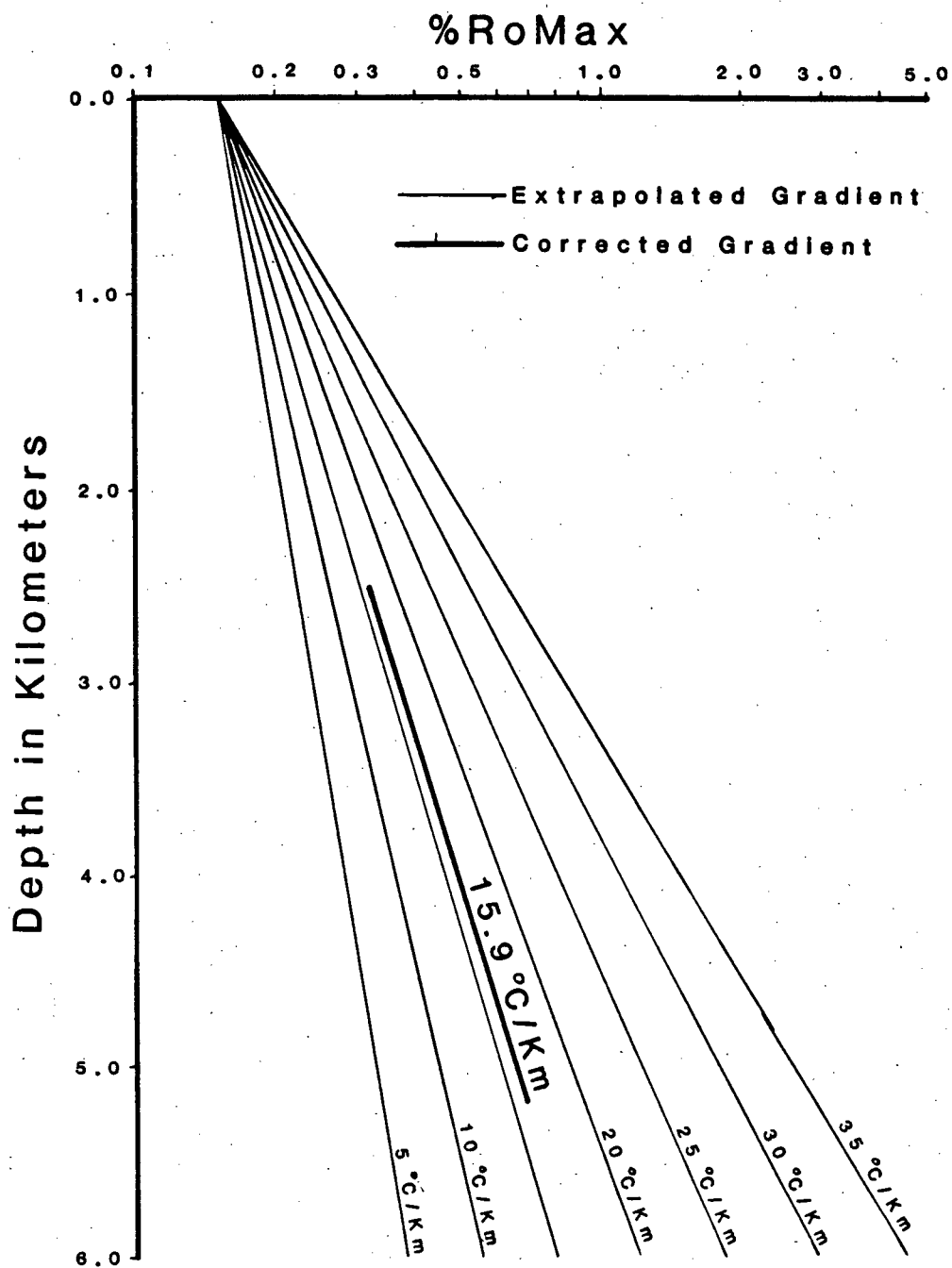
Figure 10- Geothermal gradient determination using Lopatin's (1971) method and assuming a maximum depth of burial of 5500 metres.

maximum temperature at the base of the section was 95°C using Lopatin's (1971) TTI model. Corresponding maximum temperatures using Barker's (1983) method are 14°C (0.50% R_0max) at the top of the section and 83°C (0.80% R_0max) at the 1400 m mark. Discrepancies in the temperature values determined from the two models can be attributed to a number of factors. First, considering the poor fits from the coalification gradients (i.e., $r^2 = 0.48$) the depth of burial value is accurate at best to within ±1 km. As a result, the temperature value obtained from Lopatin's geothermal gradient will also be subjected to additional error. Second, the basic differences in the assumptions of Barker's (1983) and Lopatin's (1971) models will produce obvious discrepancies in the reported temperatures.

SANDSTONE PETROLOGY AND DIAGENESIS

An examination of textural relationships between authigenic phases has been used to determine the paragenetic sequence of cements and estimate the fluid chemistry in the sandstones of the Eureka Sound Formation from Strand Fiord. Textural information was obtained from both SEM—EDS of gold coated, fractured samples and the optical examination of thin sections. Mineral identification of the coarser phases was based on optical examination of thin sections, SEM—EDS (energy dispersive spectrometry) examination of carbon coated polished thin sections and XRD analyses of the <20 μm fraction of the sandstones.

RESULTS

Petrology

Petrology of the Eureka Sound Formation was determined from the analysis of 16 thin sections of highly consolidated, fine and medium grained sandstones. Sandstone samples from the lower 1000 m of section were collected from major sandstone horizons without observing any specific sample interval. This sampling procedure was done because of the relative scarcity of sandstones through the lower part of the section. Above 1000 m, samples were taken at approximately 80 m intervals or as exposure and degree of consolidation permitted. Detailed sampling of isolated horizons was not done as the samples used in this study were not collected specifically for this study. Modal analysis of framework grains was done by point counting a minimum of 400 grains per sample to ensure that a statistically significant grain population was obtained (Solomon, 1963). Cement and porosity were calculated by identifying 400 grid points per sample as either framework, pore, or

cement. Roundness and sphericity determinations were done by comparing the shapes of 25 grains per sample with the tables of Krumbein et al. (1963) and Rittenhouse (1943). Average grain sizes were determined by measuring the long axis of 25 grains per sample. Seven of the most texturally varied samples were chosen for SEM—EDS analysis while 6 of the more compositionally complex samples were chosen for XRD whole—rock analysis.

Thin section analysis of the 16 samples revealed that all of the studied rocks are compositionally very mature. Fifteen of the samples are quartz arenites, and only one is a quartz wacke with approximately 15% clay in its matrix. Table 2 outlines the framework composition of each sample along with the number of grains counted per sample. Figure 11 demonstrates the composition of the rock clan from the Strand Fiord section using Gilbert's (1954) classification scheme (Williams et al., 1982).

The majority of the quartz is monocrystalline (77% of framework on average) and polycrystalline (14% of framework on average) grains. Chert, also included with quartz, makes up on average 5% of the framework material. Chert grains commonly appear altered in thin section. Quartz—quartz grain contacts range from floating grains (RAK—40) to sutured contacts (occurring primarily through the lower 1800 m of the section). The bulk of the samples, however, display primarily concavo—convex and long contacts indicating moderate amounts of pressure solution between both quartz overgrowths and detrital quartz grains (Adams, 1964). Texturally, samples are mature to submature as is reflected by grain roundnesses and sphericities which range from 0.3—0.6 (mode=0.5) (Krumbein et al., 1963) and 0.53—0.91 (mode=0.75) (Rittenhouse, 1943), respectively. Grain sorting is primarily moderate. In general, grain sphericity and roundness appears to improve as the sorting increases.
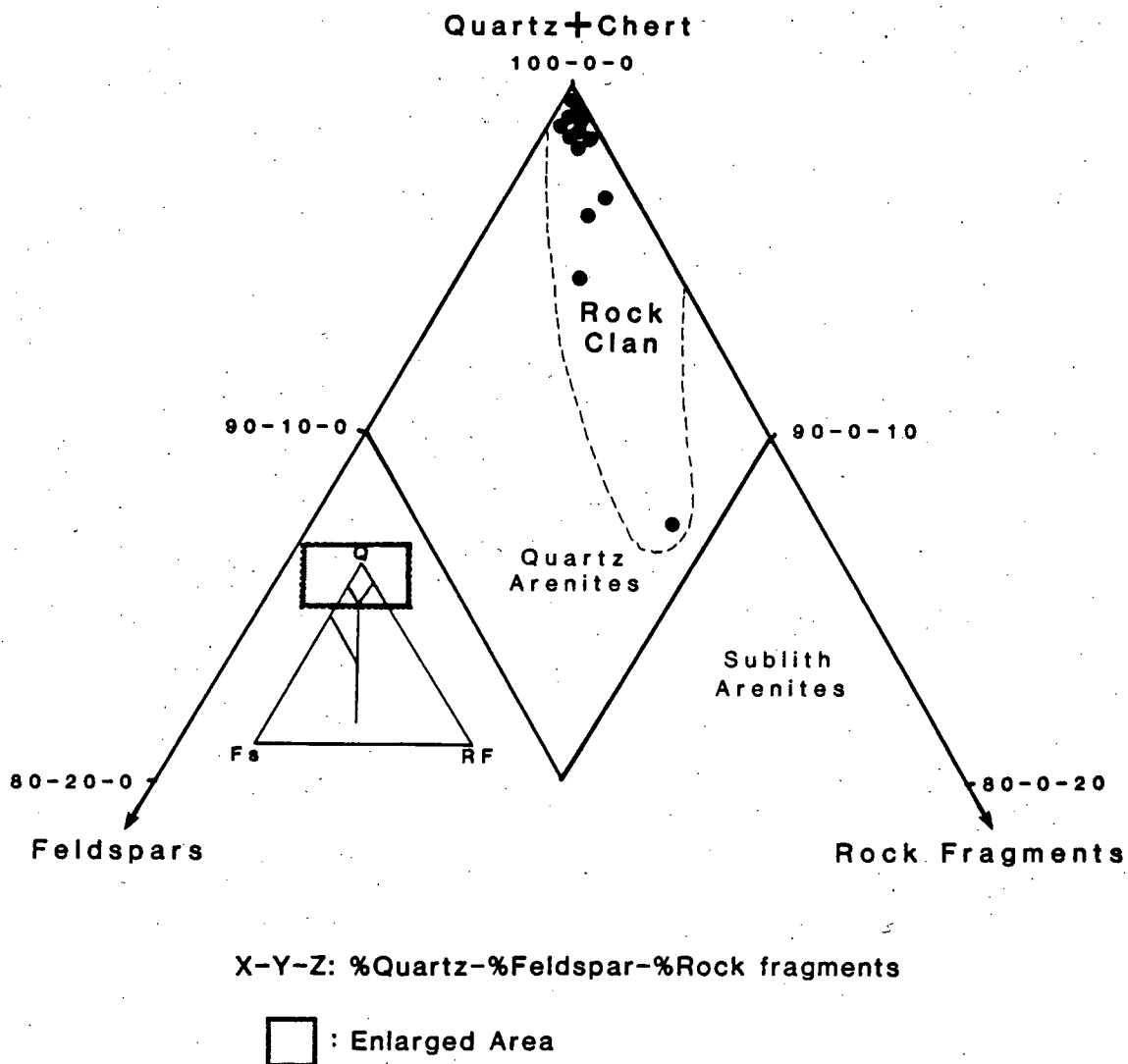
Figure 11- RAK-25 rock clan plotted on a modified Gilbert's (1954) composition triangle.

TABLE 2

Framework Petrology of Sandstones

Sample	MxtlQ	PxtlQ	Plag	Kspar	SRF	Orgs	Chert	Counts
RAK—7	66	19	Tr	1	9	Tr	4	414
RAK—10	64	32	Tr	1	2	Tr	Tr	407
RAK—13	74	12	2	Tr	2	3	6	436
RAK—18	82	16	Tr	0	0	Tr	1	525
RAK—26	90	8	Tr	0	0	1	0	410
RAK—34A	75	7	1	0	1	9	7	532
RAK—40	90	4	Tr	0	0	3	2	411
RAK—49	88	9	Tr	Tr	1	Tr	2	453
RAK—63	88	7	Tr	Tr	Tr	Tr	3	404
RAK—66	72	18	Tr	Tr	Tr	0	9	413
RAK—90	71	16	Tr	Tr	Tr	3	10	452
RAK—96	72	14	1	Tr	0	3	10	412
RAK—97	72	14	1	Tr	0	1	3	402
RAK—118	88	14	1	Tr	0	Tr	1	422
RAK—127	77	20	0	0	Tr	2	Tr	410

MxtlQ (monocrystalline quartz), PxtlQ (polycrystalline. quartz), Plag (albite), Kspar (potassium feldspar), SRF (sedimentary rock fragments), Orgs (organics/phytoclasts)

Detrital feldspars constitute no more than 3% of the total framework in any of the samples. Plagioclase is 3 to 4 times as abundant as potassium feldspar. All plagioclase grains display characteristic albite twinning. Plagioclase compositions were calculated using the Michel—Levy method (Kerr, 1977). Averaged extinction angle pairs range in value from 12.5° to 18° indicating plagioclase compositions between An_2 and An_{10}. Degraded microcline is the dominant potassium feldspar, but never occurs in amounts exceeding 1% of the total detrital fraction. All feldspars appear to be highly diagenetically altered showing evidence of kaolinitization, minor sericitization and extensive dissolution.

Phytoclasts occur as disseminated, opaque fragments in most of the 16 samples. Percentages range from trace amounts in a few samples to as much as 8% in other samples (i.e., RAK—34A).

Primary porosity is absent from sandstones examined in this study. Oversized, irregular secondary pores (Shanmugan, 1985) commonly associated with chert and highly altered feldspars are pervasive through out the section. These oversized pores are believed to form by the dissolution of aluminosilicates and possibly micro—porous chert as is discussed in a later section. Many of these oversized pores have been reduced in size by the subsequent growth of quartz overgrowths, kaolinite and dawsonite crystal aggregates into the pore spaces. Additional secondary porosity is present in those sandstones that contain abundant carbonate cement. In these calcareous sandstones, the secondary porosity appears in the form of partially dissolved carbonates (especially calcite and ankerite). Total porosity values range from virtually 0% in the finer grained, and more poorly sorted sandstones (e.g. RAK—7) to as high as 25% in the cleaner and better sorted sandstones (e.g. RAK—118).

Cements and matrix generally constitute between 1% and 20% of the total rock volume. Usually no more than one—sixth of this 20% is matrix material such as detrital clays. Table 3 outlines the distribution of the observed cements through the section. The following section examines the occurrences and morphology of the cements and authigenic minerals in more detail.

TABLE 3

Distribution of Sandstone Cements Through Section

Sample	QOG	Carbonate	Pyrite	Clay	Other
RAK 7	X_1	—	X	X_1	FeO_1
RAK 10	X_1	—	—	X_1	FeO_1
RAK 13	$X(Tr)_1$	$Ankerite_1$ $Calcite_1$	—	$Kaolinite_1$	FeO_1
RAK 18	X_1	—	—	—	—
RAK 26	X_1	—	—	$X(Tr)_1$	FeO_1
RAK 34A	—	$Ankerite_{1\,2\,3}$ $Calcite_{1\,2\,3}$	X	$X(Tr)_1$	FeO_1
RAK 40	—	$Calcite_{1\,2\,3}$ $Ankerite_{1\,2\,3}$	X	$X(Tr)_1$	— FeO_1 $Rutile_1$
RAK 49	X_1	$Calcite_{1\,2\,3}$ $Ankerite_{1\,2\,3}$	—	$X(Tr)_1$	—
RAK 63	X_1	—	—	—	—
RAK 66	X_1	—	—	—	—
RAK 90	—	$Calcite_{1\,2\,3}$ $Dawsonite_{1\,3}$ $Siderite(Tr)_{1\,2\,3}$ $Ankerite(Tr)_{1\,2\,3}$	—	$Kaolinite_{2\,3}$	FeO_1
RAK 96	$X(Tr)_1$	$Calcite_{1\,2\,3}$ $Ankerite_{1\,2\,3}$ $Dawsonite_{1\,2\,3}$ $Siderite_2$	X	$Kaolinite_{2\,3}$ $Illite_3$	—
RAK 97	X_1	$Calcite_2$ $Dawsonite_{1\,3}$ $Siderite_{1\,2}$	—	$Kaolinite_{2\,3}$ $Illite_3$	$Analcime(Tr)_3$ $Rutile_3$
RAK 118	$X(Tr)_1$	$Calcite_{1\,2\,3}$ $Dawsonite_{1\,2\,3}$ $Ankerite_{1\,2\,3}$	X	—	—
RAK 127	X_1	$Dawsonite_1$	—	—	—
RAK 129	X_1	$Fe—Calcite_{1\,2}$ $Siderite_2$	—	—	—

1=Determined Optically; 2=Determined using XRD; 3=Determined using SEM—EDS; Tr=Trace; X=present; —=absent

Discription of Authigenic Minerals

A total of 13 authigenic phases were observed in the Eureka Sound sandstones. Of the 13, only 6 were present in proportions great enough to classify them as principal authigenic minerals. The remaining 7 authigenic minerals are classified, for the purposes of this paper, as accessory—authigenic minerals. Four of the 6 principal authigenic minerals are carbonates; calcite, ankerite, siderite, and dawsonite. The remaining 2 principal authigenic phases consist of kaolinite, and quartz overgrowths. The accessory—authigenic minerals occurring through the section are illite, pyrite, iron oxide, rutile, sphene, analcime(?) and chabazite(?). In general, accessory—authigenic minerals make up a less than 1% of the total amount of cement.

Principal Authigenic Minerals

Calcite $CaCO_3$— Calcite occurs primarily as a void and fracture filling cement through most of the section. It was identified optically by its extremely high birefringence (0.172) and characteristic {0112} twinning. SEM—EDS analyses revealed that minor amounts of Fe are substituted for Ca. Well developed subhedral crystals of calcite were also visible in the pores of a number of samples. Calcite cement never exceeds 10% of the total cement.

Ankerite $Ca(Mg,Fe)(CO_3)_2$— Ankerite is the dominant cement in a number of samples. For example, in RAK—13 ankerite comprises up to 90% of the total cement. Like calcite, ankerite occurs as fracture and void infillings. Ankerite is distinguished from calcite by having generally higher birefringence and brownish stains around its cyrstal boundaries and within the crystals as seen under plane

polarized light. Furthermore, when viewed in thin section ankerite crystals are generally more corroded and anhedral than associated calcite crystals. SEM—EDS analyses show ankerite to be Mg free or poor and thus extremely Fe rich (Figure 12). Ankerite's composition generally plots near the Ca—Fe mid point on the Ca—Fe—Mg carbonate ternary diagram (Figure 13).

Siderite $FeCO_3$— Discrete siderite was not recognized optically in thin sections. Siderite identification was based on SEM—EDS analyses of polished thin sections and XRD analyses. Siderite displays characteristic diffraction peaks at 0.279 and 0.173 *nm* and produces an EDS pattern as seen in figure (14a). Like ankerite, siderite appears to be more anhedral than associated calcite and occurs in proportions less than 8% of the total cement. Siderite occurs as a primary pore filling cement (Plate 1a).

Dawsonite $NaAlCO_3(OH)_2$— Dawsonite was initially difficult to positively identify in part due to the relative lack of reported occurrences in other study areas. The best known and most studied occurrence of dawsonite is from the Green River Formation oil shales of Colorado where it occurs with other lacustrine saline carbonates such as nahcolite (Meddaugh and Salotti, 1983; Smith and Young, 1975). Other occurrences of dawsonite appear in weathered syenite tuffs in Olduvai Gorge, Tanganyika (Hay, 1963) and in rhyolitic ignimbrites near Terlano, Italy (Corazza *et al.*, 1977).

Through the upper third of the section dawsonite is the most abundant sandstone cement; it comprises approximately 100% of the cement in sample RAK—127. Dawsonite was only observed in the zone 5 and overlying sandstones. The vertical distribution of dawsonite and ankerite appears to be inversely related. In
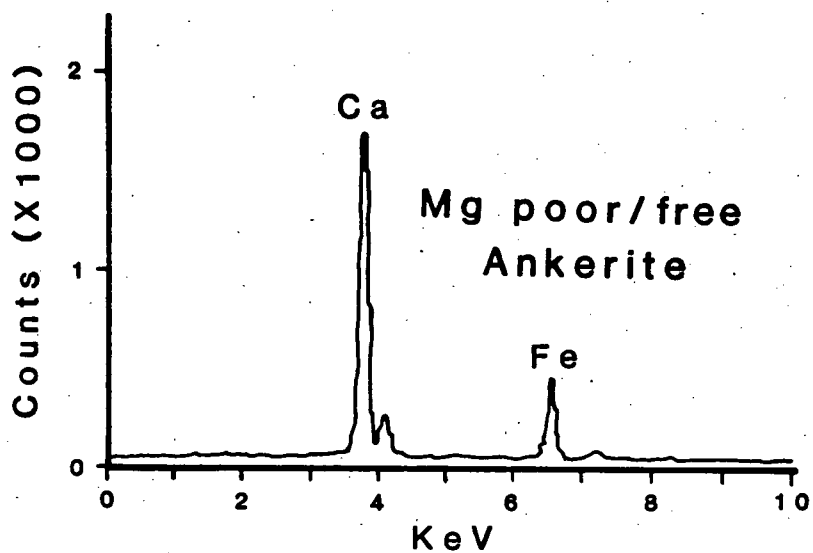
Figure 12a- Energy dispersive spectrograph of Mg poor/void ankerite.
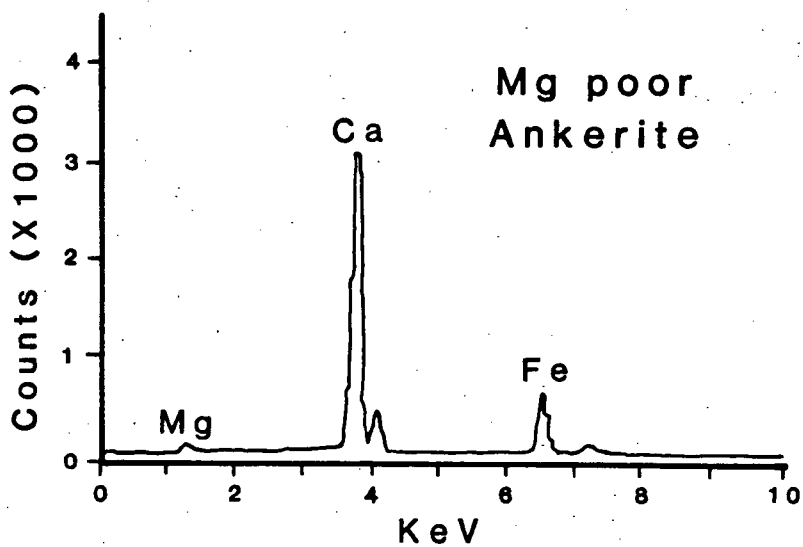
Figure 12b- Energy dispersive spectrograph of Mg poor ankerite.

CaO–MgO–FeO–CO$_2$
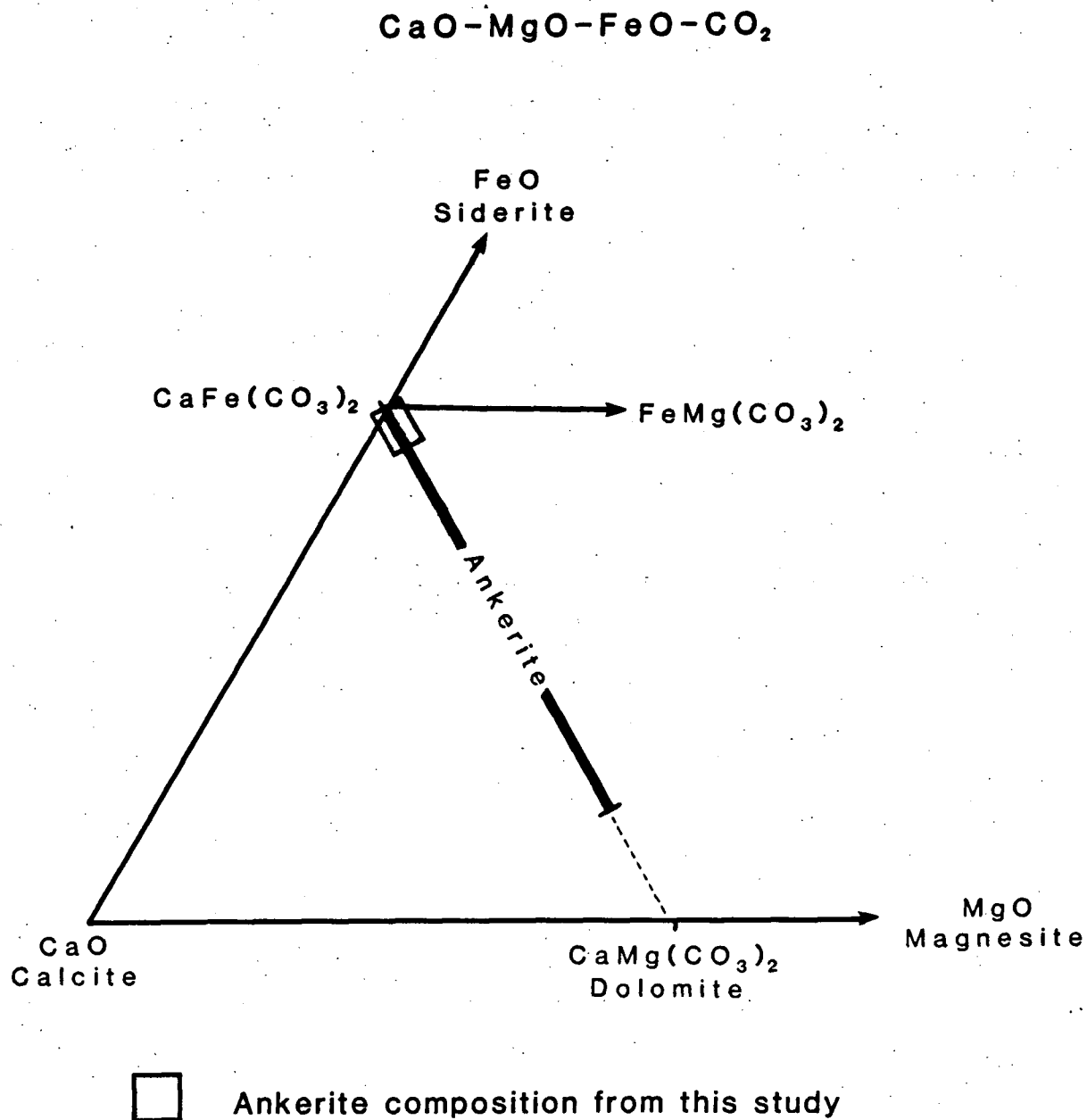
Figure 13- Approximate ankerite composition range plotted on a CaO-FeO-MgO-CO2 ternary diagram. Compositions are only approximations as determined by EDS analyses.

general, the dawsonite content per sample increases from the base of zone 5 toward the top of the section while the ankerite content correspondingly decreases over the same range (Figure 15). The significance of this trend is believed to be related to the proximity of the diapirs as is discussed in a later section.

Under the optical microscope dawsonite is recognized in plane polarized light (ppl) as clear, colorless aggregates of radiating, acicular crystals. Its birefringence is lower than that of calcite's (0.172) but considerably higher than that of kaolinites. SEM–EDS analyses are by far the most useful technique for identifying dawsonite. Figure (14b) shows a typical EDS pattern for dawsonite, showing roughly equal proportions of Na and Al. Plate 1b is a typical back scattered image of dawsonite and quartz revealing the difference in average atomic number of the two minerals. Dawsonite's crystal and aggregate morphology is shown in Plate 2c, where it is seen occupying a pore throat. Confirmation of dawsonite was made using the XRD where characteristic diffraction peaks occur at 0.570 and 0.3385 nm. Dawsonite is occasionally observed with an 'illitic' intergrowth (plate 2d) whose chemical significance is not wholly understood at this time.

Quartz SiO_2— Syntaxial quartz overgrowths are most common in the medium grained samples which had either relatively high primary porosity or oversized secondary porosity. Samples with greater amounts of clay in the matrix generally had fewer and smaller overgrowths than the cleaner arenites. The average thickness of the quartz overgrowths is approximately 3–5 μm and the overgrowths can be found on approximately 35% of all detrital quartz grains. Overgrowths comprise up to 100% of the total cement in samples RAK–18 and 26. Evidence for additional quartz cement is manifested as either or both concavo–convex and sutured grain contacts in most samples.
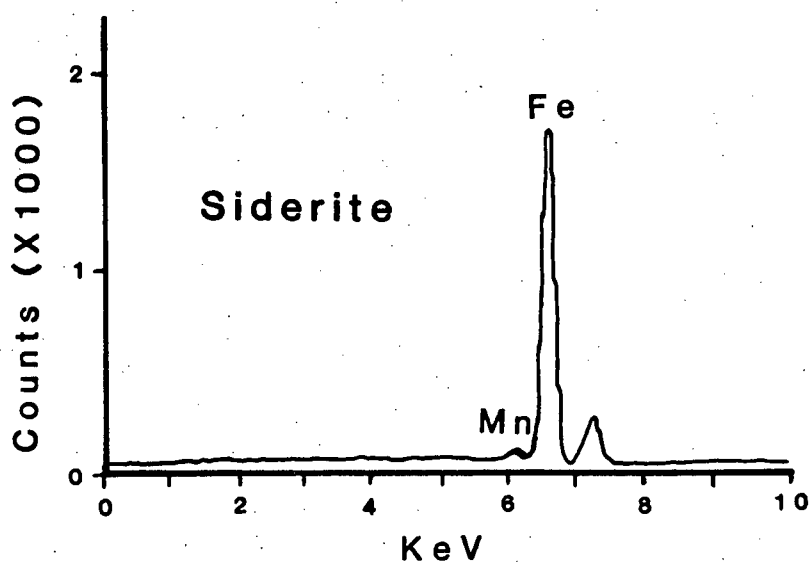
Figure 14b- Energy dispersive spectrograph of siderite.
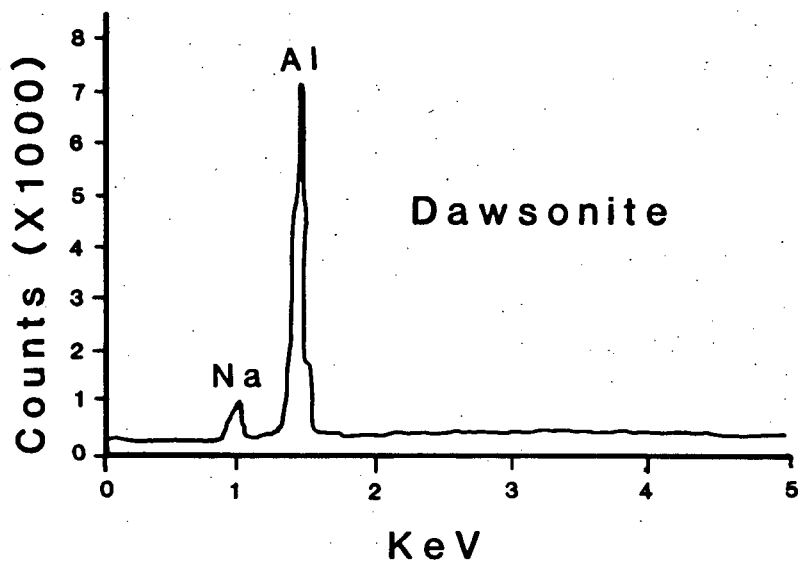
Figure 14a- Energy dispersive spectrograph of dawsonite showing equal proportions of Na and Al.
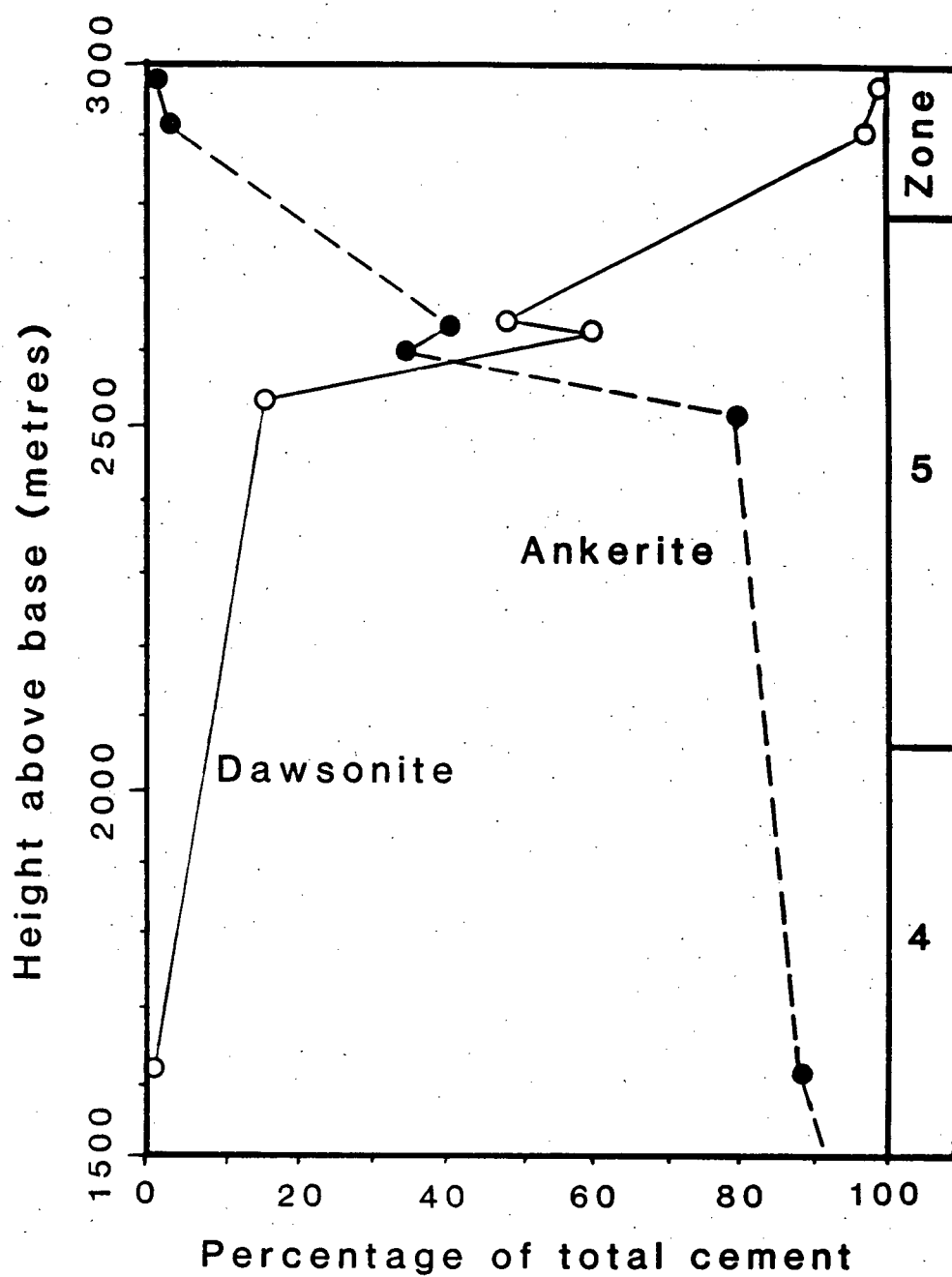
Figure 15- Variations in ankerite and dawsonite proportions with depth.

PLATE 1

Morphology, Textural Relationships, and Back Scattered Ellectron Image Appearence of Dawsonite and Associated Minerals

A.   Scanning electron micrograph of siderite (Sd) and quartz (Qu). Siderite occurs as a primary pore filling cement; polished thin section; back scattered electron image; RAK—97—25.

B.   Scanning electron micrograph of dawsonite (Dw), quartz (Qu), calcite (Cc) and plagioclase (Pg). Grey shade difference reflects the difference in average atomic number between these minerals; polished thin section; back scattered electron image; RAK—96—25.

C.   Scanning electron micrograph of acicular dawsonite (Dw) occupying a pore; calcite (Cc) occurs adjacent to an oversized pore; Dawsonite is associated with quartz (Qu) and potassium feldspar (Ks); secondary electron image; polished thin section; RAK—118—25.

D.   Scanning electron micrograph of dawsonite (Dw) intergrown with illite. Dawsonite (Dw) can also be seen replacing calcite (Cc) (see arrow); back scattered electron image; polished thin section; RAK—96—25.
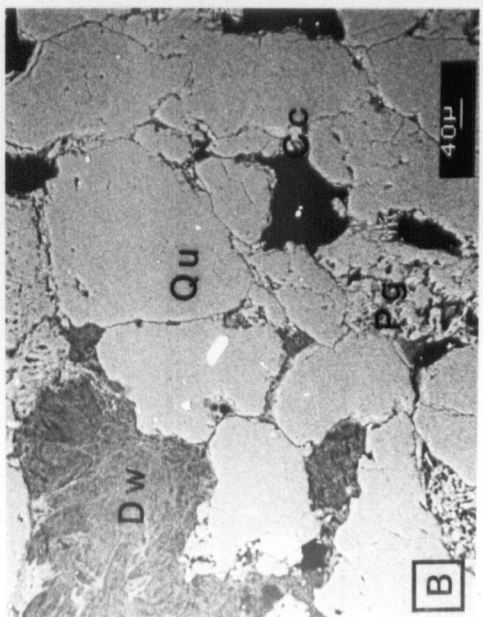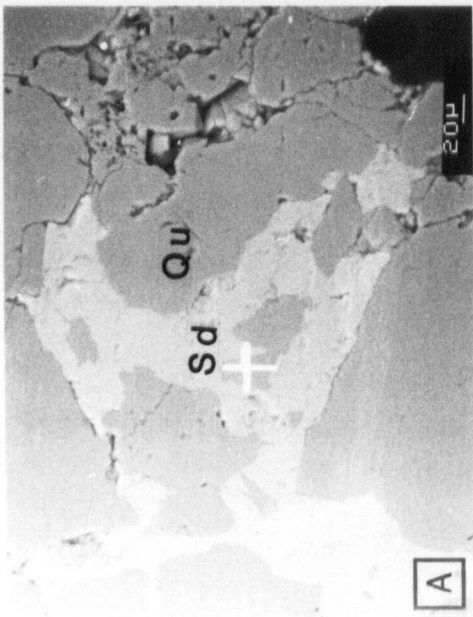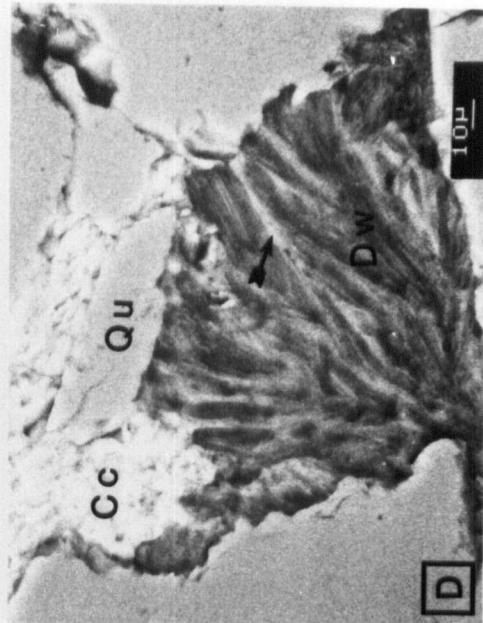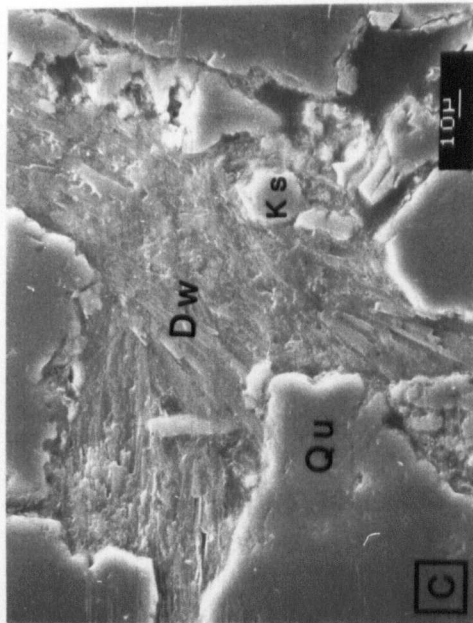
Kaolinite $Al_2Si_2O_5(OH)_4$— Kaolinite booklets are visible in many of the samples as revealed by SEM analysis. The booklets commonly occur as pore fillings (Plate 2a) and, in a number of instances, are closely associated with resorbed K—spar and Na—plagioclase. Optical identification of kaolinite was based on its vermiform habit and very low birefringence (Plate 2b). Individual kaolinite crystals range in size from 3 to 4 μm.

Accessory—authigenic Minerals

Illite— Like kaolinite, illite is a late stage diagenetic mineral as revealed by its occurrence in pores and as sporadic grain coatings. Individual illite crystals occasionally occur as grain dustings. As was mentioned previously, illite(?) also occasionally occurs as an inter growth with dawsonite.

Pyrite FeS_2— Pyrite occurs in only a few samples through the section. Euhedral pyrite crystals were observed both with the binocular microscope and in thin section. The crystals are generally very small, ranging in size from 3 to 11 μm. In plane polarized light the pyrite crystals appear slightly translucent (Plate 3a).

Iron Oxides/hydroxides FeO_x— Reddish brown iron oxides/hydroxides are recognized in a number of thin sections under plane polarized light. In most cases it is closely associated with ankerite.

Rutile/Anatase(?)/Brookite(?) TiO_2— Rutile occurs as small euhedral crystals in association with calcite and less commonly with ankerite. Identification of rutile was based solely on SEM—EDS analysis of polished thin sections (Plate 3b).

PLATE 2

Morphology and Appearence of Kaolinite

A. Scanning electron micrograph of kaolinite (Ka) lining pores; secondary electron image; fractured sample; gold coated image; RAK—96—25.

B. Micrograph of authigenic vermicular kaolinite (Ka) occluding a pore space; associated with quartz (Qu); plane polarized light; RAK—96—25.
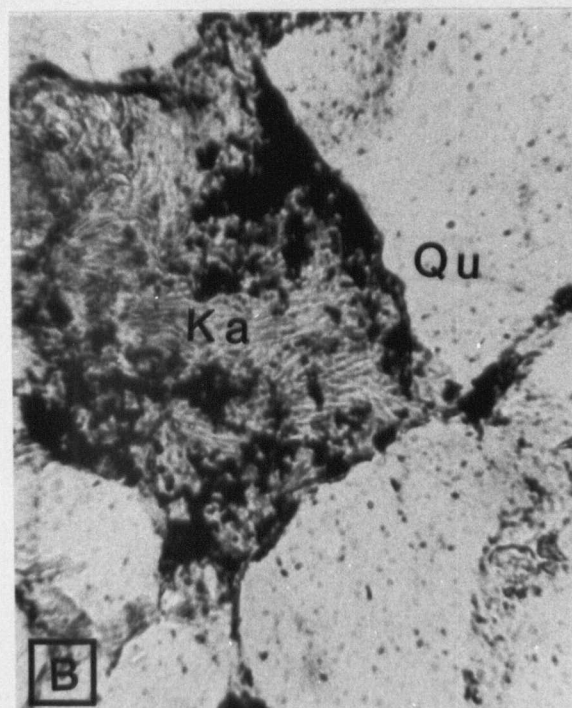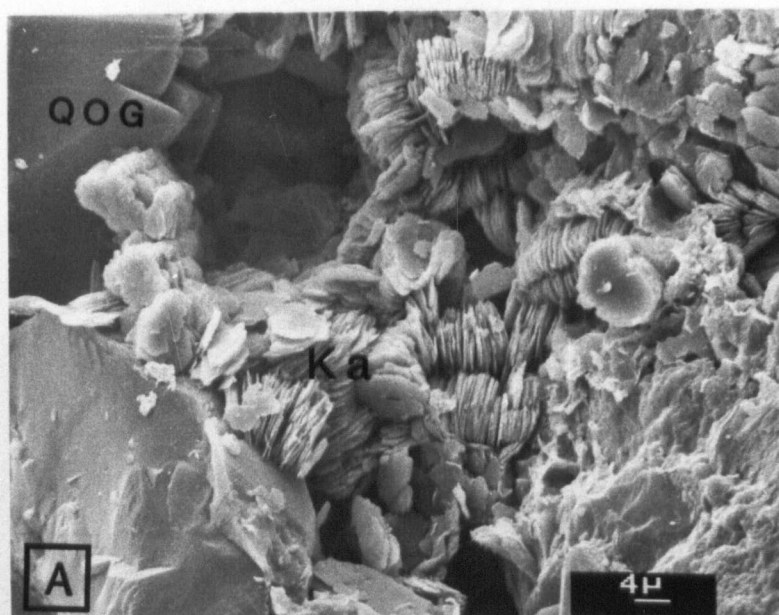
PLATE 3

Morphology and Occurence of Pyrite and Rutile

A.   Cubic pyrite associated with dawsonite (Dw) and quartz (Qu) as seen in plane polarized light; horizontal field = 0.19 mm; RAK—118—25.

B.   Scanning electron micrograph of rutile (Ru) associated with ankerite (Ak); polished thin section; back scattered electron image; RAK—96—25.
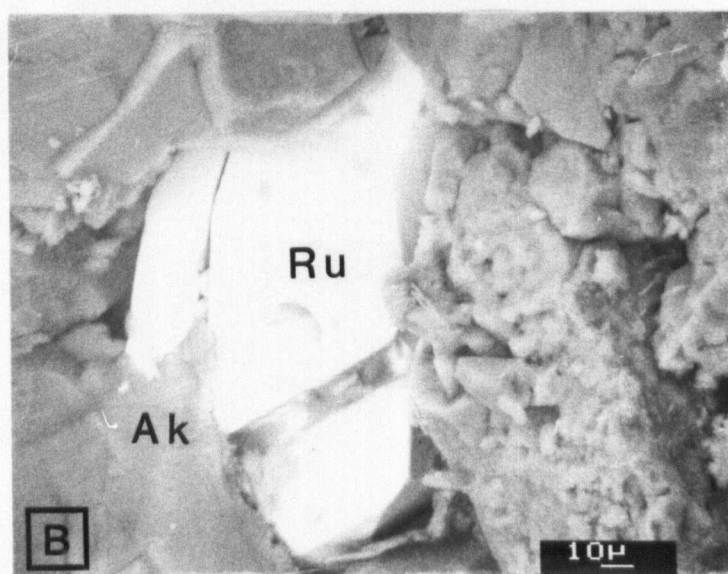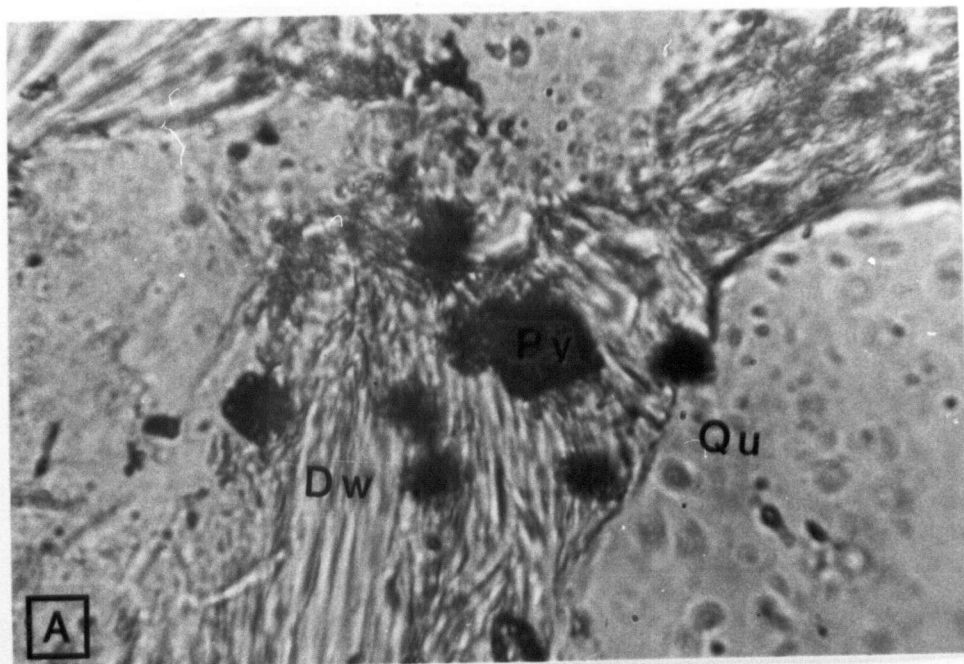
Analcime $NaAlSi_2O_6 \cdot 2H_2O$— Analcime has previously been reported in the study area by Bustin (1977). In the present study, however, the occurrence of analcime is uncertain as it was identified in only one sample based on an EDS pattern analysis from a single grain. Never was analcime observed in thin section or in SEM fracture samples. XRD analysis also failed to indicate the presence of analcime in any of the samples. Certainly, if analcime is present it only exists in extreme trace amounts.

DISCUSSION

Textural Relationships

Textural relationships between authigenic minerals, where present, are outlined below. Unfortunately, not all authigenic minerals display textural associations with all other authigenic phases and, therefore, some ambiguities exist in the paragenetic sequence. A number of relationships are, however, revealed by cement associations with quartz overgrowths.

Syntaxial quartz overgrowths coated with kaolinite booklets or dawsonite crystals commonly project into pore spaces (Plate 4a, b) suggesting that quartz overgrowth formation pre—dated both kaolinite and dawsonite genesis. Quartz overgrowths are also seen projecting into the oversized pores created by the dissolution of feldspars and chert grains. Veneers of illite occur as coverings on quartz overgrowths. Strong evidence for calcite cementation post—dating quartz overgrowth formation can be seen in plate 5a,b, which shows calcite cement replacing a quartz overgrowth and its nucleus. Note that the clay dust rim between the overgrowth and the nucleus has not been replaced by the calcite. Both embayed contacts and quartz 'islets' within calcite and ankerite are extremely

PLATE 4

Morphology and Textural Relationships Between Dawsonite and Quartz Overgrowths

A. Scanning electron micrograph of dawsonite (Dw) post—dating quartz overgrowth formation. Note acicular and radiating habit of dawsonite; fractured sample; gold coated; secondary electron image;RAK—96—25.

B. Thin section micrograph under crossed nicols showing same relationship as in plate 6a; dawsonite (Dw), quartz overgrowth; crossed nicols; horizontal field=0.77 mm; RAK—90—25.
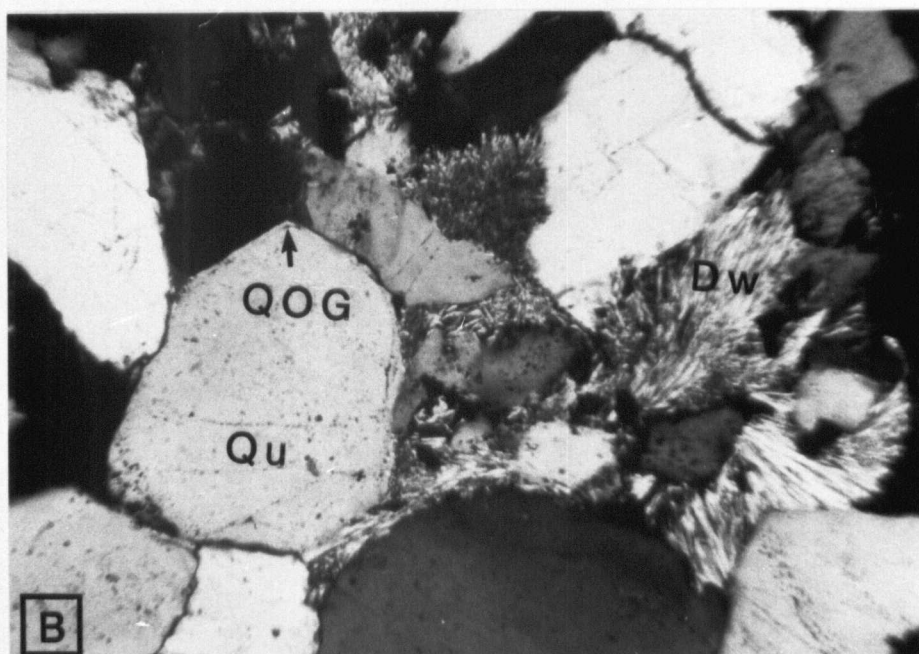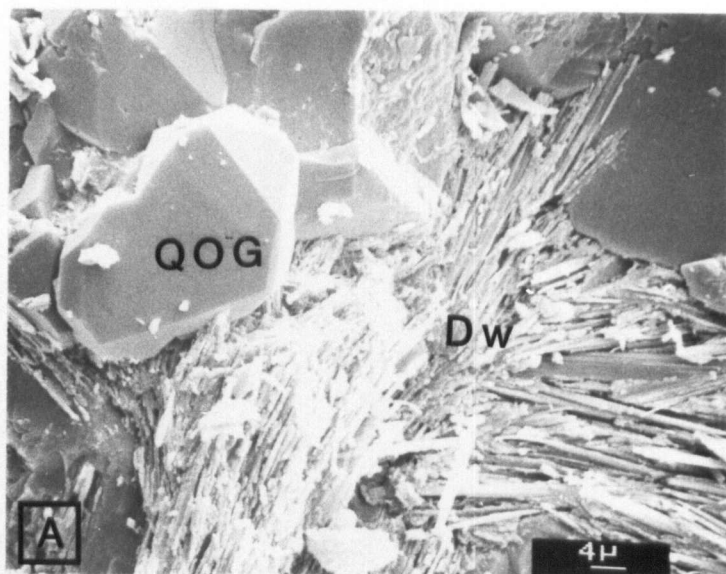
common. The relative timing of formation of siderite and ankerite is uncertain due to inconclusive textural relationships. Ankerite, however, most likely formed after the formation of quartz overgrowths as it replaces calcite crystals within overgrowths (Plate 6a, b). It is therefore concluded that at least two stages of quartz overgrowth formation existed during the evolution of the studied strata, early in the paragenetic sequence prior to the precipitation of calcite and after the dissolution of the framework aluminosilicates but prior to the precipitation of kaolinite and dawsonite.

Additional textural information is drawn from examining the relationships between the carbonates and the other diagenetic phases. Euhedral calcite and FeO_x were commonly observed in association with anhedral ankerite. Although not conclusive, this relationship suggests that a later stage calcite and FeO_x are products in an ankerite dissolution reaction. Plates 7a & b shows resorbed calcite encased in dawsonite crystals suggesting that the two are either contemporaneous or, more probably, that the calcite pre—dates the dawsonite. Kaolinite booklets were also occasionally observed on euhedral calcite crystals within pore spaces. This evidence supports the theory that calcite predates the kaolinite. Ankerite precipitation/formation occurred before the dissolution of the framework aluminosilicates as ankerite cement boundaries are coincident with "ghost" aluminosilicate grain and oversized pore boundaries.

Plate 8a demonstrates the relationship between illite and dawsonite. Dawsonite can be seen both with an illitic covering and as an intergrowth with illite(?). Kaolinite booklets and dawsonite can be seen in Plate 8b. The observed relationship between kaolinite and dawsonite suggests that dawsonite and kaolinite are either syntaxial or the kaolinite pre—dates the dawsonite. Figure 16 outlines a paragentic

PLATE 5

Textural Relationships Between Ankerite and Quartz Overgrowths

A. Micrograph of ankerite (Ak) replacing quartz overgrowth and the quartz nucleus (Qu). Notice that the overgrowth 'dust rim' (see arrow) is preserved in the carbonate; crossed nicols; horizontal field = 0.77 mm; RAK—49—25.

B. Enlargement of plate 5a; horizontal field = 0.19 mm.
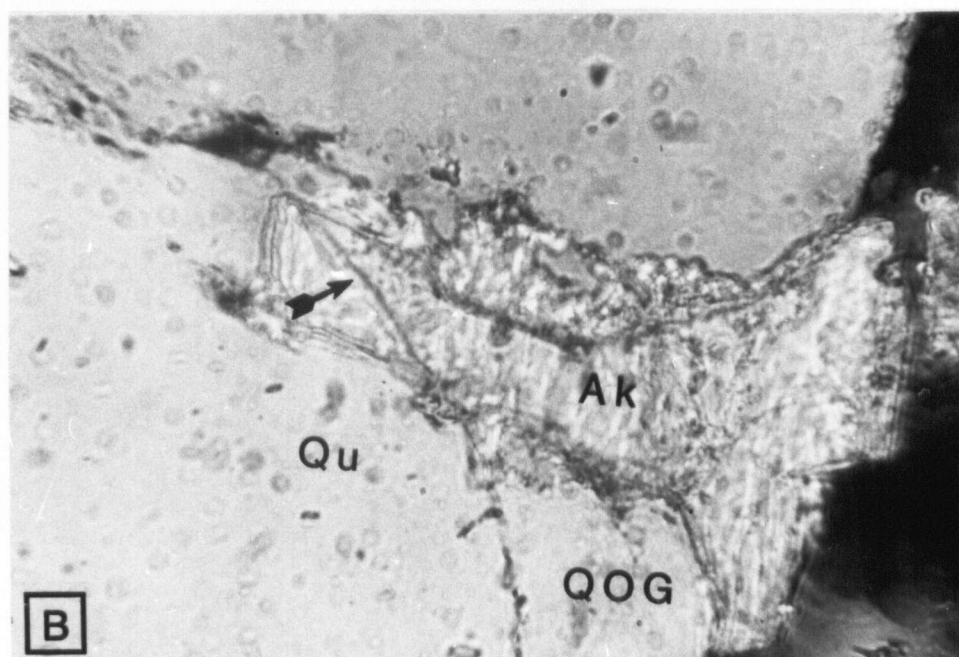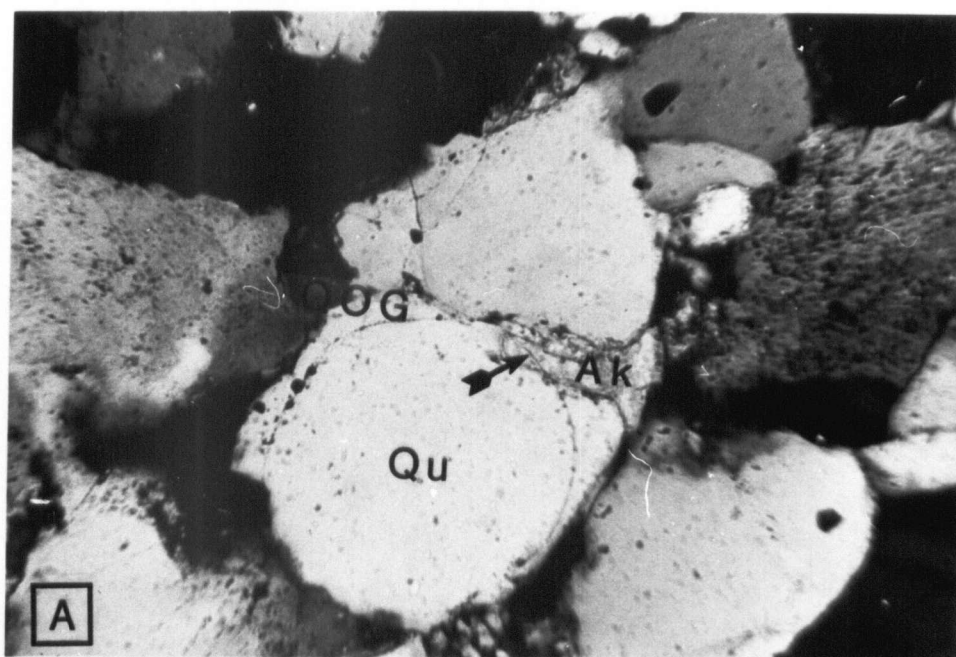
PLATE 6

Textural Relationships Between Calcite, Ankerite, and Quartz Overgrowths

A.   Ankerite (Ak) altering to Calcite (Cc) euhedra within a quartz overgrowth; crossed nicols; horizontal field = 0.58 mm; RAK—49—25.

B.   Enlargement of plate 13a; horizontal field = 0.19 mm.
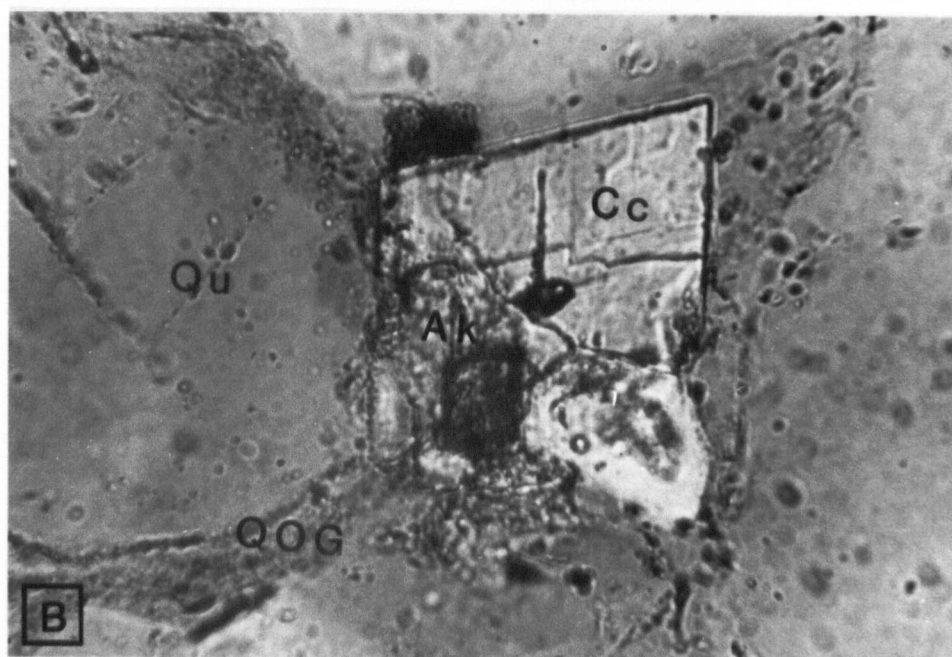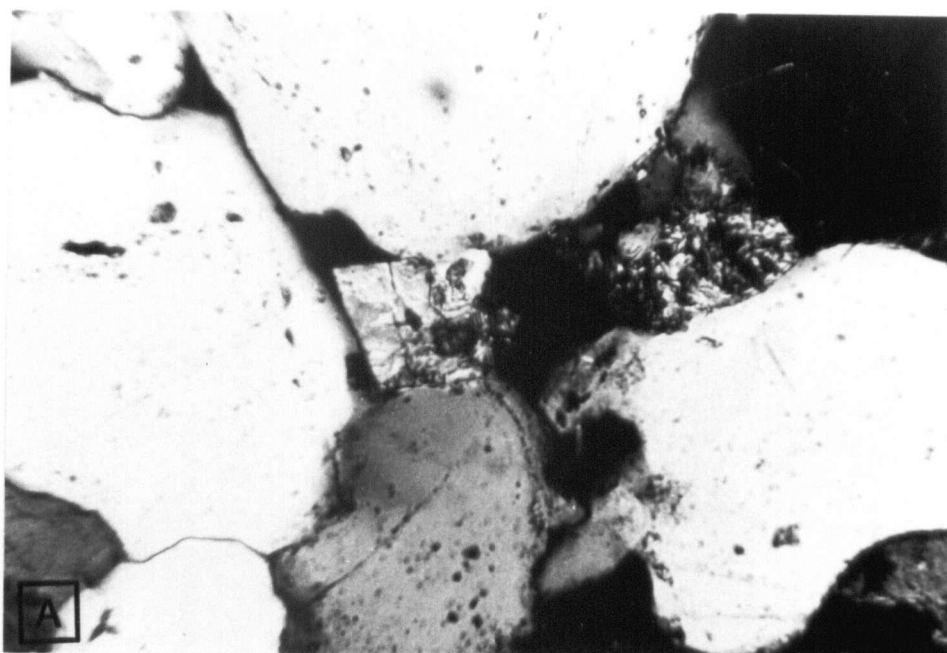
PLATE 7

Textural Relationship Between Dawsonite and Other Carbonates

A. Scanning electron micrograph of dawsonite (Dw) surrounding a corroded ankerite (Ak) crystal. Textural relationship suggests that the ankerite predates the dawsonite; gold coated fractured sample; secondary electron image; RAK—96—25.

B. Thin section micrograph similar to plate 14a showing dawsonite (Dw) replacing a calcite (Cc) crystal; crossed nicols; horizontal field = 0.85 mm; RAK—96—25.
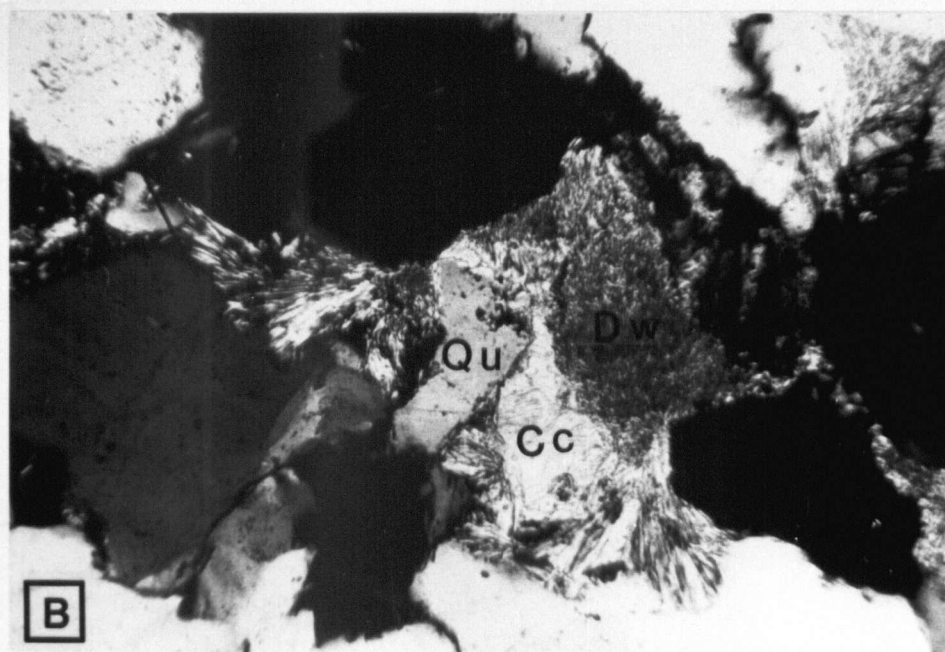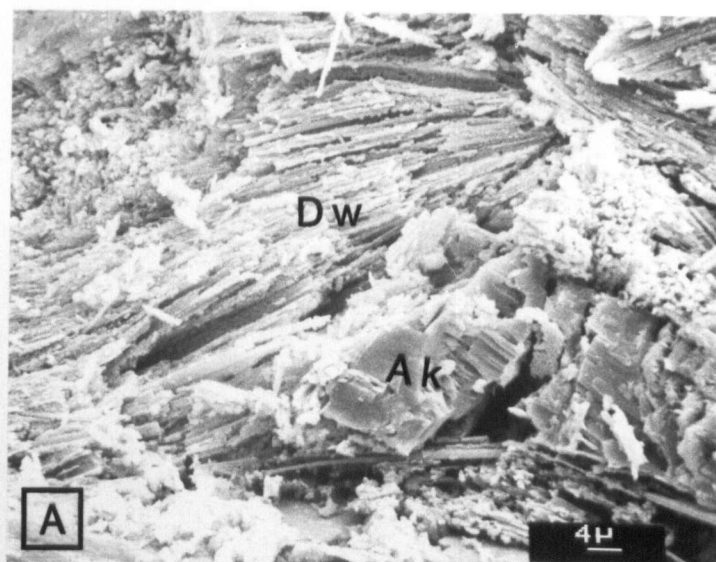
PLATE 8

Textural Relationships Between Dawsonite and Other Silicates

A.   Scanning electron micrograph displaying textural relationship between kaolinite (Ka) and dawsonite (Dw). Relationship suggests that kaolinite is either pre— or syn—genetic with dawsonite; gold coated fractured sample; secondary electron image; RAK—96—25.

B.   Scanning electron micrograph of dawsonite (Dw) replacing both calcite (Cc) and plagioclase (Pg) and occurring with illite(?) (arrow). polished thin section; back scattered electron image; RAK—96—25.
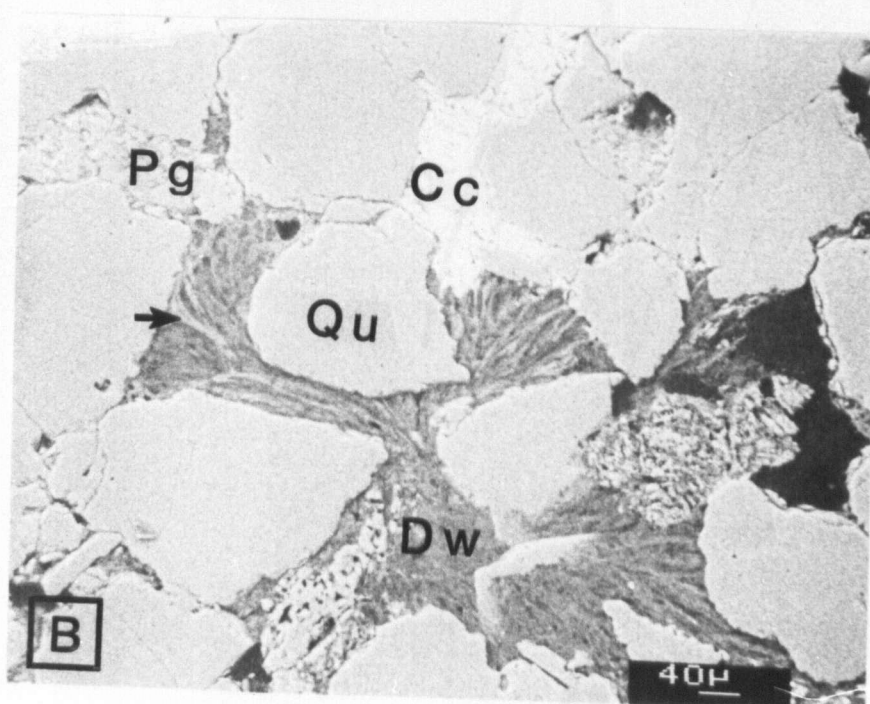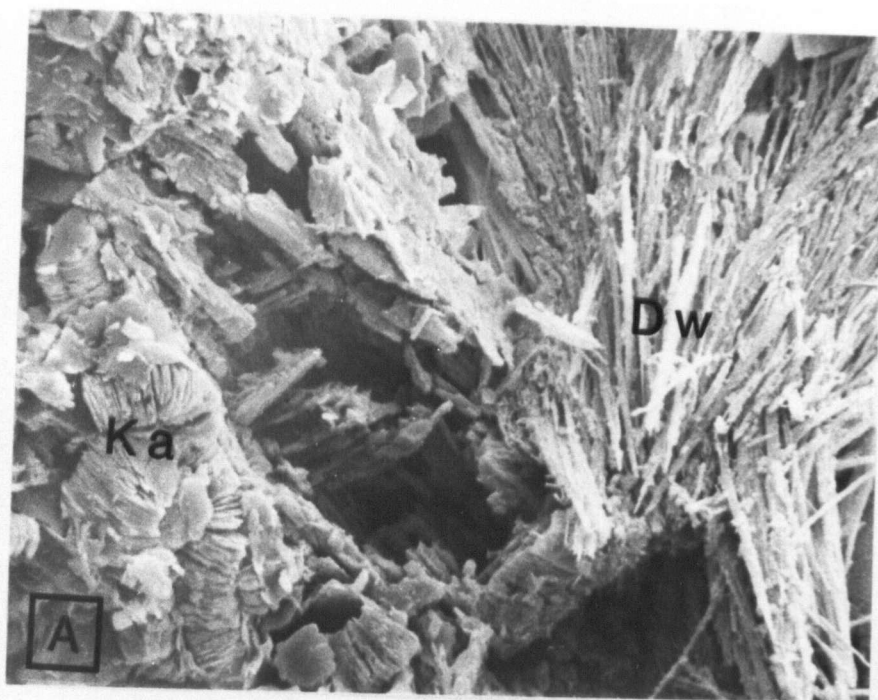
sequence based on information derived from total combined textural information.

Fluid Chemistry

Chemical considerations of the observed authigenic mineral assemblage suggest that numerous episodes of changing pore fluid chemistry have existed in the Eureka Sound strata since the time of their deposition. The presence of siderite and pyrite, for example, suggests a period when Eh was low (i.e., <0.35 v (Curtis and Spears, 1968)) and Fe^{2+} activity relatively high. In order to facilitate the formation of both pyrite and siderite, however, sulfide activity had to vary with time and/or depth. For example, pyrite is reported to form under conditions of non—restricted water circulation and elevated sulfur activity (Curtis and Spears, 1968) while siderite formation is favored by conditions of restricted water circulation, elevated $Fe^{2+}:Ca^{2+}$, and very low sulfide activity (Matsumoto et al., 1981). Pyrite is, therefore, suggested to be an earlier phase than siderite, although textural information in support of this is inconclusive. It is believed that the anaerobic reduction of sulfate, in the presence of excess Fe^{2+}, near the sediment/water interface created conditions favorable for pyrite formation. Pyrite formation is believed to give way to siderite formation with increasing depth as CO_2 activity increases and sulfide activity decreases. Changes in both the CO_2 and sulfide activities are believed to be mainly controlled by the biochemical degradation of organic matter during early diagenesis.

Initial quartz overgrowth precipitation is thought to have occurred at relatively shallow depths early in the paragenetic sequence when silica solubility is generally low. At the low temperatures of shallow burial the solubility of quartz is approximately 6 mg l^{-1}, significantly lower than the amount of silica present in

Paragenetic Sequence

Quartz Overgrowth
Calcite
Siderite
Ankerite
Pyrite
Feldspar Dissolution
Dawsonite
Kaolinite
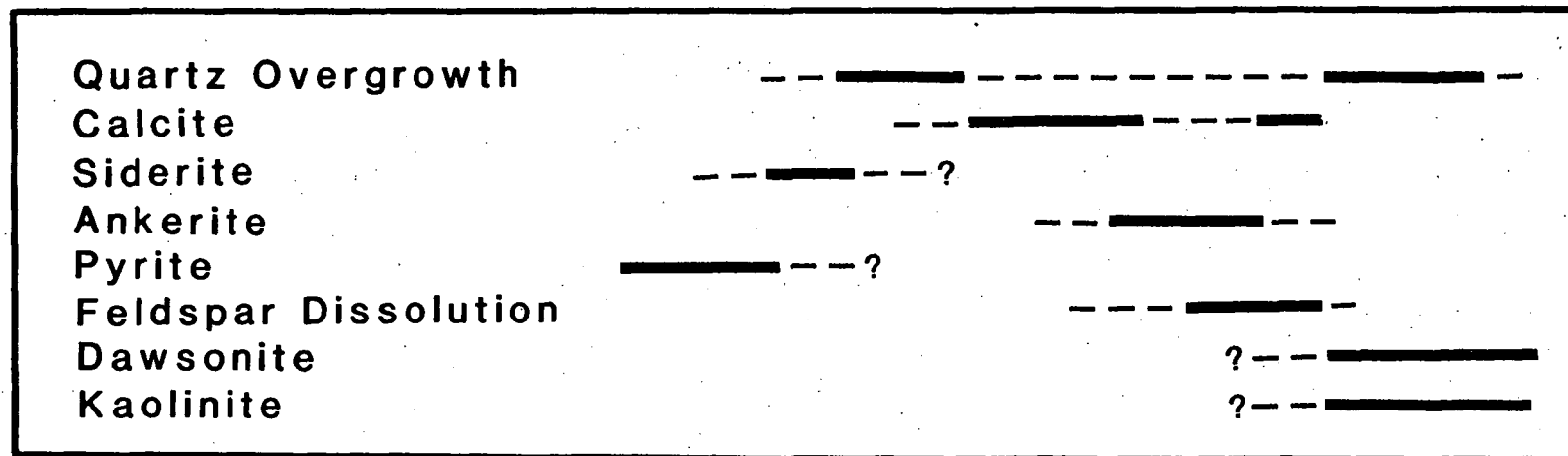
Figure 16- Diagram of paragenetic sequence

near surface and fluvial waters . Under these shallow burial conditions where silica solubility is low quartz will generally precipitate in quantities proportional to the volume of fluid moved through the rock. With increasing depth and temperature, however, more silica is required to be in solution to precipitate quartz as the solubility of quartz increases by an order of magnitude from 6 mg l^{-1} at 20°C to 63 mg l^{-1} at 100°C (Ehlers and Blatt, 1980 (original source not referenced)). The first episode of quartz overgrowth precipitation is, therefore, believed to have occurred during shallow burial when temperatures were <20°C and near surface water circulation relatively unrestricted.

Although the silica necessary to precipitate the early quartz overgrowths is believed to have been derived from external fluids, later stage overgrowths are thought to have precipitated from locally derived silica which may have been produced by a combination of sources including:

1) the dissolution of framework aluminosilicates and micro—porous chert;

2) silica released during compaction as a result of pressure solution;

3) silica released during the illitization of smectite in adjacent shales.

The dissolution of the framework aluminosilicates, precipitation of kaolinite and dawsonite and the presence of calcite may be explained by considering the effects of organic diagenesis on inorganic diagenesis. The thermal maturation of organic matter is now commonly accepted to result in the cleaving of functional groups from phenols, volatiles, carboxylic acids, and short chained aliphatics from the larger aromatic, aliphatic and alicyclic parent molecules. In rocks where there are large amounts of coal and disseminated organics, such as those with in the Eureka Sound Formation, carboxylic acid concentrations can be exceedingly high. For example, Carothers and Kharaka (1978) demonstrated that carboxylic acid

concentrations can exceed 5000 mg l^{-1} in some oil field formation waters. Carboxylic acids, when in the presence of Al^{3+}, are known to bond with the Al^{3+} to form water soluble complexes. The mobility of Al^{3+} in solution is enhanced by an order of magnitude when complexed with acetic acid and by 3 orders of magnitude when complexed with oxalic acid (Surdam et al., 1984). The net effect of increasing the mobility of Al^{3+} in solution is to enhance the removal of aqueous Al^{3+} from the system and, thereby, destabilize the aluminosilicates to a point where they begin to dissolve. As these Al^{3+}—complexed fluids migrate through the rock they eventually encounter zones where the Al^{3+} complex is believed to destabilize (possibly due to changes in solution pH (Surdam et al., 1984) and result in the precipitation of kaolinite and possibly dawsonite (see following section on Dawsonite: chemical constraints).

Surdam et al. (1984) have also demonstrated that the presence of organic acids in solution has a profound effect on the carbonate chemistry. While the presence of carboxylic acids tends to destabilize aluminosilicates the same acids can decrease the solubility of calcite with increasing P_{CO_2} by buffering the pH. In the absence of carboxylic acids the reverse is true: calcite solubility increases with increasing P_{CO_2} (Holland and Borcsik, 1976). The presence of dissolution features in the aluminosilicates and presence of pre—aluminosilicate—dissolution carbonates (ankerite and Fe—calcite) in the Eureka Sound sandstones suggests that the P_{CO_2} was relatively high (Surdam et al., 1984) and that carboxylic acids were buffering carbonate precipitation and destroying aluminosilicates. The iron necessary for the formation of ankerite may have a number of sources: Fe released during the transformation of smectite to illite, the dissolution of siderite, the reduction of. colloidal iron oxides, and the dissolution of biotite and amphibole. Following the

dissolution of the aluminosilicates it is believed that enough organically complexed Al^{3+} remained in the system to favor the precipitation of post—aluminosilicate—dissolution kaolinite and dawsonite.

Dawsonite: Chemical Constraints

The thermochemical data necessary to calculate the stability of dawsonite are drawn from a number of sources. First, the heat capacity (Cp) data used to derive coefficients for the Maier—Kelly heat capacity function:

$$Cp = a + bT + c/T^2$$

were taken from Ferrante et al. (1976). Figure 17 shows the heat capacity function fit to Ferrante et al's data. The molar volume of dawsonite was calculated using the crystallographic data of Corazza et al. (1977). The standard state (298.15°K, 0.1MPa) enthalpy of formation (H^o) and entropy (S^o) were taken from Robie et al. (1978). Free energies of formation (G^o) for the additional sodium carbonate phases considered in the partial pressure and activity—activity diagrams were collected from Garrels and Christ (1965). Thermochemical data for all remaining phases were drawn from Helgeson (1969; 1978). Before the H^o of dawsonite could be used with the Helgeson data set it had to be adjusted in order to provide consistency with the other phases in the data set. Helgeson adopted a value for the H^o of corumdum of -1661655.0 jnsupminus,sup1, in contrast to the calorimetrically derived value of -1675700.0 jn^{-1} (Robie et al., 1978). In order to provide for internal consistency, the dawsonite H^o was adjusted by this difference. Table 4 presents the thermochemical data for dawsonite used in the following distribution of species
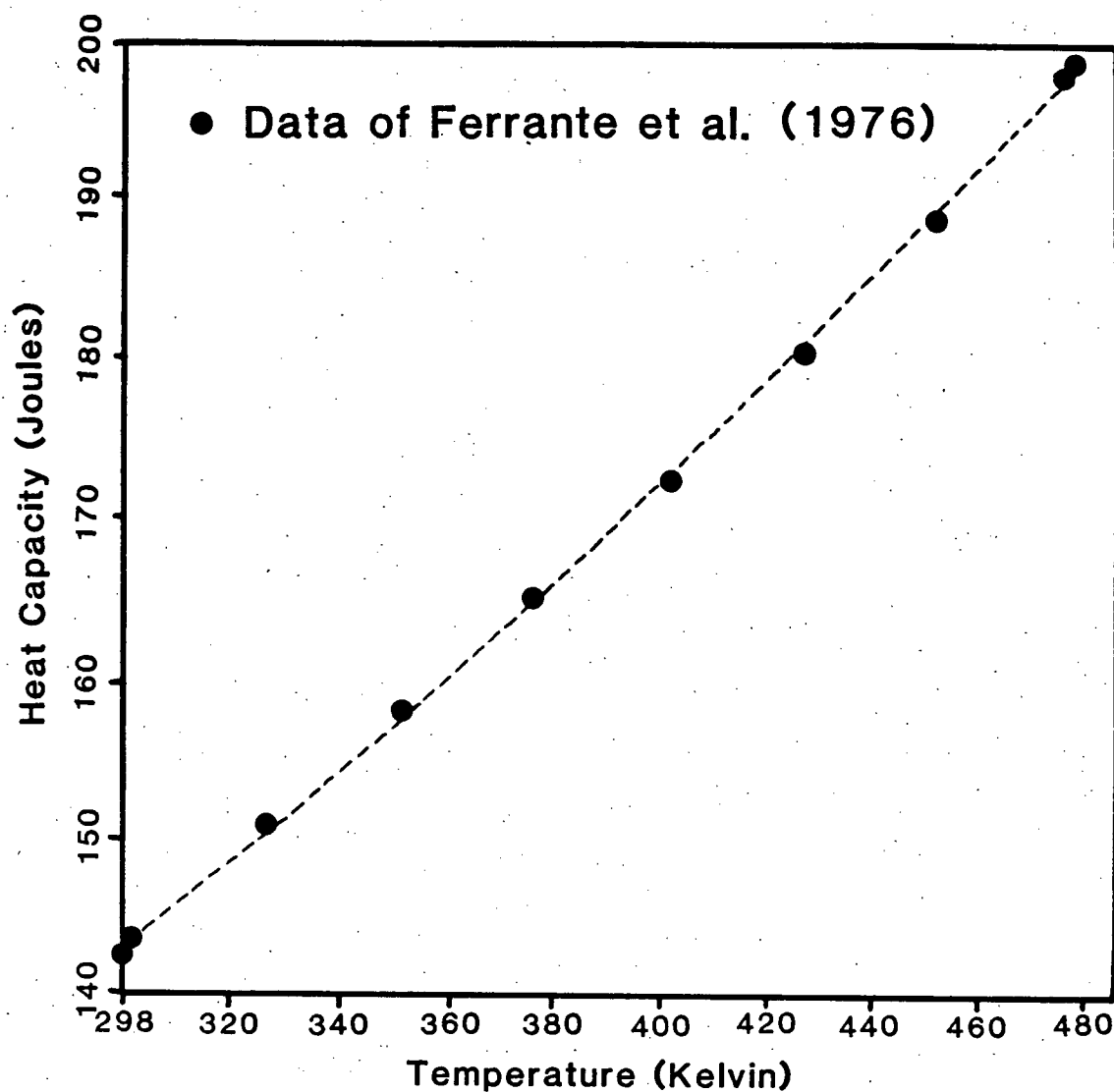
Figure 17· Dawsonite heat capacity function fit to the data of Ferrante *et al.* (1976).

calculations.

The stability of dawsonite relative to other sodium carbonates was examined in a series of activity–activity and partial pressure diagrams prior to performing the distribution of species calculations. Due to the absence of heat capacity coefficients for the sodium carbonates considered these stability analyses are limited to 298.15 °K and 0.1 MPa (Table 5). Balanced reactions, logK values and the free energies of the various reactions represented in Figures 18, 19 and 20 are listed in Tables 6 and 7. Figures 18 through 20 demonstrate the control that variations in Al^{3+}/H^+ ratios, P_{CO_2}, Na^+/H^+ ratios, and activity of water have on the topology of the dawsonite stability field. Figures 18 through 20 may, in fact, suggest that dawsonite is more common under low temperature geologic P_{CO_2}, a_{H_2O}, $a_{Al^{3+}}$, a_{Na^+} conditions than previously realized (see following section re: distribution of species). For example, a recent personal communication (B. Rottenfuser) has shown that previously undetected dawsonite has been identified in the samples of the Gething Formation of the Peace River Oil Sands. Other factors, however, such as the $a_{H_4SiO_4}$ undoubtedly have some controlling effect on the distribution of dawsonite, but this has not been pursued in this study. Stability conditions of dawsonite are, however, strongly influenced by pH and the activity of Al^{3+}. Figure 19 to 21 demonstrate that an increase in 1 $loga_{H^+}$ unit reults in a significant increase in the size of the dawsonite field with respect to P_{CO_2} and a_{H_2O}. The chemistry of sea water and the fluid chemistry of a number of formation waters are plotted on figures 18, 19 and 20 to illustrate the chemical domain of a few natural systems within $P_{CO_2}-a_{H_2O}-a_{Al^{3+}}-a_{Na^+}-H^+$ space.

The reason for performing a distribution of species on the authigenic assemblage was to approximate the activities of aqueous species and gases in
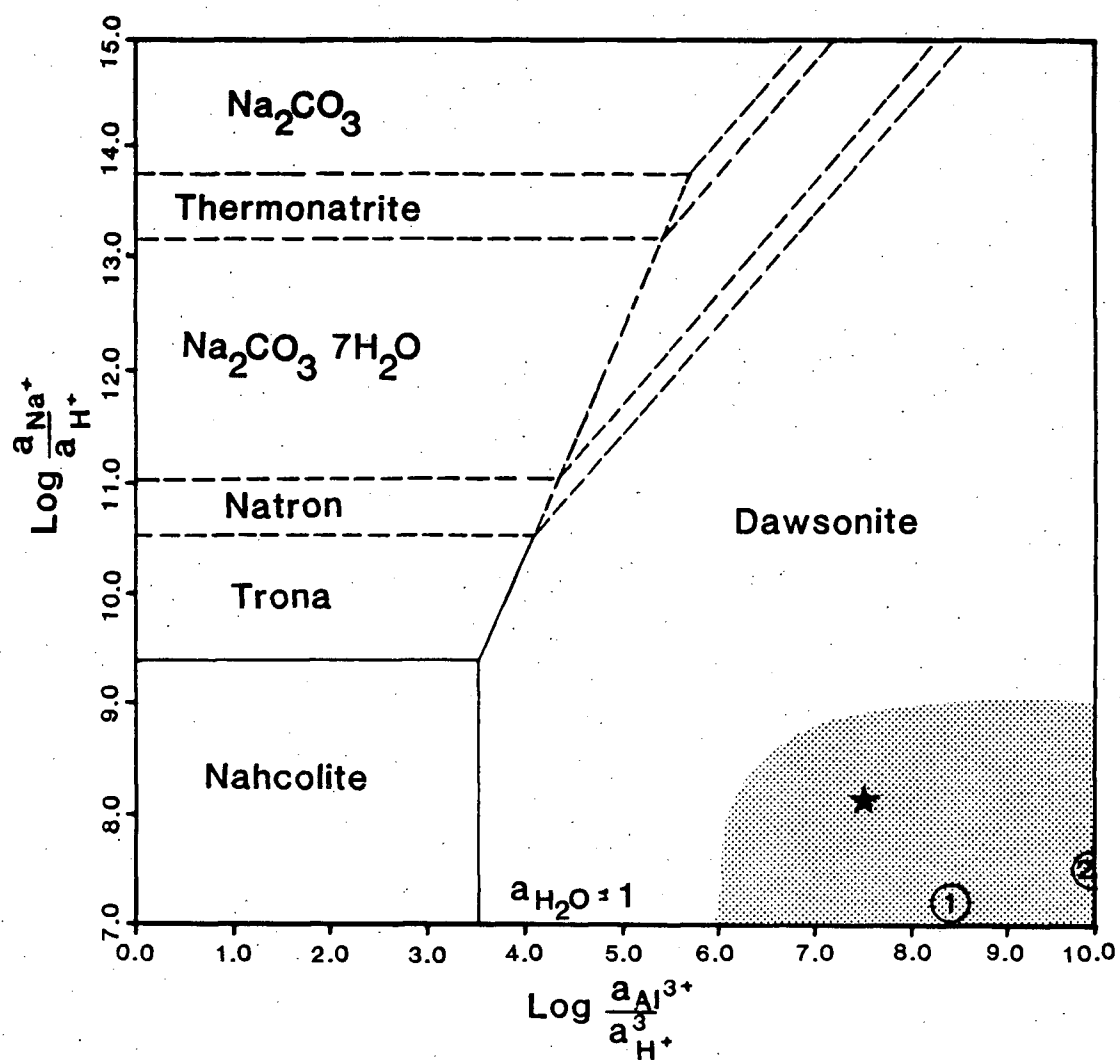
Figure 18- Plot of $Log[A_{Na^+}/A_{[H^+]}]$ versus $Log[A_{Al^+} {}^3/A^3{}_{H^+}]$.
1=Shannon Sandstone, 2=Ocean water, Star=Eureka Sound Formation.
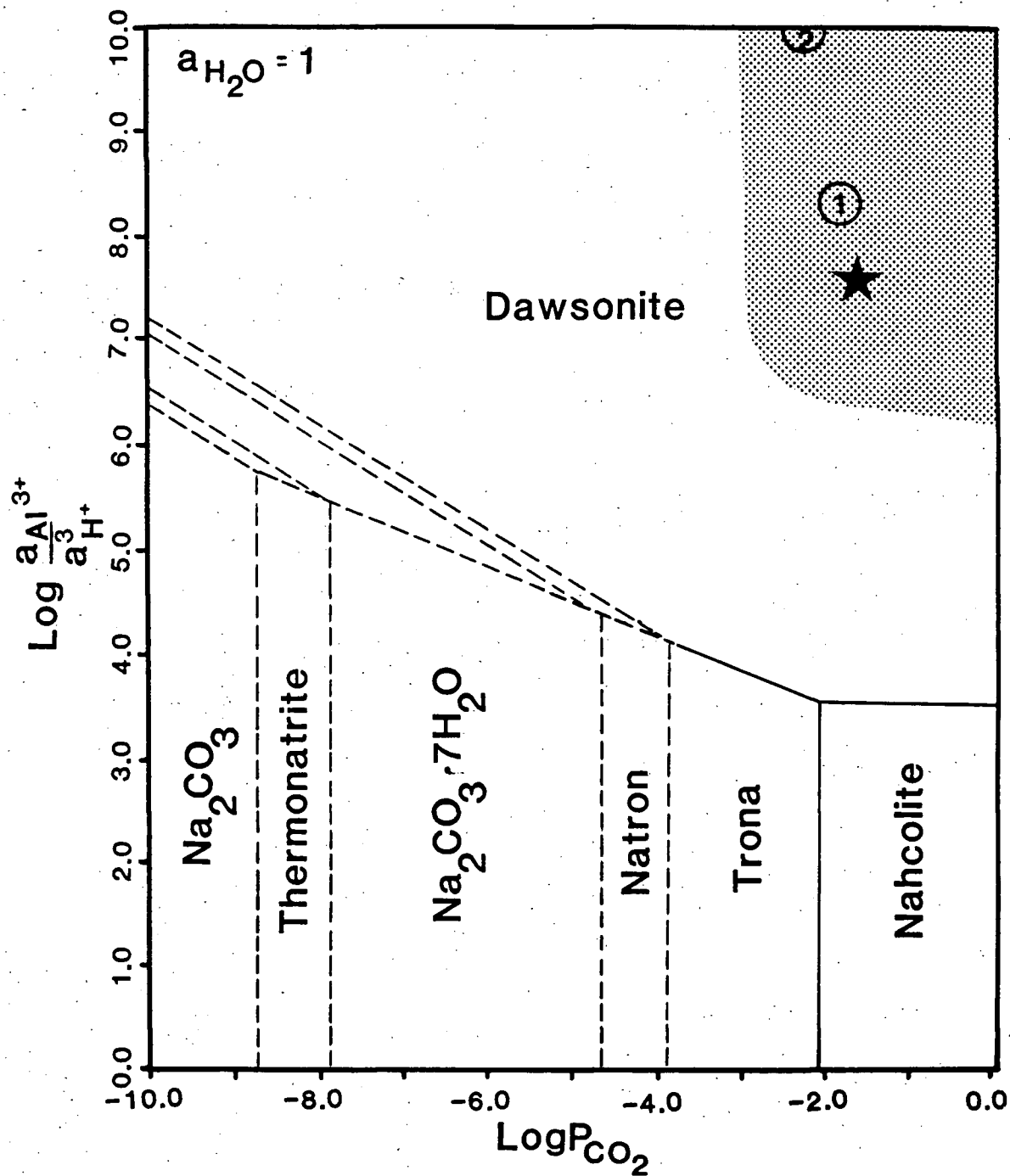
Figure 19- Plot of $Log[A_{Al}+{}^3/A^3{}_{H^+}]$ versus $LogP_{CO_2}$. 1=Shannon and Blairmore Sandstones, 2=Ocean water, Star=Eureka Sound Formation.
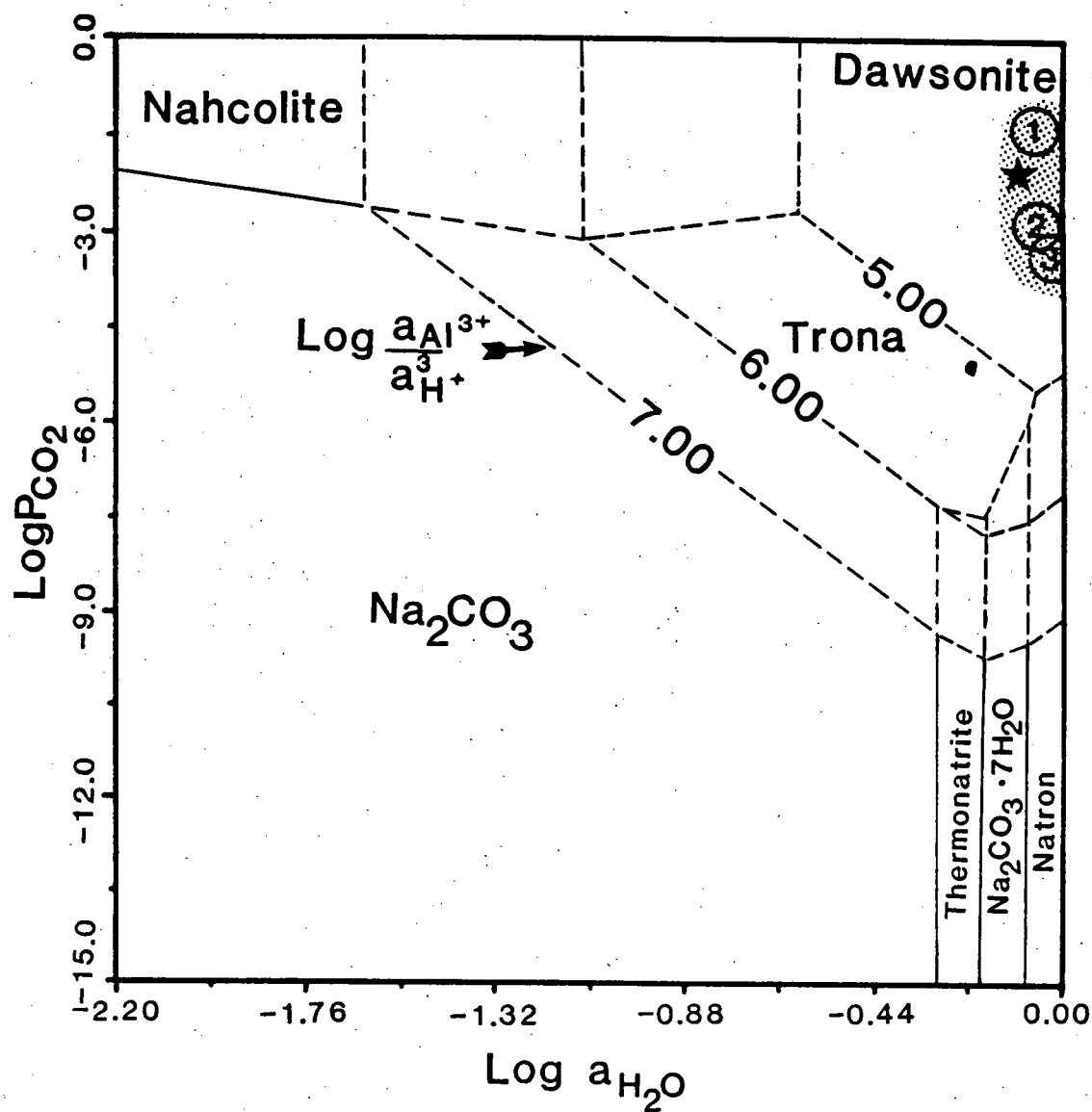
Figure 20- Plot of $LogP_{CO_2}$ versus $LogA_{H_2O}$. 1=Shannon Sandstone, 2=Blairmore Sandstone, 3=Ocean water, Star=Eureka Sound Formation.

TABLE 4

Standard Enthalpy and Entropy of Formation of Dawsonite with a, b and c Heat Capacity Coefficients

$\Delta H^\circ(298)$ J/N	S° J/NK$^\circ$	a	b	c
−1956947.5	132.0	14.8213156	0.37051717	1563478.4

Heat capacity function: $Cp = a + bT + c/T^2$

equilibrium with the rock. Distribution of species calculations were done using a computer progam (THB2:PATH.O, Brown and Perkins) that treats the chemical system as a grand matrix of inter—dependant reactions and solves all equations simultaneously. A formal description of the theory is presented in Perkins (Masters Thesis). Limitations do exist, however, regarding the versitility of the computer program. For example, non—trivial factors such as reaction kinetics are not considered in the computer program. In addition, solid solution phases such as albite—anorthite and ankerite cannot be handled directly by the program. When considered, the free energies of such phases had to be hand calculated and added to the program separately. Distribution of species calculations at temperatures higher than 298.15°K were also not possible with albite and ankerite without estimating their respective Cp values. Such a treatment was beyond the scope of this project. As a result, runs at 298.15°K served as first approximations for aqueous species activities used at higher temperatures. Pure albite and pure calcite replaced An_{10} and ankerite for runs at temperatures greater than 298.15°K. The free energies of An_{10} and ankerite at 298.15°K were calculated using the following formula of ideal

TABLE 5

Names, Chemical Formulae, and Free Energies of Formation of the Sodium

Carbonates Considered in the Included Activity/Activity and Partial Pressure Diagrams

Mineral	Formulae	Free Energy (Kcals)
Natron	$Na_2CO_3 \cdot 10H_2O$	-819.54_2
Trona	$Na_3H(CO_3)_2 \cdot 2H_2O^*$	-570.40_3
Thermonatrite	$Na_2CO_3 \cdot H_2O$	-307.49_2
Sodium Carbonate	Na_2CO_3	-250.4_1
Nahcolite	$NaHCO_3$	-203.6_1
(?)	$Na_2CO_3 \cdot 7H_2O$	-649.12_2
Dawsonite	$NaAl(CO_3)(OH)_2$	-426.86_4

* Trona also commonly reported as $Na_2CO_3 \cdot NaHCO_3 \cdot 2H_2O$
1. Rossini et al. (1952)
2. Saegusa (1950)
3. Garrels and Thompson, unpublished (Garrels and Christ, 1965)
4. Robie et al. (1978)

mixing:

$$\mu = \Sigma_i \mu_i x_i + nRT(\Sigma_i x_i \ln x_i)$$

where: μ_i = the free energy of the end member i

x_i = the mole fraction of end member i

n = number of solution sites (?)

R = 8.417 Joules/mole °K

T = 298.15 °K

All computer runs are isothermal and isobaric with pressures restricted to 0.1 MPa.

Equilibrium within the considered system is assumed to exist between all phases

and species within that system. It is important to note that the following treatment

is only intended as a first approximation calculation as the fluid chemistry of the

TABLE 6

System: $H^+-Al^{+3}-Na^+-H_2O$

Reaction	ΔG	$LogKeq$
Trona + Na^+(aq) = $2Na_2CO_3$ + H^+(aq) + $2H_2O$(l)	18.809	−13.790
Trona + Na^+(aq) = 2Thermonatrite + H^+(aq)	18.009	−13.203
Trona + Na^+(aq) + $18H_2O$(l) = 2Natron + H^+(aq)	14.329	−10.505
Trona + Na^+(aq) + $12H_2O$(l) = $2Na_2CO_3 \cdot 7H_2O$ + H^+(aq)	15.029	−11.018
Trona + $2Al^{+3}$(aq) + $2H_2O$(l) = 2Dawsonite + Na^+(aq) + $5H^+$(aq)	−2.529	1.854
Nahcolite + Na^+(aq) = Na_2CO_3 + H^+(aq)	15.789	−11.576
Nahcolite + Na^+(aq) + H_2O(l) = Thermonatrite + H^+(aq)	15.389	−11.282
Nahcolite + Na^+(aq) + $10H_2O$(l) = Natron + H^+(aq)	13.549	−9.933
Nahcolite + Na^+(aq) + $7H_2O$(l) = $Na_2CO_3 \cdot 7H_2O$ + H^+(aq)	13.899	−10.190
Nahcolite + Al^{+3}(aq) + $2H_2O$(l) = Dawsonite + $3H^+$(aq)	5.120	−3.754
Na_2CO_3 + H_2O(l) = Thermonatrite	−0.400	0.293
Na_2CO_3 + $10H_2O$(l) = Natron	−2.240	1.642
Na_2CO_3 + $7H_2O$(l) = $Na_2CO_3 \cdot 7H_2O$	−1.890	1.386
Na_2CO_3 + Al^{+3}(aq) + $2H_2O$(l) = Dawsonite + Na^+(aq) + $2H^+$(aq)	−10.669	7.822
Thermonatrite + $9H_2O$(l) = Natron	−1.840	1.349
Thermonatrite + $6H_2O$(l) = $Na_2CO_3 \cdot 7H_2O$	−1.490	1.092
Thermonatrite + Al^{+3}(aq) + H_2O(l) = Dawsonite + Na^+(aq) + $2H^+$(aq)	−10.269	7.529
Natron = $Na_2CO_3 \cdot 7H_2O$ + $3H_2O$(l)	0.350	−0.257
Natron + Al^{+3}(aq) = Dawsonite + Na^+(aq) + $2H^+$(aq) + $8H_2O$(l)	−8.429	6.180
$Na_2CO_3 \cdot 7H_2O$ + Al^{+3}(aq) = Dawsonite + Na^+(aq) + $2H^+$(aq) + $5H_2O$(l)	−8.779	6.436
Trona + H^+(aq) = 2Nahcolite + Na^+(aq) + $2H_2O$(l)	−12.769	9.361

considered system is very poorly constrained and many of the thermodynamic and computer program limitations may reduce the system to a state of unrealistic simplicity. By considering the assemblage listed in Table 8 it was possible to constrain the P_{CO_2}, $a_{Al^{3+}}$, a_{Na^+}, pH, a_{SiO_4}, and carbonate species activities for any given molality of Ca^{2+}. Calcium molality was chosen as the independant variable because its activity was the only one of all the species considered that was not fixed by the assemblage considered. By varying the molality of Ca^{2+} it was, therefore, possible to determine aqueous species activities under conditions where

TABLE 7

System: $Al^{+3}-H^+-H_2O-CO_2$

Reaction	ΔG	LogKeq
$Trona + CO_2(g) = 3Nahcolite + 1H_2O(l)$	−2.831	2.076
$2Trona = 3Thermonatrite + 2H_2O(l) + CO_2(g)$	10.691	−7.838
$2Trona + 25H_2O(l) = 3Natron + CO_2(g)$	5.171	−3.791
$2Trona + 16H_2O(l) = 3Na_2CO_3 \cdot 7H_2O + CO_2(g)$	6.221	−4.561
$Trona + 3Al^{+3}(aq) + 5H_2O(l) + CO_2(g) = 3Dawsonite + 9H^+(aq)$	12.529	−9.185
$Nahcolite + Al^{+3}(aq) + 2H_2O(l) = Dawsonite + 3H^+(aq)$	5.120	−3.754
$Na_2CO_3 + H_2O(l) = Thermonatrite$	−0.400	0.293
$Na_2CO_3 + 10H_2O(l) = Natron$	−2.240	1.642
$Na_2CO_3 + 7H_2O(l) = Na_2CO_3 \cdot 7H_2O$	−1.890	1.386
$Na_2CO_3 + 2Al^{+3}(aq) + 5H_2O(l) + CO_2(g) = 2Dawsonite + 6H^+(aq)$	4.380	−3.218
$Thermonatrite + 9H_2O(l) = Natron$	−1.840	1.349
$Thermonatrite + 6H_2O(l) = Na_2CO_3 \cdot 7H_2O$	−1.490	1.092
$Thermonatrite + 2Al^{+3}(aq) + CO_2(g) + 4H_2O(l) = 2Dawsonite + 6H^+(aq)$	4.789	−3.511
$Natron = Na_2CO_3 \cdot 7H_2O + 3H_2O(l)$	0.350	−0.257
$Natron + 2Al^{+3}(aq) + CO_2(g) = 2Dawsonite + 6H^+(aq) + 5H_2O(l)$	6.629	−4.860
$Na_2CO_3 \cdot 7H_2O + 2Al^{+3}(aq) + CO_2(g) = 2Dawsonite + 6H^+(aq) + 2H_2O(l)$	6.279	−4.603
$2Nahcolite = Na_2CO_3 + CO_2(g) + H_2O(l)$	5.851	−4.290
$2Nahcolite + 9H_2O(l) = Natron + CO_2(g)$	3.611	−2.647
$2Nahcolite + 6H_2O(l) = Na_2CO_3 \cdot 7H_2O + CO_2(g)$	3.961	−2.904
$Thermonatrite + CO_2(g) = 2Nahcolite$	−5.451	3.996
$2Trona = 3Na_2CO_3 + CO_2(g) + 5H_2O(l)$	11.891	−8.718

halite (i.e., the source of Na^+ for dawsonite) begins to go into solution (i.e., where $logQ_{halite} > logK_{halite}$) and thereby approximate an upper limit on solution salinity.

Post tectonic/late stage pore waters within the Eureka Sound Formation at Strand Fiord were theoretically determined to be highly saline. Results from the analysis are presented in Table 9. Sodium concentrations as high as 95 to 105 g l^{-1} are proposed at mid section with P_{CO_2} values as high as 0.14 atm. Similarily

TABLE 8

Components Considered in Distribution of Species Analyses

T=298.15 °K   P=0.1 MPa

Components	Formula
Dawsonite	$NaAl(\overline{CO_3})(OH)_2$
Alpha Quartz	SiO_2
Kaolinite	$Al_2Si_2O_5(OH)_2$
Ankerite	$CaFe(CO_3)_2$
Albite—90	$Na_9Ca_1Al_{11}Si_{29}O_{80}$
Calcite	$CaCO_3$
Water	H_2O
Calcium ion	Ca^{2+}

T=333.15 °K   P=0.1 MPa

Components	Formula
Dawsonite	$NaAl(\overline{CO_3})(OH)_2$
Alpha Quartz	SiO_2
Kaolinite	$Al_2Si_2O_5(OH)_2$
Low Albite	$NaAlSi_3O_8$
Calcite	$CaCO_3$
Water	H_2O
Calcium ion	Ca^{2+}

high Na^+ concentrations are common primarily in saline lakes and formation water brines formed from such lakes. Sodium enrichment in the Eureka Sound strata is believed to result from the liberation of Na^+ upon the dissolution of halite from adjacent diapir cores. The presence of dawsonite is, therefore, believed to be attributed to the enrichment of Na^+ in combination with relatively high P_{CO_2}, low

silicic acid activities, and the eventual destabilization of the carboxylic acid—Al^{3+} complex.

Distribution of species results also indicate that for each run the $logQ_{paragonite} > logK_{paragonite}$ irrespective of temperature. Reasons must, therefore, be considered to explain paragonite's absence from a system which *thermodynamically* favours its presence. As was noted earlier, the program used in this study does not take reaction kinetics into consideration. Reaction kinetics may, in this case, exert some control on the absence of paragonite although quantification of this theory is beyond this study. Organic inhibitors, as well, may in some way retard the nucleation of paragonite from solution.

Results from the preceding thermodynamic analysis suggests 2 possible insights. First, dawsonite may be more common in sedimentary rocks than is suggested by its relative scarcity from the literature. The preceding activity/activity and partial pressure diagrams have shown that the chemical conditions necessary to promote the precipitation of dawsonite at standard state temperature and pressure (STP) are found in a range of present day sedimentary and surficial environments. Barring the effects that those chemical factors not considered in this study (i.e., Eh, silicic acid activity, etc) have on the stability of dawsonite it appears reasonable to assume that dawsonite is more abundant in the rock record than previously believed. It may be quite possible that dawsonite's presence has previously been either disregarded, misidentified or completely overlooked. This statement is substantiated by personal communications with other investigators who have identified dawsonite in strata where it has previously been overlooked.

TABLE 9

Comparison of Eureka Sound Formation Fluid Chemistry with the Fluid Chemistry of other Natural Systems (mg l^{-1})

Location	Na^+	Al^{3+}	$LogAl^{3+}$	pH	HCO_3^-	$LogP_{CO_2}$	Ref.
Ocean Water	10,560	1.9	0.27	8.1	140	−3.07	2
Great Salt Lake, Utah	83,600	—	?	7.4	251	?	1
Danby Lake, Calif.	137,580	—	?	—	tr	?	1
Saline Valley, Calif.	103,000	—	?	7.35	614	?	1
Frio Sandstone	9,450	1.7	0.23	7.0	415	?	2
Blairmore Sandstone	31,500	4.1	0.61	6.8	140	−2.5	2
Shannon Sandstone	6,300	0.6	−0.22	7.6	1.01	−1.7	2
*	*	*	*	*	*	*	*
Upper Eureka Sound	117,000	0.0	−8.83	7.1	66.1	−1.99	Exp.
Mid Eureka Sound	99,000	0.0	−6.63	5.8	297	0.14	Exp.

1. Eugster and Hardie, 1978
2. White, 1965

The second implication of the preceding thermodynamic treatment is that the presence of dawsonite in the Eureka Sound strata supports the findings of other investigators who suggest that the evaporite diapirs in the Arctic Archipelago are cored with halite. In this study, halite is modelled as the source of Na for the dawsonite. As the studied sandstones contain only 1 authigenic Na-rich phase it was possible to calculate the prevailing chemical conditions which allowed dawsonite to

precipitate while keeping all other Na-rich phases in solution (i.e., halite). The results show that at the point where halite begins to go into solution and dawsonite precipitates the Na concentration in solution is as high as that in many present day saline lakes and formations. In addition, only those phases which are present in the samples have thermodynamic stability under the conditions calculated by the distribution of species program. In other words, with the exception of pyrophyllite, the chemical conditions calculated in the distribution of species program do not favor the precipitation of any phases other than those *observed* in the samples.

SHALE MINERALOGY AND DIAGENESIS

Clay mineral analyses may yield valuable genetic and diagenetic information about strata. In studies by Burst (1969), De Segonzac (1970), Millot (1970), Folscolos *et al*, (1976) and Hower *et al*, (1976) it has been shown that relationships exist between depth of burial and various diagenetic parameters relating to clays. For example, studies by Burst (1969), Foscolos (1973), Eberl and Hower (1976), and Foscolos *et al* (1976) have shown that as depth of burial increases so does the sharpness ratio and crystallinity of illite. Perry (1969), Reynolds and Hower (1970), and Hower (1981) have shown that as depth of burial increases the percentage of smectite present in illite/smectite mixed layers generally decreases. In other studies (Wilson and Pittman, 1977; Perry and Gillot, 1979; Sedimentology Research Group, 1981; Almon and Davies, 1981), the detrimental effects of detrital and authigenic clay minerals on reservoir recovery characteristics have increased the need to better understand the role that clays play in reservoir mechanics.

This chapter examines the clay mineralogy and variations in a number of diagenetic parameters through the studied section.

EXPERIMENTAL

Clay Sample Preparation

Twenty five shale samples were chosen from 100 m intervals for x—ray diffraction analyses. Each sample was initially ground in a rock crusher to reduce rock fragment size to approximately 5 mm^3. The samples were then washed in

de—ionized water to remove any clay contaminants which may have been introduced by the rock crusher. Although care was taken when cleaning the crusher between samples, the design of the rock crusher made it impossible to guarantee that some clays were not passed from one sample to the next during sample preparation. Once dry, each sample was ground to a fine powder in an agate mortar and placed in a one litre bucket filled with de—ionized water. The clays were dispersed in the water by stirring and then allowed to settle for a period of 8 hours. After eight hours the top 8 cm of supernatant, containing the <2.0 um fraction (Jackson, 1969), were syphoned off into a separate container and left to stand for 10 to 14 days. Once the clays had settled completely out of the solution the supernatant was discarded and the remaining slurry was set aside for cation exchange treatment and further size fractionation.

Before the clays were saturated with a cation each sample was separated into coarse (0.2 to 2.0μm) and medium (<0.2μm) size fractions via centrifugation. One hundred ml plastic test tubes were filled to 1 cm with the clay sample solution and topped to 10 cm with de—ionized water. Samples were then centrifuged at 2000 rpm for 50 minutes using an IEC® centrifuge with a number 240 head (after Brown, 1965 and Jackson, 1969). After centrifuging, the supernatant, containing the less than 0.2 μm fraction was syphoned off and reserved for later treatments.

The coarse fraction of each sample was again separated into three portions that were subsequently:

1) left untreated;

2) saturated with K^+ and;

3) saturated with Mg^{2+}.

Cation exchange was accomplished by following techniques outlined by Brown (1965) and Jackson (1969). Twenty to 25 mg of sample was placed in a 15 ml test tube and flocculated in a 1N cation—chloride solution (i.e., KCl or $MgCl_2$). Cation saturation was completed by successively centrifuging and decanting the suspension four times in the 1N cation—chloride solution. Finally, excess salts were removed from the sample by washing in 50% methanol, 95% methanol and two successive washings in 95% acetone. It was necessary when saturating a sample with Mg^{2+} to first acidify the solution in order to avoid precipitating $Mg(OH)_2$ out of solution upon addition of Mg^{2+}. Acidification was accomplished by adding 0.1N HCl drop wise to the initial solution until the pH was between 3.5 and 4. Ten N magnesium acetate was used in place of $MgCl_2$ in the first cation—solution bath.

Oriented Samples

Once cation saturation was complete an equal volume of water was added to the remaining volume of the clay slurry. This thinned slurry was then pipetted onto a glass slide and allowed to dry at room temperature. Once dry, each slide was x—rayed and then glycolated.

Clay samples were glycolated by placing the slides face—up in a vacuum desiccator over ethylene glycol for approximately 24 hours. The samples were x—rayed immediately after being removed from the desiccator in order to minimize the amount of interlayer glycol lost through evaporation (Kunze, 1955; Srodon, 1980).

Finally, clays saturated with K^+ were placed in an electric furnace and heated for 2 hours at 500°C. At the end of this time the samples were removed and

placed in a desiccator where they were left to cool. This procedure minimized the amount of atmospheric water resorbed by clays upon cooling. Once cool the samples were again x—rayed.

Unoriented Samples

Unoriented samples were prepared by scraping the dried material off of oriented sample mounts with a razor blade and re—crushing the clays to create a fine powder. This powder was then poured into a "welled" aluminum sample holder and x—rayed.

Instrumental Techniques

All clay samples were x—rayed on a Philips® x—ray diffractometer using a CuKα source and Ni filter. The scan speed used on all samples other than those saturated with Mg^{2+} was $2°$ per minute with a time constant of 2 seconds. Voltage and amperage were set at 40 kV and 20 mA, respectively. All oriented sample preparations were scanned between $3-18°$ 2θ. Those samples that had been exchange saturated with Mg^{2+} and glycol were scanned between $3-18°$ 2θ and $42-48°$ 2θ at a scan speed of $1°$ per minute with a time constant of 1 second. These samples were also scanned at $1/2°$ per minute between 17 and $18°$ 2θ in order to determine a more precise (002)10/(003)17 reflection location for calculating the percentage of illite in illite/smectite mixed layer clays. The K^+ saturated samples were used to examine for variations through the section in the illite crystallinity index (Kubler, 1966) and sharpness ratio of the 1.0 nm peaks (Weaver, 1961). Mg^{2+}—glycol saturated samples were used for percent illite determinations and discrete layer silicate identification.

Unoriented sample preparations were scanned between 50–58° 2θ at 2° per minute in order to examine the (060)10 reflection. The position of this reflection was used to differentiate between di– and trioctahedral 2:1 silicates (Jackson, 1956).

Analytical Techniques

Analytical techniques used for specific clay mineral analyses have been divided into the following categories:

– Clay mineralogy.

– Semi–quantitative mineralogy.

– Mixed layer analyses.

– Sharpness ratio and illite crystallinity index.

Clay Mineralogy

Identification of clay minerals was based on changes in diffraction peak locations following different sample treatments. Identification criteria were as follows:

1) Kaolinite– has (00l) d–spacings of 0.715 nm and 0.35 nm which are unaffected by cation saturation and glycolation. These peaks dissappear upon heating at 500°C for 2 hours.

2) Illite– has a (001) d–spacing of 1.0 nm which varies slightly depending on the amount of smectite present (Reynolds & Hower, 1970). The 1.0 nm peak increases in intensity and sharpness upon saturation with K^+. Heating to 500°C leaves this peak unaffected. Jackson (1956) reports that dioctahedral illite produces a (060) reflection at 0.15 nm while trioctahedral illite has a (060) peak in the 0.1525–0.1534 nm range.

3) Chlorite— has (00l) spacings of 1.4 and 0.715 nm which can be confused with vermiculite and kaolinite. It is distinguished from all but non—Al^{3+} vermiculite (Brown, 1969) by saturating with K^+. Upon treatment with K^+, non—Al^{3+} vermiculite collapses to 1.0 nm while chlorite and Al^{3+} vermiculite persist at 1.4 nm. After heating to 500°C for 2 hours all 1.4 nm vermiculite will collapse to 1.0 nm while the 1.4 nm chlorite peak will increase in intensity.

4) Vermiculite— has a (001) d—spacing of 1.4 nm when saturated with Mg^{2+} at a relative humidity of approximately 40% (Brindley, 1980). This d—spacing increases to roughly 1.52 nm when glycolated and collapses to 1.0 nm when heated to 500°C for 2 hours.

5) Smectite— like vermiculite, smectite collapses to 0.95—1.0 nm when heated for 2 hours at 500°C. Brindley (1980) demonstrates how saturation with different cations will result in different (00l) d—spacings. For the purpose of this study, smectite (001) d—spacings at 40% relative humidity are approximately 1.1—1.25 nm and 1.1 nm for Mg^{2+} and K^+ saturated samples, respectively. Glycolated samples expand to approximately 1.69 nm.

6) Mixed layer clays— the identification of illite/smectite mixed layers is discussed in a later section.

Semi—quantitative Mineralogy

Semi—quantitative estimates of the relative proportion of each clay type in each sample was determined by methods outlined by Bayliss *et al.* (1970). The height of the reflections at 0.7 nm (kaolinite), 1.0 nm (illite), 1.4 nm (vermiculite), 1.4 nm (chlorite), and 1.7 nm (smectite) were measured on Mg^{2+} saturated samples. A correction factor of 8:8:2:2:2 was then multiplied by the respective peak

heights to compensate for Lorentz polarization (Bustin and Bayliss, 1979).

The above mentioned procedure quantifies only the proportions of each clay *type* present in a sample but says nothing about how those clays are distributed between mixed layered and discrete clays. To quantify the distribution of discrete smectite, discrete illite, and mixed layer illite/smectite present the following technique was employed:

1) Diffractograms of Mg saturated clays were examined for reflections in the 15.65–17.65° 2θ range. If discrete smectite and illite were present there would be reflections at 15.78° and 17.65° 2θ, respectively (Reynolds and Hower, 1970).

2) The ratio of illite to smectite in illite/smectite mixed layers (see following section) was calculated for each sample. This value was then normalized to 1 smectite (i.e., X_{illite}:1). The X_{illite} value of this term will be referred to as 'X_I'.

3) If, from the diffractograms, it was determined there was no discrete smectite present it was assumed that of all the smectite from the *total* clay calculations was tied up in the illite/smectite mixed layers. This value of total smectite (S_{tot}) was then multipied by X_I to determine the percentage of illite (I_{mix}) in the I/S mixed layers. The sum of I_{mix} and S_{mix} (the percentage of smectite in I/S) gave the total percentage of I/S mixed layers present. The difference between I_{mix} and the total percentage of illite in the sample (I_{tot}) represented the percentage of illite that occurs as discrete illite.

4) If I_{mix} was greater than I_{tot}, I_{tot} was assigned completely to I/S mixed layers and a new S_{mix} was calculated. Intuitivly, the new S_{mix} would have to be less than or equal S_{tot}. The difference in S_{mix} and S_{tot} would, therefore, be unaccounted for if it had been previously determined that discrete smectite was

not present. This 'residual' smectite would have to be attributed to error, other smectite mixed layers (i.e., chlorite/smectite) or the presence of discrete smectite in such small proportions that the (002)10/(003)17 reflection was too weak to be recognised. This approach produced values for the *maximum* possible percentage of both I/S mixed layers and discrete smectite and a *minimum* possible percentage of discrete illite that could have been present in each sample.

Mixed layer Analyses

Both mixed layer illite/smectite and mixed layer chlorite/smectite were analysed in the current study. It was attempted to determine the percentage of chlorite in mixed layer chlorite/smectite by using the techniques of Reynolds and Hower (1970), who used shifts in the location of second and third order peaks as a measure of % chlorite in glycolated samples. Due to the presence of vermiculite at approximately 1.4 nm and kaolinite at 0.71 nm the true positions of the chlorite/smectite peaks were masked and the determination of % chlorite in chlorite/smectite mixed layers was, therefore, not possible in this study.

Two different methods were considered for determining the percentage of illite in the illite/smectite mixed layers. The first followed the method of Srodon (1980) where the difference in 2θ between two reflections in the 42–48° 2θ region was used as a measure of the proportion of illite. The second method determines the proportion of illite based on the positioning of the (002)10/(003)17 peak (Reynolds and Hower, 1970). The former method is believed by the author to be a more accurate measure of %–illite as the latter neglects to take 'small domain size' into account (domain size being that volume of a structure which scatters x–rays coherently (Srodon, 1980)). Srodon (1980) reports

that a small domain size will contribute to shifting of the (002)10/(003)17 peak location and thus introduce additional error to the analysis.

Problems associated with Srodon's (1980) method are that for mixed layers containing >80% illite two reflections in the 42–48° 2θ range cannot be differentiated due to overlap of the peaks.

Using Reynold and Hower's (1970) method, the proportion of illite in illite/smectite mixed layers was determined by comparing the diffractograms obtained from the clay analyses with the data of Reynolds and Hower (1970) (Table 10).

This method required performing a linear interpolation of Reynolds and Hower's data. The objective of this interpolation was to express their data as a series of linear equations from which illite proportions could be determined given the position of the (002)10/(003)17 peak. Although the data of Reynolds and Hower (1970) appears to have a sigmoidal distribution with respect to illite proportion and the positioning of the second and third order reflection peaks there is no *theoretical* justification for fitting higher order polynomials (i.e., cubic) to the data. In addition, as the experimental error associated with the data was not reported it can only be assumed that the relationship is at best linear.

Example

A diffractogram indicates that no reflections occur at 15.78° 2θ, therefore, no discrete smectite is present. Mixed layer percent—illite calculations reveal that mixed layers are composed of 85% illite and 15% smectite. Therefore,

Illite/smectite ratio = 85:15
Normalized ratio = 5.66:1
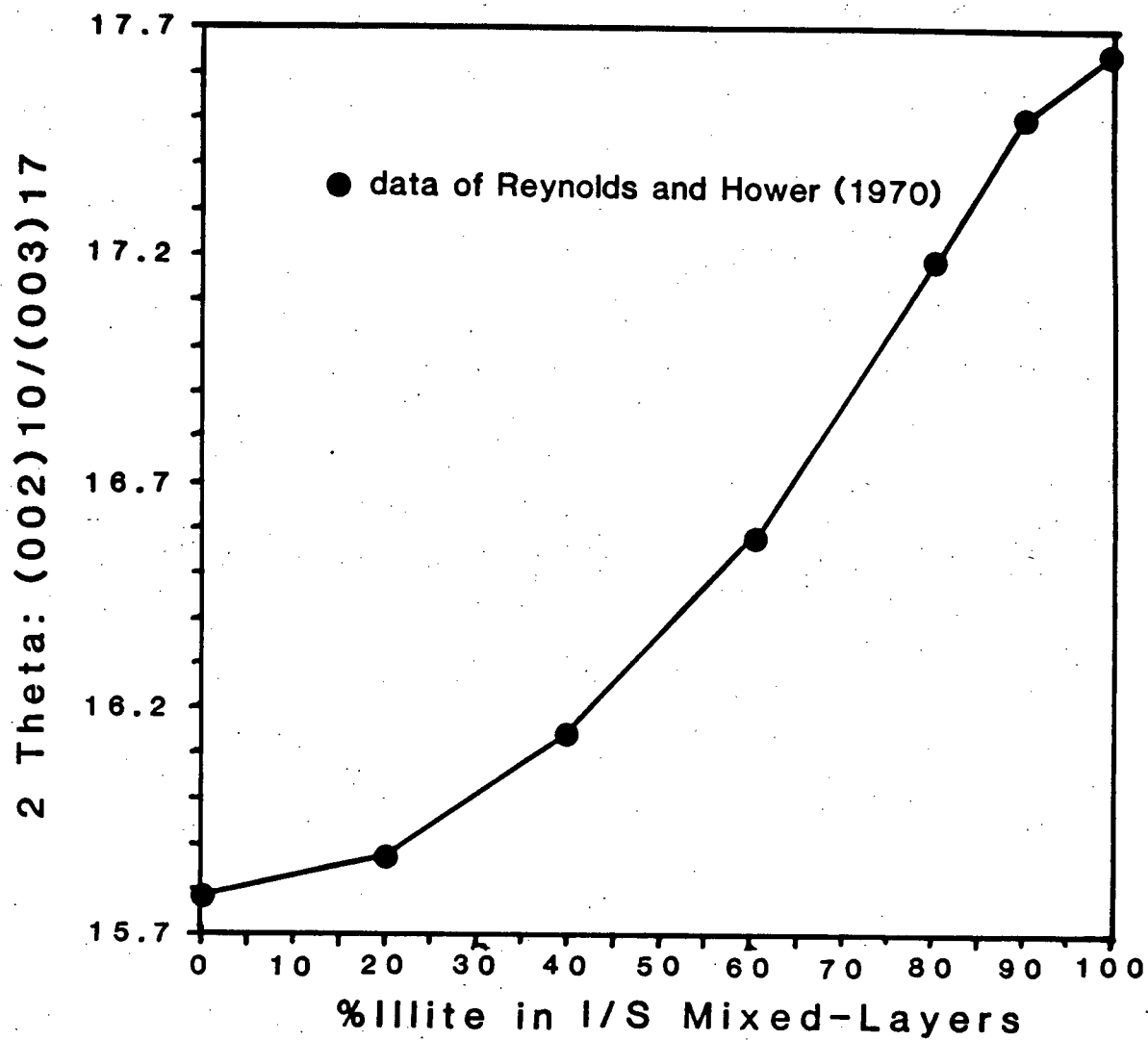
Figure 21- Plot of variations in (002)10/(003)17 illite peak location with variations in %illite in illite/smectite mixed-layer clays.

TABLE 10

Positions of the (002)10/(003)17 Diffraction Peak for Various % Illite in Illite/Smectite

Values

% Illite in I/S	(002)10/(003)17: 2θ
0	15.78
20	15.87
40	16.15
60	16.58
80	17.19
90	17.50
100	17.65

Data of Reynolds and Hower, 1970

$$X_I = 5.66$$

Total—clay calculations reveal that the sample is composed of:

55% kaolinite
40% illite
4% smectite
1% vermiculite

therefore,

$I_{tot} = 40$
$S_{tot} = S_{mix} = 4$
$I_{mix} = S_{mix} * X_I = 23$

and, therefore,

Total % I/S mixed layers $= I_{mix} + S_{mix} = 27\%$
Total % discrete illite $= I_{tot} - I_{mix} = 17\%$

Sharpness Ratio and Illite Crystallinity Index

Two 1.0 nm peak shape parameters are used in this study to approximate the degree of shale diagenesis in the studied section. These parameters are Weaver's (1961) sharpness ratio which compares the height of the peak at 1.0 nm to the height of the reflection at 1.05 nm and illite crystallinity, which is measured using Kubler's (1964) 'illite crystallinity index' where the (001) peak width is measured at half height. As scan speeds and chart speeds can vary from one study to another it is more convenient to report illite crystallinity values in degrees $\Delta 2\theta$ rather than millimeters.

RESULTS

Clay Mineralogy

Appendices 1—3 show the diffraction peak locations for all samples with each different treatment. From an examination of these tables the clay mineralogy of each sample and the section in general was determined. The results indicate that kaolinite, illite, and possibly vermiculite persist through the entire section. There is, however, some variation in the relative proportion of illite (see following section). Chlorite is apparently restricted to zone 4 while smectite is apparently less abundant through zone 4 than elsewhere. Di—octahedral 2:1 silicates persist through the entire section (Table 11).

TABLE 11

Variations in Smectite (060) d—spacing (in nm) Through Section

Height	Di—octahedral (0.149—0.151)	Tri—octahedral (0.152—0.153)
656	0.149	—
748	0.1505	—
892	0.1510	—
919	0.1507	—
1058	0.1496	—
1070	0.1499	—
1120	0.1512	—
1268	0.1497	—
1330	—	—
1551	0.1511	—
1699	0.1510	—
1830	0.1507	—
2100	0.1502	—
2173	0.1505	—
2243	0.1510	—
2358	—	—
2419	0.1492	—
2967	0.1501	—

Semi—quantitative Mineralogy

Semi—quantitative results of total—clay percentages through the studied section are listed in Table 12. General trends indicate that as the percentage of kaolinite decreased with increasing depth through zone 4, the percentage of total illite increased. At the boundary between zones 3 and 4 there is a sharp reversal in their relative proportions. Through zones 2 and 3, kaolinite and illite proportions remained approximately constant. The major point of interest with respect to

smectite is that through the upper 2/3 of the studied section the percentage of smectite was low (<2%) and remained approximately constant with increasing depth. Below zone 4 there was a sharp increase in the percentage of total smectite to approximately 4%, which remained high to the base. Figure 22 demonstrates graphically how the sample compositions vary with depth.

Table 13 outlines the distribution of clay—types through the the studied section. The main trend to note here was that both discrete illite and chlorite were restricted to zone 4. Mixed layer illite/smectite was relatively absent through this same interval. Figure 23 indicates graphically how the the relative proportions of clay vary with depth.

Percent Smectite in Illite/Smectite Mixed layers

An examination of the diffractograms from the present study revealed that only one peak was present in the 42—48° 2θ range in all samples. The absence of two peaks in this range suggested, using Srodon's (1980) method, that no where in the section did the %—smectite in illite/smectite mixed layers exceed 15%.

In a separate attempt to determine a value for the %—smectite it was assumed that the domain size of all samples through the section was large enough to minimize the amount of error attributable to small domain size. This assumption permitted the application of Reynold and Hower's (1970) method of %—illite determination.

Figure 24 illustrates the variations in the percentage of illite with depth that were calculated through the section using Reynolds and Hower's (1970) method. In
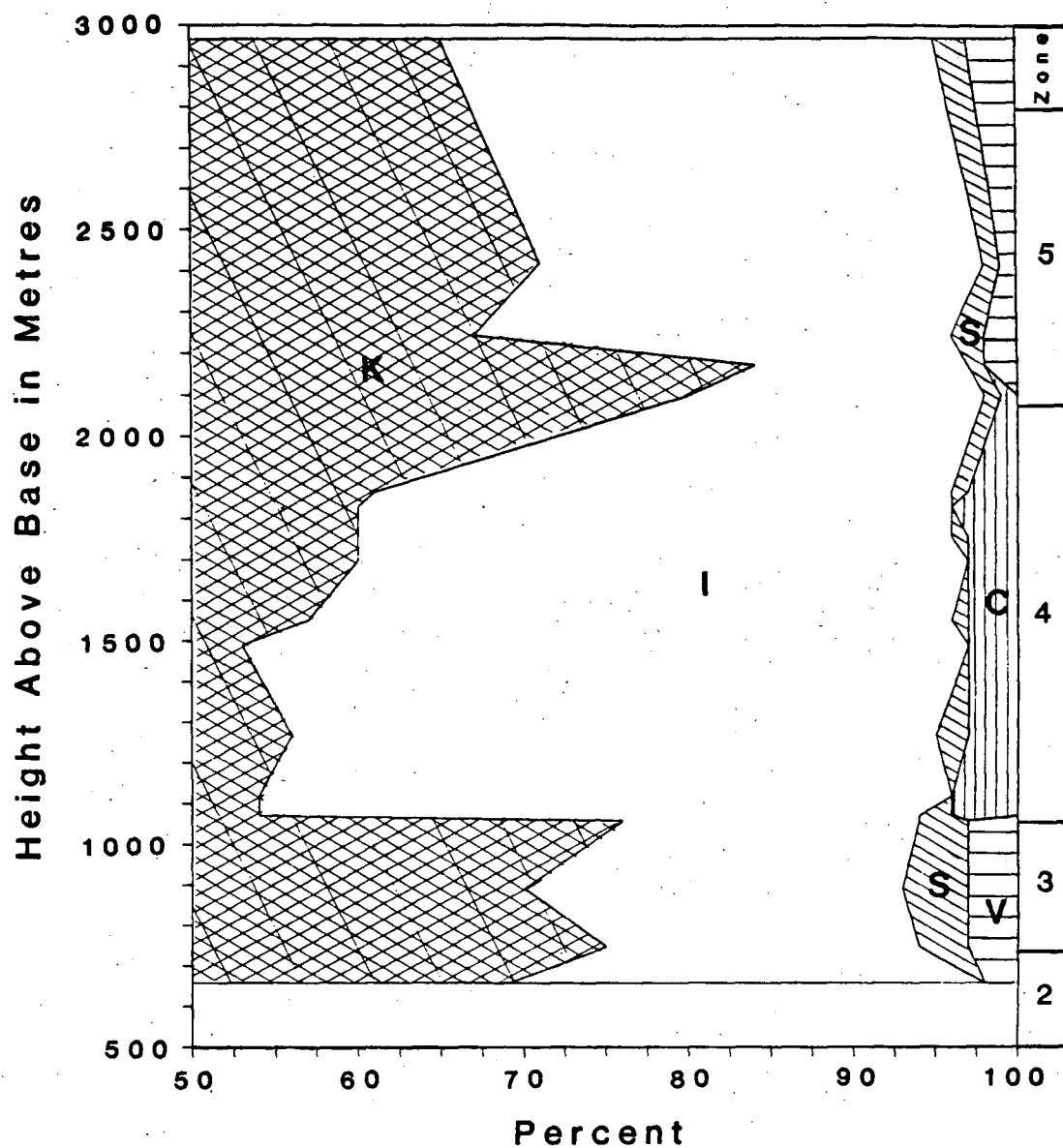
Figure 22. Plot of variations in shale composition with depth and through individual paleo-environments. K= kaolinite, I= *total* undifferentiated illite, V= vermiculite, C= chlorite and/or non-Al vermiculite, S= total smectite.
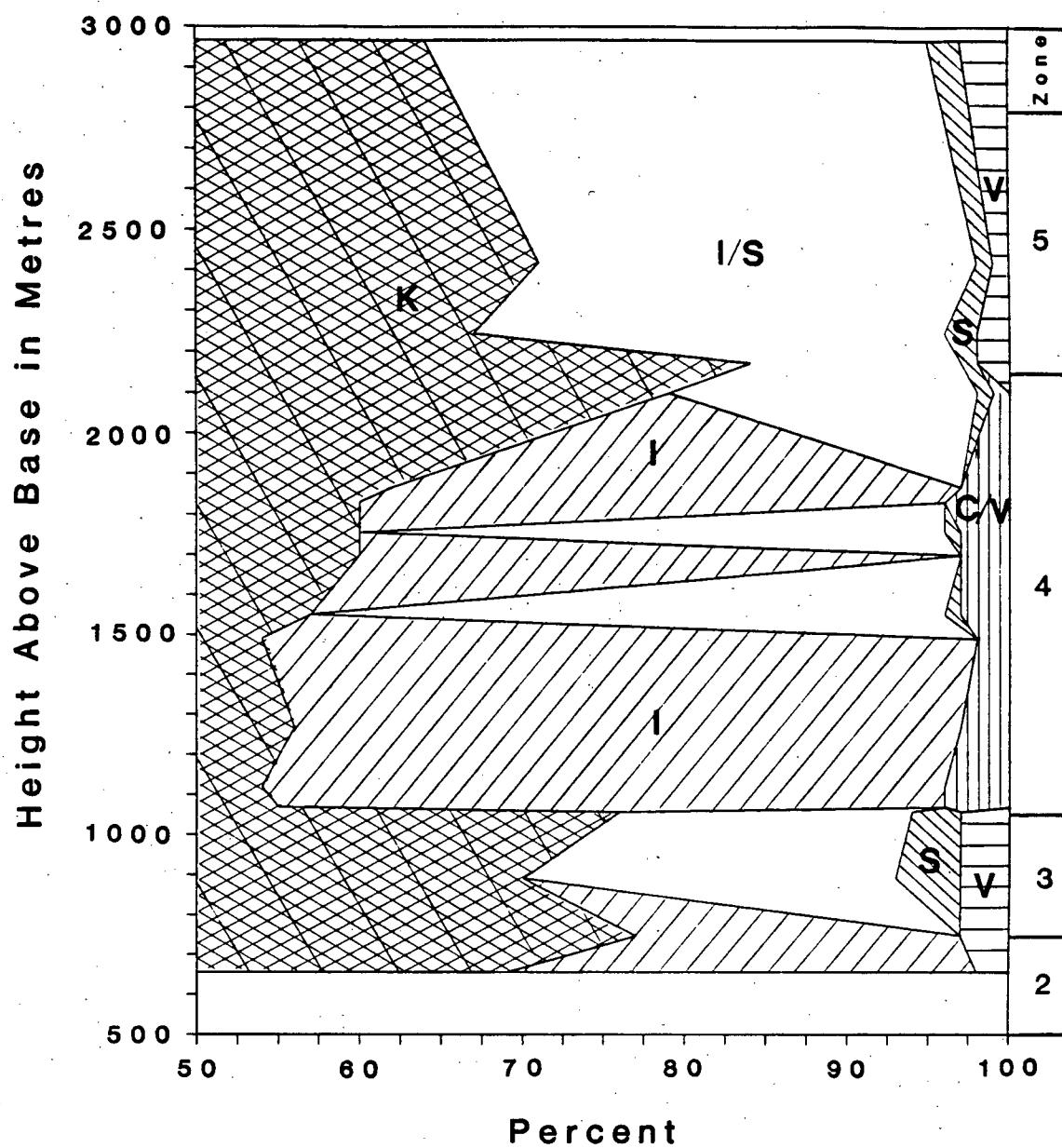
Figure 23- Plot of variations in shale composition with depth and through individual paleo-environments. K= kaolinite, I= discrete illite, I/S= illite/smectite mixed-layers, S= discrete and undifferentiated smectite, V= vermiculite, C= chlorite and/or non-Al vermiculite.
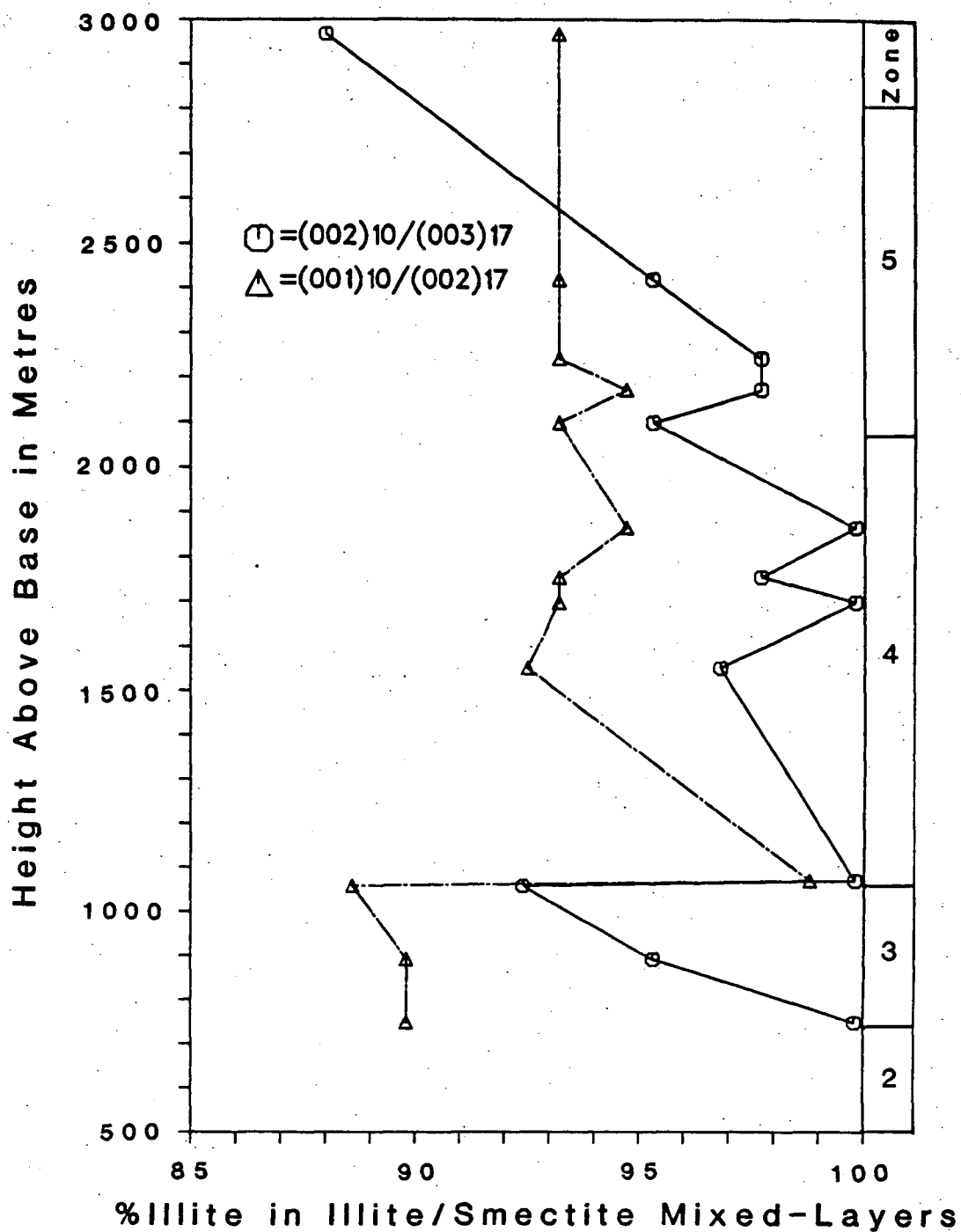
Figure 24- Plot of variations in the percentage of illite in illite/smectite mixed-layered clays with depth and through the individual paleoenvironments of RAK-26.

TABLE 12

Semi—quantitative Mineralogy of Studied Section with Undifferentiated Illite

(%)

Heigh a/b	Kao	Ill	Chl	Verm	Smec
656	69	29	0	2	0
748	75	19	0	3	3
892	70	23	0	3	4
1058	76	18	0	3	3
1070	54	40	4	?	2
1120	55	42	4	?	0
1268	56	39	3	?	2
1490	54	44	3	?	0
1551	57	39	3	?	1
1699	60	37	3	?	0
1755	60	36	3	?	1
1830	60	36	4	?	0
1866	62	35	3	?	1
2100	79	18	1	?	1
2173	84	13	0	2	1
2243	67	29	0	2	2
2419	71	27	0	1	1
2967	64	30	0	3	2

Height a/b= height above base (metres), Kao= kaolinite, Ill= total illite, Smec= total smectite, Verm= vermiculite, Chl= chlorite

general, the percentage of illite at the top of the section ($\sim$88%) increases to approximately 100% at the base of zone 4. Below zone 4 there is a relatively sharp increase in the percentage of smectite and decrease in the percentage of illite. Within zone 3 the illite percentage again increases toward the base of the section.

TABLE 13

Semi—quantitative Mineralogy of Studied Section with Differentiated Illite

(%)

H a/b	Kao	Ill(d)	Smec(d)	Chl	Verm	Ill/Smec
656	69	29	0	0	2	0
748	75	20	0	0	3	0
892	70	0	4	0	3	23
1058	76	0	3	0	3	18
1070	54	41	0	4	?	0
1120	55	42	0	4	?	0
1268	56	43	0	3	?	0
1490	54	44	0	3	?	0
1551	57	0	1*	3	?	39
1699	60	37	0	3	?	0
1755	60	0	1*	3	?	36
1830	60	36	0	4	?	0
1866	62	35	0	3	?	0
2100	79	0	1*	1	?	18
2173	84	0	1*	0	2	13
2243	67	0	2*	0	2	29
2419	71	0	1*	0	1	27
2967	64	0	2*	0	3	31

H a/b= height above base (metres), Kao= kaolinite, Ill(d)= discrete illite, Smec(d)= discrete smectite, Verm= vermiculite, Chl= chlorite, Ill/Smec= illite/smectite mixed layers

(*) indicates *maximum* possible value
i.e., (002)10/(003)17 reflection at 5.62—5.66A was weak or absent.

Illite Crystallinity Index

Illite crystallinity values were found to decrease with increasing depth through the upper 2/3 of the section. Crystallinity values decreased from approximately 0.85 $\Delta 2\theta$ at the top of the section to approximately 0.33 $\Delta 2\theta$ at the base of zone 4 (Table 14). Within zones 2 and 3, the crystallinity of illite appears to show no

relationship to increasing depth (Figure 25). Whether this random distribution of illite crystallinity throughout zones 2 and 3 is real or not is discussed in a later section.

Sharpness Ratio

Sharpness ratio values show a similar trend to that of illite crystallinity. The ratio increases more or less linearly from approximately 1.20 at the top of the section to approximately 1.60 close to the base of zone 4 (Table 15). Below zone 4, however, the sharpness ratio decreases linearly to approximately 1.05 at the base of zone 2 (Figure 26)..

DISCUSSION

Shale analysed from the domain of diagenesis usually contains both a detrital and diagenetic clay component. Only after low grade metamorphic pressures and temperatures are attained will the *majority* of the detrital clay component no longer exist in a form which has been unaffected by its physical and chemical environment (i.e., increasing temperature and pressure, variations in pore water chemistry, etc.). Care must, therefore, be taken when interpreting clay analyses to differentiate results attributable to the detrital component from those attributable to the diagenetic component.

An examination of the shale composition plots (Figures 22 and 23) indicates that paleo—environments and provenance, rather than authigenic mineralogy, exert primary control on producing the observed distribution of clay minerals with depth. This does not, however, totally dismiss the presence of a diagenetic component .
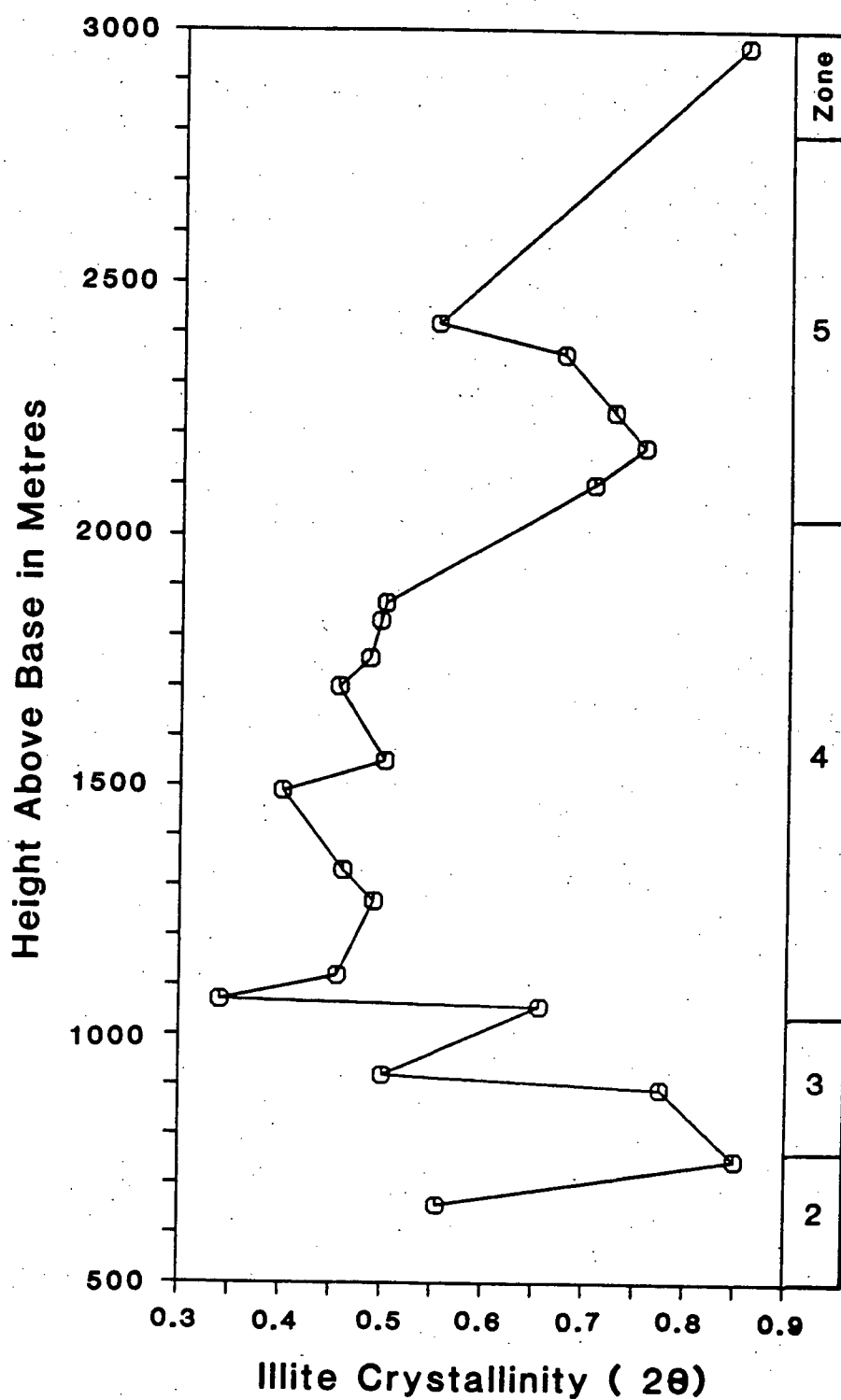
Figure 25- Plot of variations in illite crystallinity through section and individual paleo-environments.
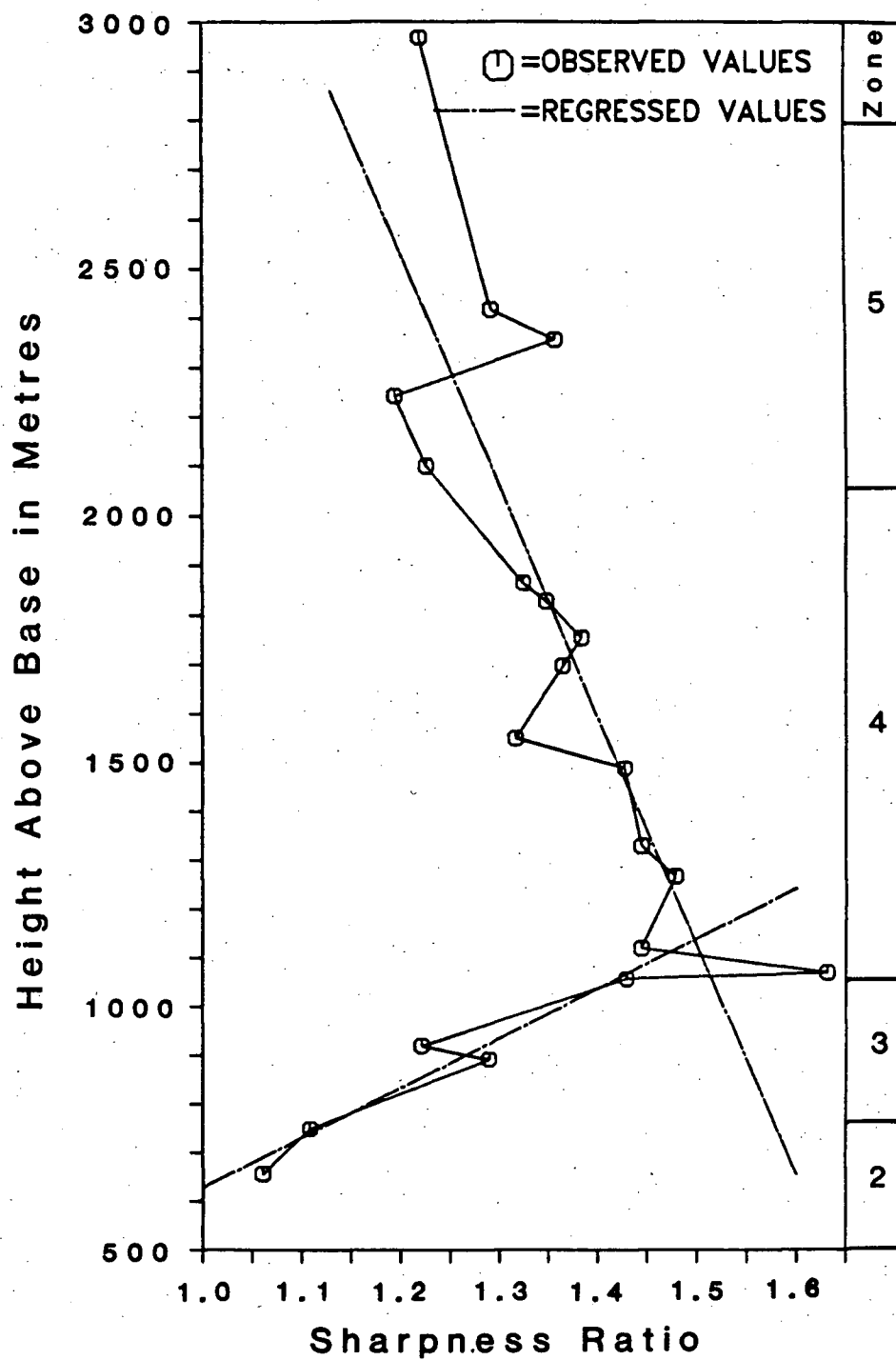
Figure 26- Plot of variations in the 1.0:1.05 nm peak sharpness ratio through section and individual paleo-environments.

TABLE 14

Variations in Illite Crystallinity with Depth

Height above base (m)	Illite Crystallinity Index
656	0.55
748	0.85
892	0.77
919	0.50
1058	0.65
1070	0.34
1120	0.45
1268	0.49
1330	0.46
1490	0.40
1551	0.50
1699	0.45
1755	0.49
1830	0.49
1866	0.50
2100	0.70
2173	0.75
2243	0.73
2358	0.67
2419	0.55
2967	0.65

In these plots it can be seen that the gross changes in mineralogy and reversals in clay proportion trends occur primarily at zone (lithofacies) boundaries. For example, chlorite is restricted to zone 4, kaolinite content decreases through zone 4, and smectite and kaolinite proportions increase sharply at the boundary between zones 3 and 4. Enigmatic shifts in illite crystallinity values, sharpness ratios and the percentage if illite in I/S mixed layers at zone boundaries (i.e., zones 3 and 4) also suggests that lithofacies exert control on trends in clay diagenesis parameters.

TABLE 15

Variations in Sharpness Ratio with Depth

Height above base (m)	Sharpness Ratio
656	1.060
748	1.108
892	1.289
919	1.220
1058	1.429
1070	1.631
1120	1.444
1268	1.478
1330	1.444
1490	1.427
1551	1.316
1699	1.364
1755	1.383
1830	1.347
1866	1.324
2100	1.225
2173	1.194
2243	1.356
2358	1.291
2419	1.219
2967	1.219

Control, in this case, coming from variations in either detrital mineralogy or fluid chemistry unique to each zone (i.e., P_{H_2O}, P_{CO_2}, [cation]).

Within each zone, and in some cases through adjacent zones, there is evidence to support the diagenetic overprinting of the detrital mineralogy. For example, the increases in illite crystallinity, sharpness ratio values and %illite in I/S from the top of the section to the base of zone 4 supports diagenetic alteration of illite. Similarly, coincident increases and decreases of different clay minerals over

specific intervals suggests that possible diagenetic reactions *may* be taking place. Before examining the diagenetic trends and some of the associated problems, however, it is first necessary to identify the "diagenetic facies" that is represented by the Eureka Sound strata along Kanguk Peninsula.

*Diagenetic Facies and Sub—*facies

Although there exists no universally accepted definition of diagenesis the 1980 *Glossary of Geology* (Bates *et al.*, 1980) defines diagenesis as:

> 'chemical, physical, and biological changes undergone by a sediment after its original deposition...exclusive of surficial alteration and metamorphism.... It embraces the processes...that occur under pressure (up to 1 kilobar) and temperature (maximum range of 100°C to 300°C) that are normal to the surficial or outer part of the earth's crust.'

The temperature and pressure constraints used in this definition may be misleading, however, because they imply that the lower limits of metamorphism are absolute (i.e., P>1Kb) and defined without regard to phase stability fields. Because metamorphic facies are delineated in P—T space by the mineral assemblage stability fields, a preferred criteron for marking the diagenetic/metamorphic boundary is given by Winkler (1967).

> 'Metamorphism has begun and diagenesis has ended when a mineral assemblage is formed which cannot originate in a sedimentary environment.'

Although Winkler's definition may perhaps be preferred it is still not without fault. For example, if it is assumed that a 'sedimentary environment' extends no deeper than the sediment/water interface then diagenesis has ended once pyrite begins to precipitate just below the sediment/water interface. It, therefore, now becomes apparent that in having to define a 'sedimentary environment' a certain degree of

cyclicity is introduced into trying to define diagenesis. Winkler's definition of diagenesis could perhaps be improved if it contained a more rigorous definition of a 'sedimentary environment'. Figure 27 indicates the deliniation of diagenesis in P—T space relative to metamorphism.

Attempts to establish a pre—metamorphic facies subdivision scheme (i.e., ankizone and diagenesis) based on 1.0nm peak morphology parameters have been relatively unsuccessful. This is primarily due to the fact that previous investigators have defined pre—metamorphic facies in terms of mineral assemblages (i.e., ankizone=illite, laumonite, lawsonite, prehnite, pumpellyite) and then attempted to delineate the facies in terms of some other parameter that is a function of more than just temperature and pressure (i.e., illite crystallinity values). As a result, a range of illite crystallinity values as varied as the chemistry of the units from which they were derived have been used to mark the diagenesis/ankizone boundry (i.e., $0.32\Delta2\theta$ (Sagon and de Segonzac, 1970), $0.43\Delta2\theta$ (Islam and Hesse, 1983), $0.56\Delta2\theta$ (Frey et al, 1980), $0.64\Delta2\theta$ (Chennaux et al, 1970)). Using the temperatures and pressures derived from the previous chapter on coal (i.e., maximum of $95^{\circ}C$ and 1.27Kbars) the studied strata appear to lie within diagenetic, rather than ankimetamorphic, P—T space (Figure 27).

Traditionally, the crystallinity of illite, sharpness ratios and proportion of smectite in illite/smectite mixed layers have been used to delineate diagenetic substages. One nanometre peak morphology parameters, however, have recently been shown to be less—than—reliable indicators of pressure and temperature due to their maturation dependence on factors such as variable cation activities (Eberl and Hower, 1978). Inaccuracies are especially prevalent in pre—ankizone stages where water and cation circulation is less restricted. For example, variations in [K^{+}/other
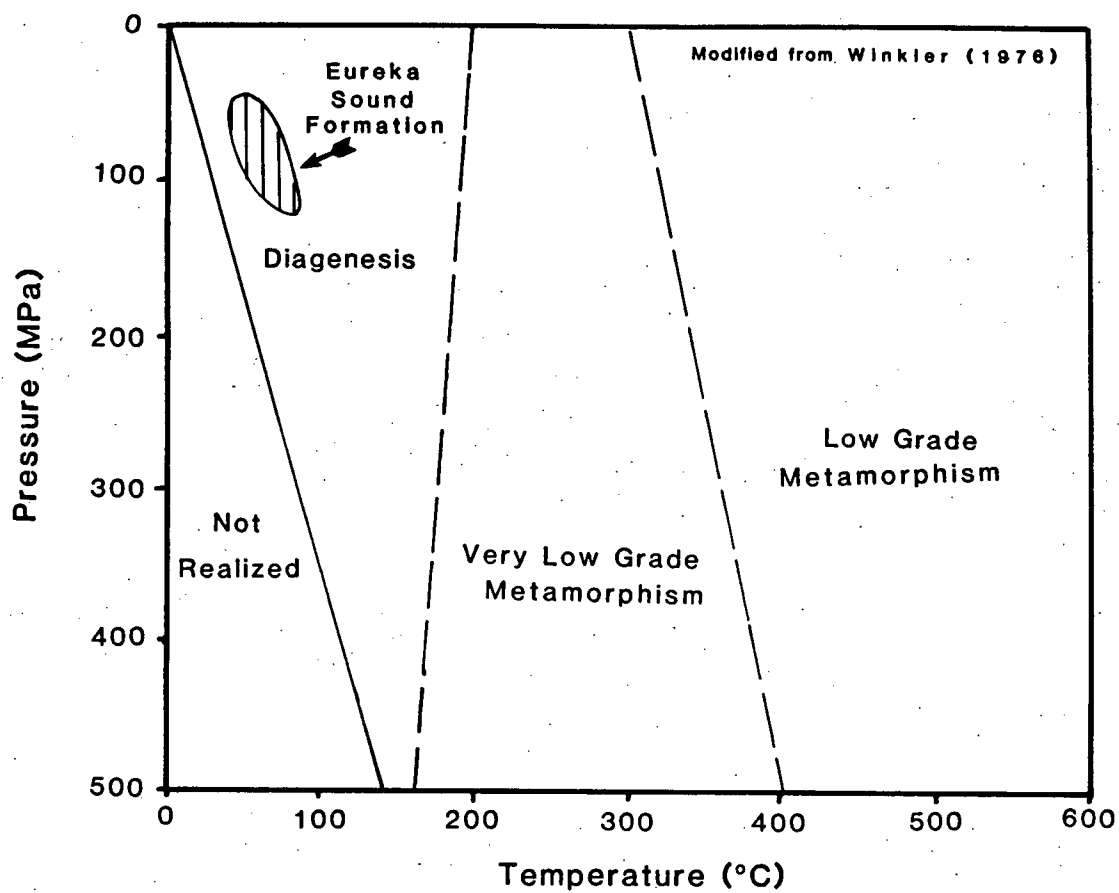
Figure 27. Plot of diagenetic facies in P-T space.

cations] are known to have a significant effect on clay diagenesis parameters. Low $[K^+/Na^+ + Ca^{2+}]$ are suggested by Eberl and Hower (1978) to retard the illitization of smectite while the crystallinity of illite is said by Hower et al (1976) to be directly, related to the activity of K^+ in solution.

Additional problems arise when using clay diagenesis parameters to delineate diagenetic sub–stages. According to Foscolos et al (1976) and Foscolos (1980) variations in expandable layer chemistry and source rock contributions of micaceous material may contribute to the 1.0 nm peak morphology during the early and middle stages of diagenesis. Weaver and Broekstra's (1984) findings support this observation noting that at temperatures less than $360^\circ C$ the width of the (001) peak is affected by the amount and composition of the I/S component present (Srodon, 1978, 1984; Weaver et al., 1984; Srodon and Eberl, 1984). It is, therefore, suggested that variations in 1.0 nm peak morphology parameters with depth are simply reflections of variations in the smectite content of the mixed layers and, therefore, reflections of variations in formation fluid and lithology chemistry. Thus, because illite crystallinity and sharpness ratios are a function of more than just temperature, assigning rocks to a maturation–temperature based classification scheme based on 1.0 nm peak morphology parameters would be in error.

Diagenetic sub–facies are less commonly delineated using $R_o max$ criteria. Because of the extreme temperature dependence and cation independence of vitrinite maturation on organic matter, a diagenetic sub–classification scheme defined by $R_o max$ values appears to be superior. The present study, therefore, uses the classification scheme of Foscolos et al. (1970) to define the diagenetic sub–facies at Strand Fiord. As was mentioned previously, the mean maximum reflectance at the base of the section is approximately 1.0%. Near the top of the section the $R_o max$

decreases to a minimum of approximately 0.48%. These R_0max brackets correspond to eodiagenesis (i.e., where R_0max <0.5%) to early mesodiagenesis (i.e., where R_0max=0.5—1.5%). For comparative purposes the diagenetic stage defined by the clay parameters (i.e., illite crystallinity of up to 0.4 $\Delta 2\theta$) correspond to late meso— (i.e., R_0max= 1.0—1.5%) to early telo— (R_0max$\geq$1.5%) diagenesis. As was mentioned earlier, because thermal disequilibrium with the coals exists the R_0max values are believed to be slightly retarded. It, therefore, seems reasonable that the measured R_0max values would correspond to a lower—than—true diagenetic stage and that the clay parameters *may*, in this case, approach a more accurate measure of the diagenetic stage.

Consideration of Shifts in Clay Parameters with Depth

An examination of figures 24, 25 and 26 indicate that a number of problems exist regarding clay diagenesis parameters that must be considered. These problems include:

1) Why is there a decrease in the sharpness ratio and increase in illite crystallinity index below zone 4. (Such trends are the opposite to what is generally expected with increasing depth).

2) How is the sharp decrease in illite proportion in the I/S mixed layers accounted for at the boundary between zones 3 and 4?

Both of these questions can be answered in part by considering the effects of detrital clay variation with depth.

The primary factors believed to be responsible for producing the observed shifts in clay diagenesis parameters are higher P_{CO_2} and P_{H_2O} in the zone 3 shales than in overlying units. Previously proposed theories, such as a shift from

dioctahedral smectite to trioctahedral smectite between two units (Bustin, 1977) must be discounted in this case as an examination of (060) peaks indicates that trioctahedral 2:1 silicates are absent from the entire section.

Late diagenetic decarboxylation of organic matter is generally accepted to increase the acidity of an environment through the production of CO_2 . Foscolos et al (1980), Hurst and Irwin (1982) and Srodon and Eberl (1984) suggest that illite responds to increasing acidity by 'opening' its interlayer spaces. The result of 'opening' illite is that bonds between interlayer cations and tetrahedral sheets are weakened whereby interlayer K^+ may be lost or substituded with other cations. In order to preserve charge neutrality, elemental rearrangement within the tetra— and octahedral layers could favor the retrograde conversion of illite to illite—smectite under sufficiently hydrated and sodium—rich conditions. An increase in P_{CO_2}, therefore, can produce changes in the illite crystal lattice which will be reflected in illite crystallinity, sharpness ratio and the proportion of illite in I/S values given that the cation chemistry is correct. The increase in kaolinite proportions within zones 2 and 3 supports the idea that the environment was acidic and K^+—poor as kaolinite is known to be stable under low pH, low [K^+/H^+] conditions.

A second theory which may account for the observed shifts in clay parameter trends is the presence of a possible P_{H_2O} differential between zones 3 and 4. Studies by Eberl and Hower (1978) have suggested that smectite will resist illitization under conditions of elevated P_{H_2O}. Denoyer de Segonzac (1970) also notes that under sufficiently hydrated conditions smectite will resist being transformed to illite. Low [K^+/other cations], supported by the persistence of kaolinite through zones 2 and 3, may also retard the illitization of smectite.

Consideration of Variations in Sample Mineralogy with Depth

As was mentioned previously, due to the coincidence of clay boundaries and paleo—environments it is believed that the trends in bulk shale mineralogy represent trends in detrital mineralogy rather than the diagenetic production of one clay at the expense of another. Chemical microenvironments may, however, exist which produce authigenetic variations in clays within each separate zone. Likewise, intrazonal trends in mineralogy which appear to represent diagenetic reactions with depth may be nothing more than changes in paleo—environment such as deepening of the basin, dissipation of flow energy and competence.

A good deal of evidence suggests that the chlorite occurring through zone 4 is of detrital rather than authigenic origin. First, authigenic chlorite was not detected in the zone 4 sandstones. Granted that the fluid chemistry could have differed some what between the sandstone and adjacent shales, both the absence of chlorite from, and presence of Mg—poor/free ankerite (see previous chapter) in, the sandstones may suggest that the bulk formation fluid chemisty was depleted in Mg.

Second and third, previously reported diagenetic chloritization reactions are said to occur under conditions of higher temperature and Mg activity than observed at Strand Fiord. For example, Boles and Frank (1979) found, in a study of the Wilcox Group of southwest Texas, that the following chloritization reaction occurred over a temperature range of 150—200°C vs the 54—100°C range at Strand Fiord.

$$3.5Fe^{2+} + 3.5Mg^{2+} + 9H_2O + 3Kao = Chlorite + 14H^+$$
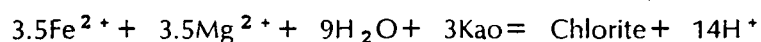
The Mg^{2+} and Fe^{2+} necessary for the conversion of kaolinite to chlorite was believed to be derived from the illitization of smectite. Magnesium concentrations in

the Eureka Sound strata from Strand Fiord are believed to be too low to promote the diagenetic formation of chlorite as ankerites from the section are found to be Mg^{2+} void to extremely Mg^{2+} poor (i.e., <5% Mg in Fe—Mg solution sites). A second chloritization reaction which produces the observed trends in clay mineralogy through zone 4 is presented by Hower et al (1976) where by smectite is converted to illite and chlorite as follows:

$$smectite + K^+ = illite + quartz + chlorite$$
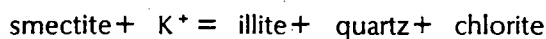
This reaction, as well, must be discounted as the previous section modelled that low K^+ activity may have contributed to producing the problems in clay diagenesis parameters.

A final factor which supports the detrital origin of chlorite is that the chlorite is restricted to, and of constant proportion through, zone 4. The chlorite is also associated with a lesser amount of kaolinite than occurs elsewhere through the section which may suggest a change in either source rock or provenance from humid to arid or temperate conditions (i.e., minimal leaching of the soil, moderate pH). Additonal kaolinite, in this case, could come from neoformation in a an environment of low [K^+] and a high Al:Si ratio (Zen, 1959; Rex and Martin, 1966). An alternatively humid source terrain could also produce the observed trends in chlorite and kaolinite through zone 4 if the chlorite source terrain was close to the depositional environment whereby transport time and distance would be short. Alternatively, if transport distances were greater and degraded 2:1 silicated were delivered to a Mg—enriched environment chlorite could still form from the aggradation of Mg^{2+} by the degraded 2:1 silicates. A study by Perry and Hower (1970) found a trend in mineralogy similar to that through zone 4 in a well from the Gulf coast that was interpreted as reflecting only detrital mineralogy. Basically,

an increase in the chlorite and discrete illite content was found to correspond to a change in depositional environment from middle and outer neritic to offshore.

SUMMARY AND CONCLUSIONS

General Summary

The major conclusions drawn from the present study are as follows:

1) The offset in the coalification gradient in the study area is attributed primarily to the preferential horizontal migration of heated Na^+—enriched waters into permeable units (coal seams and sandstones) from stratigraphically adjacent diapirs. Additional minor contributions to producing the observed offset are thought to come from bulk thermal conductivity differences between the lithologies that contain the organic matter.

2) Low r^2 values from the coalification gradients are attributed to the cessation of high heat flow from the diapirs before thermal equilibrium with the organic matter was attained. This reduction in heat flow is thought to be associated with the unrooting of diapirs with their source at depth.

3) The pre—tectonic thickness of Eureka Sound, and possibly Beafort, Strata is thought to lie between 5200 and 6800 m. Low r^2 values from the coalification gradients subject these thickness values to a moderate degree of uncertainty, however, these thicknesses are in relative agreement with previously proposed tectonic models.

4) Time-temperature modelling of the coalification gradients suggest that a geothermal gradient of 18.3 °C/km is recorded in the studied strata. Temperatures at the top of the section were calculated using methods of Lopatin (1971) and Barker (1983) to be 45°C and 14°C, respectively. Mid—section maximum .

temperatures of 75°C and 83°C, respectively, were calculated using these same methods. Again, due to the low r^2 values from the coalification gradients these calculated temperatures only serve as first approximations of actual temperatures.

5) Six principal authigenic phases were detected in the sandstones from the studied section. These include: dawsonite, ankerite, calcite, siderite, kaolinite and quartz overgrowths. Also present are a number of accessory authigenic phases which include pyrite, FeO_x, illite, rutile and sphene.

6) Two generations of quartz overgrowths are recognized in the studied sandstones. The first formed early in the diagenetic sequence prior to the initial precipitation of calcite. The second formed after the dissolution of the framework aluminosilicates but prior to the precipitation of kaolinite and dawsonite.

7) Two generations of calcite precipitation are also recognized. Initial calcite precipitation occurred relatively early in the diagenetic sequence after the precipitation of first generation quartz overgrowths but prior to the precipitation of ankerite. Second generation calcite formed late in the diagenetic cycle (possibly post tectonically) prior to the precipitation of kaolinite and dawsonite but after the precipitation of ankerite.

8) The precipitation of dawsonite is synchronous with the precipitation of kaolinite. Both minerals are thought to precipitate as the Al^{+3}—organic complexes responsible for the dissolution of the aluminosilicate eventually destabilize and release free Al^{+3} back into solution. The Na^+ necessary for the precipitation of dawsonite is thought to originate from the dissolution of halite in adjacent diapirs.

9) The distribution of clay minerals with depth is believed to reflect primarily detrital and chemical variations between lithofacies rather than the diagenetic alteration of clay minerals. However, *within* the separate lithofacies there is evidence to support the diagenetic alteration of illite and illite/smectite mixed layers with depth.

These above mentioned conclusions are used in the following section to summarize the diagenetic and sedimentologic developement of the Eureka Sound Formation at Strand Fiord.

Discussion

Diagenetic analyses from the previous 3 chapters suggest that 6 separate bio- and physiochemical events are recorded in the Eureka Sound strata at Strand Fiord. These events include:

1) **Subaerial Weathering—** Although poor control is had on the paleogeography of the Eureka Sound Formation source area at Strand Fiord it is believed, due to the high percentage of kaolinite in the shales, that erosion of the sediment source occurred under predominantly humid conditions. As a result, the only major clay types other than kaolinite to be delivered to the basin would have been degraded 2:1 and 2:1:1 silicates. A possible exception, however, is seen in zone 4 where the chlorite may be of detrital origin if its transport distance had been relatively short and subaerial degradation minimal.

2) **Subaqueous Aggradation and Neoformation-** Prior to the deposition and burial of the degraded clay minerals within the different sedimentary environments a number of modifications occurred to these minerals while still in the water

column and at the sediment/water interface. First, in zones 2, 3, and 5 aggregation of Na^+, K^+, and Ca^{+2} by the degraded 2:1 silicates occurred to form smectite and illite in Mg^{+2}-poor, $K^+ + Na^+$ enriched environments. Second, in zone 4 aggregation of Mg^{+2} by the degraded 2:1:1 silicates in a Mg^{+2} enriched K^+ depleted environment lead to the production of chlorite. Rapid flocculation and possible neoformation of kaolinite also occurred in zone 4 there was a high Al^{+3}/Si^{+4} ratio and low K^+/H^+ ratio (Figure 28).

3) **Sediment/Water Interface Reactions (Diagenesis A)-** Both pyrite and siderite formed during diagenesis A under near surface conditions where the Eh was relatively low ($<0.35v$ and Fe^{+2} activity relatively high. Pyrite and siderite did not form synchronously, however, but rather the former gave way to the latter with depth as sulfide activity decreased and P_{CO_2} increased on passing from the zone of sulfate reduction to the zone of methanogenesis. Eventually, as the concentration of Fe declined the precipitation of siderite ceased.

4) **Shallow Burial (Diagenesis B)-** As sediment compaction progressed pressure solution resulted in the the early mobilization of silica and, in this case, the subsequent formation of first generation quartz overgrowths. Also during the early stages of shallow burial the smectite-illite transformation was still primarily in the first stage of smectite dehydration where little or no lattice rearrangement was occurring. As a result very little, if any, Fe^{+2} was being liberated by the illite into the formation waters at this time. First generation calcite which precipitated at this time formed, therefore, under conditions of reduced Fe^{+2} activity and elevated CO_2 partial pressure.

Subaqueous Aggradation and Neoformation
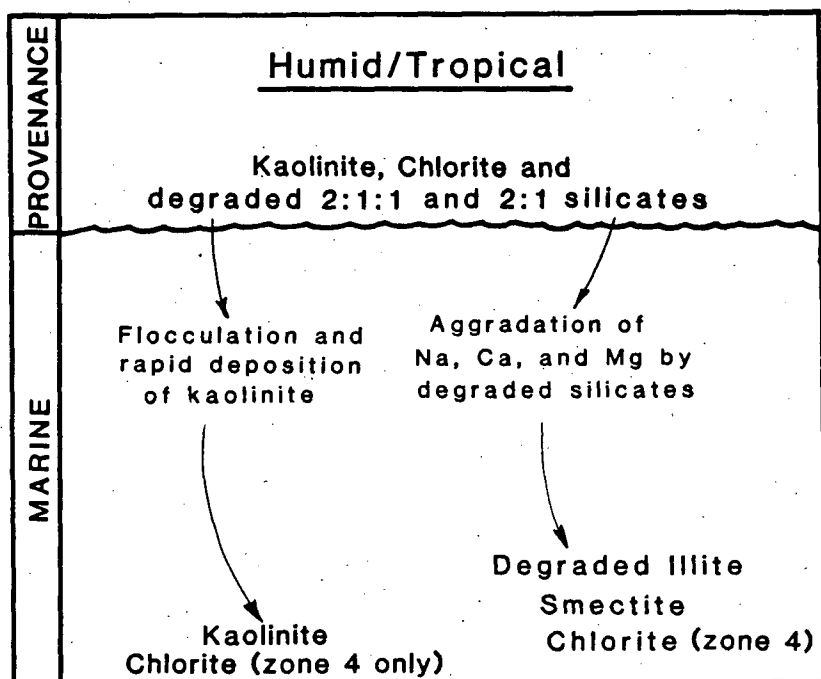
Figure 28- Summary diagram of early stage subaqueous aggradation and neoformation of clay minerals under humid/tropical source conditions.

5) **Deep Burial (Diagenesis C)-** During the deep burial diagenetic stage, just prior to the onset of the Eurekan Orogeny, the studied strata were buried to a maximum depth of between 5500 and 6800 m. Hydrostatic pressures at this time were close to 127 MPa at the base of the section with temperatures of up to 95°C. It was under these conditions that porosity enhancement within the sandstones began to occur as increased carboxylic acid activity resulted in the dissolution of the framework aluminosilicates through organic complexing with Al^{+3}. Second generation calcite cementation also occurred during this stage in association with the framework aluminosilicate dissolution (Figure 29). Prior to the dissolution of the aluminosilicates, however, ankerite precipitated at the expense of the previous generation carbonates in response to increasing Fe^{+2} associated with the illitization of smectite and continued high CO_2 partial pressures.

Within the shales during diagenesis C, intra-zonal variations in fluid chemistry and permeability lead to the following phenomena:

a) Zones 2 and 3- retardation of smectite-illite transformation due to elevated P_{H_2O} and low $[K^+/Na^{+2}+Ca^{+2}]$. Possible retrograde conversion of smectite to illite due to elevated P_{CO_2} and $[H^+/K^+]$.

b) Zones 4 and 5- conversion of smectite to illite due to lower P_{H_2O} than in the previous stages. Conversion of previous carbonates to ankerite through the liberation of Fe^{+2} in the smectite-illite transformation.

Toward the end of diagenesis C second generation quartz overgrowths formed as silica continued to be released into solution through the progressive illitization of smectite in the associated shales.

Deep Burial (Diagenesis C)
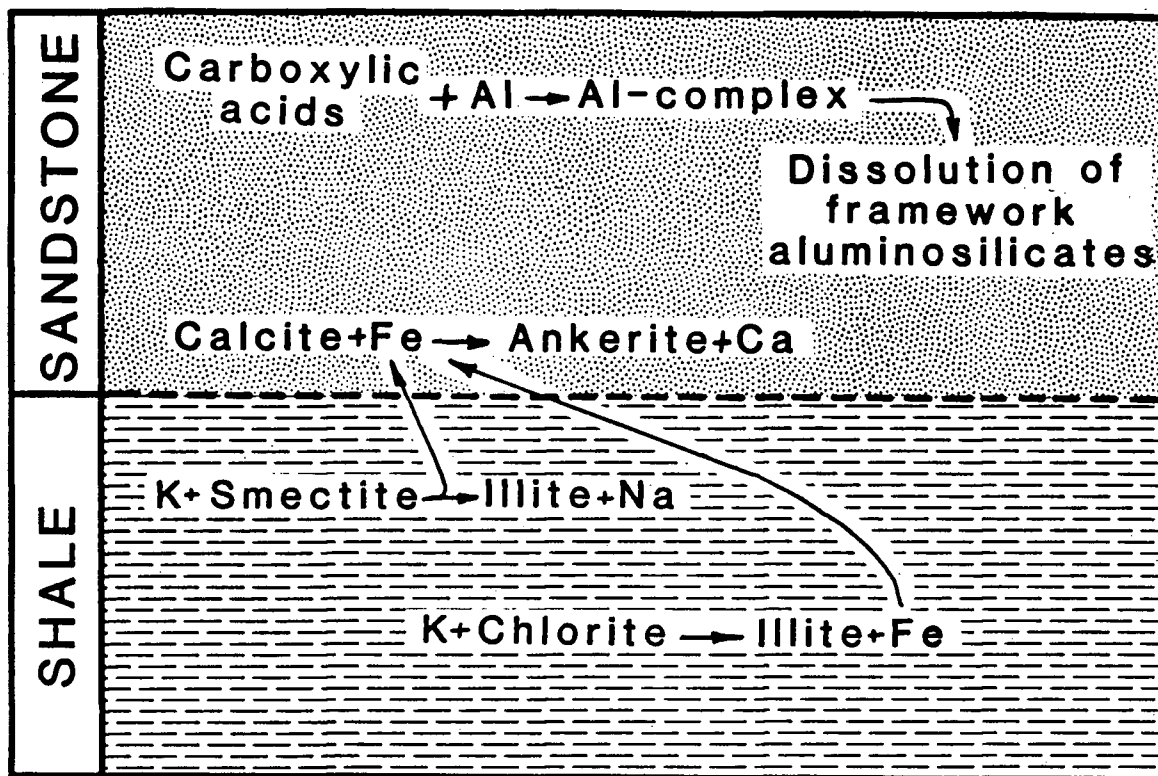
Figure 29- Summary diagram of deep burial diagenetic environment.

6) **Syn-/post Orogenic Reactions (Diagenesis D)-** It is the syn- and post-orogenic diagenetic events that leave the most prominent imprint on the many diagenetic parameters of the Eureka Sound Formation at Strand Fiord. Up until this point, the thermal maturation of the strata had been relatively uniform and free from complications created by heat flow anomalies. However, with the progression of the Eurekan Orogeny and associated diapir mobilization diagenetic conditions were created in the strata which altered the strata's relatively simple paragenetic history. Heat flow anomolies created by proximity of the strata to the diapirs in the area produced a significant alteration of the maturation signature on the organic matter. Not only did the circulation of the heated waters from the diapir tend to selectively mature that vitrinite in the sequence which was associated with the most permeable strata (i.e., the coals v.s. the phytoclasts) but the waters also left a mineralogic trace of their presence in the sandstones. Due to the water's source of origin (i.e., the halite core of the diapirs) they were greatly enriched in Na^+. Aluminum concentrations as well began to increase as the organically complexed Al^{+3} produced during the deep burial diagenesis stage began to destabilize with changing pH and liberate Al^{+3} back into solution. The net result was to create an environment that was enriched in both Na^+ and Al^{+3} under a sufficiently high P_{CO_2} to favor the near synchronous precipitation of dawsonite and kaolinite (Figure 30).

Hydrostatic pressure during diagenesis D was lower than during diagenesis C as uplift and erosion resulting from the Eurekan Orogeny tended to reduce the thickness of the overlying strata. Temperatures, on the other hand, remained sufficiently high for that period immediately following uplift while the diapirs remained rooted to their source at depth. The strata began to cool only once

Syn/post Orogenic (Diagenesis D)
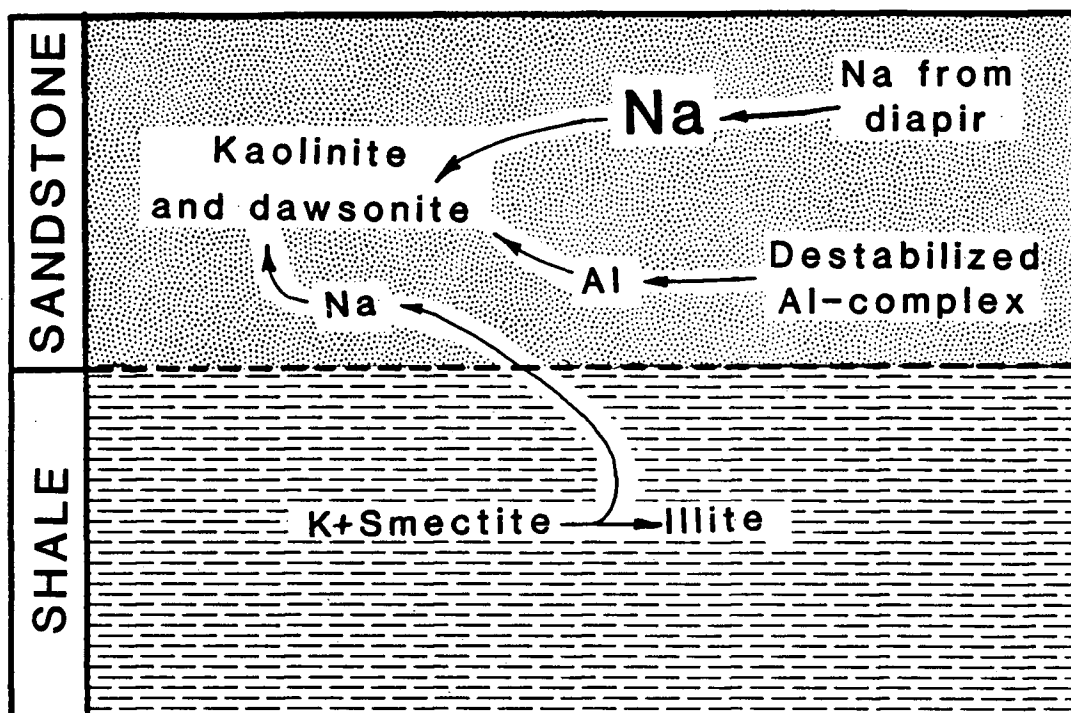
Figure 30- Summary diagram of post/syn-tectonic diagenetic environment.

the diapirs began to separate from their source and migrate further upwards toward shallower depths.

REFERENCES

Almon, W. R., and Davies, D. K., 1981, Formation damage and the crystal chemistry of clays: *In:* F. J. Longstaffe , ed., Short Course in Clays and the Resource Geologist: Mineralogical Association of Canada Short Course, Calgary, p. 81-103.

American Society for Testing and Materials (ASTM), D-2797 (Reapproved, 1980), Preparing coal samples for microcopical analysis by reflected light: Philadelphia, Pennsylvania.

Balkwill, H. R., 1973, Structures and teconics of the Cornwall Arch, Amond Ringes and Cornwall Islands, Arctic Archipelago; *In:* Geology of Arctic Canada (J. D. Aitker and D. Glass (eds.)), Geological Association of Canada and Canadian Society of Petroleum Geologists, Symposium Procedings, p. 39-62.

Balkwill, H. R., 1978, Evolution of the Sverdrup Basin, Arctic Canada: American Association of Petroleum Geologists Bulletin, v. 62, p. 1004-1028.

Balkwill, H. R., Bustin, R. M., and Hopkins, W. S., 1975, Eureka Sound Formation at Flat Sound, Axel Heiberg Island, and the chronology of the Eurekan Orogeny: Geological Survey of Canada, Report of Activities, Paper 75-1B p. 205-207.

Balkwill, H. R., and Bustin, R. M., 1980, Late Phanerozoic structures, Canadian Arctic Archipelago: Paleogeography, Paleoclimatology, Paleoecology, v. 30, p. 219-227.

Balkwill, H. R., Hopkins, W. S., and Wall, J. H., 1982, Lougheed Island, District of Franklin: Geological Survey of Canada, Memoir 388.

Barker, C. E., 1983, Influence of time on metamorphism of sedimentary organic matter in liquid-dominated geothermal systems, western North America: Geology, v. 11, p. 384-388. American Society of Agronomy, Inc., Madison, Wisconson, 1965.

Bates, B. L. and Jackson, J. A., 1980, eds., Glossary of Geology, Second edition, American Geological Institute, Falls Church, Va., 749 p.

Bayliss, P., Levinson, A. A., and Klovan, J. E., 1970, Mineralogy of bottom sediments, Hudson Bay, Canada: Bulletin of Canadian Petroleum Geologists, v. 18, p. 467-473.

Black, C. A., Methods of Soil Analysis, Pt. 1, Physical and Mineralogical Properties, includin Statistics of Measurements and Sampling;

Boles, J. R., 1978, Active ankerite cementation in the subsurface Eocene of southwest Texas: Contrib. Mineral. Petrol., v. 68, p. 13-22.

Boles, J. R., and Franks, S. G., 1979, Clay diagenesis in the Wilcox Sandstones of southwest Texas: Implications of smectite diagenesis on sandstone cementation: Journal of Sedimentary Petrology, v. 49, no. 1, p. 55-70.

Bostick, and Alpern, B., 1977, Principles of sampling, prepation and constituent selection for microphotometry in the measurement of maturation of sedimentary organic matter: Journal of Microscopy, v. 109, pt. 1, p. 41-47.

Brown, G., 1961, X-ray Identification and Crystalline Structure of Clay Minerals, Second edition, Mineralogical Society of London, 544 p.

Bruce, C. H., 1984, Smectite dehydration- its relation to structural developement and hydrocarbon accumulation in northern Gulf of Mexico Basin: American Association of Petroleum Geologists Bulletin, v. 68, p. 673-683.

Burst, J. F., 1969, Diagenesis of the gulf coast clayey sediments and its possible relation to petroleum migration: American Association of Petroleum Geologists Bulletin, v. 53, p. 73-93.

Bustin, R. M., 1977, The Eureka Sound and Beaufort Formations, Axel Heiberg and West -central Ellesmere Island, District of Franklin. Unpublished M.Sc. thesis, The University of Calgary, Calgary, 207 p.

Bustin, R. M., in press, Organic maturity of late Cretaceous and Tertiary coal measures, Canadian Arctic Archipelago. Coal Geology.

Bustin, R. M., Hills, L. V., and Gunther, P. R., 1977, Implications of coalification levels, Eureka Sound formation, northwestern Arctic Canada: Canadian Journal of Earth Science, v. 14, p. 1588-1597.

Bustin, R. M. and Bayliss, P., 1979, Clay mineralogy of the Eureka Sound and Beaufort formations, Axel Heiberg and West central Ellesmere Islands, eastern Canada, Arctic Archipelago: Bulletin of Canadian Petroleum Geology, v. 27, no. 4, p. 446-452.

Bustin, R. M., Cameron, A. R., Grieve, D. A. and Kalkreuth, W. D., 1983, Coal Petrology: Its Principles, Methods and Applications. Geological Association of Canada Short Course Notes, v. 3, 273 p.

Carothers, W. W., and Kharaka, Y. K., 1978, Aliphatic acid anions in oil field waters- implications for origin of natural gas: American Association of Petroleum Geologists Bulletin, v. 62, p. 2441-2453.

Chave, K. E., 1960, Evidence of sea water from chemistry of deeper subsurface waters of ancient basins: American Association of Petroleum Geologists Bulletin, v. 44, p. 357-370.

Chennaux, G., Dunoyer de Segonzac, G., and Petracco, F., 1970. Genese de la pyrophyllite dans le paleozoique du Sahara occidental. Acad. Sci., C. R., Ser. D, v. 270, no. 20, p. 2405-2408.

Clark, S. P. Jr. (ed.). Handbook of Physical Constants, Revised Edition. GSA memoir 97.

Corazza, E, Sabelli, C., and Vanucci, S., 1977, Dawsonite: new mineralogical data and structural refinement: Neus Jahrbuch fur Mineralogie, v. 1977 p. 381-397.

Crossey, L. J., Frost, B. R., and Surdam, R. C., 1984, Secondary porosity in laumontite bearing sandstones. In: Clastic Diagenesis, D. A. McDonald and R. C. Surdam (eds.), American Association of Petroleum Geologists Memoir 37, p. 225-238.

Curtis, C. D., and Spears, D. A., 1968, The formation of sedimentary iron minerals: Economic Geology, v. 63, p. 257-270.

Davies, G. R., 1975, Hoodoo I-41: diapiric halite facies of the Otto Fiord Formation in the Sverdrup Basin, Arctic Archipelago: Geological Survey of Canada Paper 75-1, pt. C., p23-29.

Denoyer de Segonzac, 1970, The transformation of clay minerals during diagenesis in lower grade metamorphism: Sedimentology, v. 15, p. 281-396.

Eberl, D., 1984, Clay mineral formation and transformation in rocks and soils: Phil. Trans. Royal Soc. London, A311, p. 241-257.

Eberl, D. and Hower, J., 1976, Kinetics of illite formation: Geological Society of America Bulletin, v. 87, p. 1326-1330.

Ehlers, and Blatt, H., 1982, Petrology: igneous, sedimentary and metamorphic, P. C. Vapnek (ed.), W. H. Freeman and Co..

England, T., 1984, Thermal maturation of the Western Canada Sedimentary Basin in the Rocky Mountain Foothills and Plains of Alberta south of the Red Deer River: M. Sc. Thesis, University of British Columbia.

Eugster, H. P., 1978: Saline Lakes. Lakes-Chemistry, Geology, Physics. A. Lerman (ed.). Springer-Verlag, New York, pp. 237-293.

Ferrante, M. J., Stuve, J. M., and Richardson, D. W., 1976, Thermodynamic data for synthetic dawsonite: United States Bureau of Mines Report of Investigations, v. 8129 p. 13 p.

Fortier, Y. O., Blackadar, B. F., Glenister, B. F., Greiner, H. R., McLaren, D. J., McMillan, N. J., Norris, A. W., Roots, E. F., Souther, J. G., Thorsteinson, R., Tozer, E. T., 1963, Geology of the north-central part of the Arctic Archipelago, Northwest Territories (Operation Franklin). Geological Survey of Canada, Memoir 320.

Foscolos, A. E., and Kodama, H., 1974, Diagenesis of clay minerals from lower Cretaceous shales of northeastern British Columbia: Clays and Clay Minerals, v. 22, p. 319-335.

Foscolos, A. E., and Powell, T. G., 1978, Mineralogy and geochemical transformation of clays during burial diagenesis (catagenesis): Relation to oil generation, *In*: Developements in Sedimentology 27, Mortland M. M. and Farmer, V. C. (eds.), Elsevier.

Foscolos, A. E., 1984, Diagenesis 7. Catagenesis of argillaceous sedimentary rocks: Geoscience Canada, v. 11, p. 67-75.

Frey, M., Teichmuller, M., Teichmuller, R., Mullis, J., Kunzi, B., Brestschmidt, A., Gruner, U., and Schwizer, B., 1980. Very low grade metamorphism in external parts of the central Alps: illite crystallnity, coal rank and fluid inclusion data. Ecolgae Geologicae Helvetiae, 73, p. 173-203.

Fricker, P. E., 1963, Geology of the Expedition Area, western central Axel Heiberg Island, Canadian Arctic Archipelago. Axel Heiberg Island Research Reports, McGill University, Montreal. Geology No. 1.

Fujii, K., Sumic, Y., Shoda, K., and Miki, K., 1982, Effect of degradinite on coal properties and its conversion at Ikeshima Coal Mine: American Association of Petroleum Geologists Bulletin, v. 66, p. 968.

Garrels, R. M., and Christ, C. L., 1965, Solutions, minerals and equilibria: San Francisco, Freeman, Cooper, and Co., 450 p..

Gould, D. B., and DeMille, G., 1964, Piercement structures in the Arctic Islands: Bulletin of Canadian Petroleum Geology, v. 12, p. 719-753.

Gretener, P. E., 1981, Geothermics: Using temperature in hydrocarbon exploration: American Association of Petroleum Geologists Education Course Note Series #17.

Hancock, N. J., and Taylor, A. M., 1978, Clay mineral diagenesis and oil migration in the Middle Jurassic Brent Sand Formation: J. Geol. Soc. Lond., v. 135, p. 69-71.

Hay, R. L., 1963, Zeolite weathering in Oldavai Gorge, Tanganyika: GSA Bulletin, v. 74, p.1281-1286.

Helgeson, H. C., 1969, Thermodynamics of hydrothermal systems at elevated temperatures: AJS, v. 267, p. 729-804.

Helgeson, H. C., Brown, T. H., Nigrini, A., and Jones, T. A., 1970, Calculation of mass transfer in geological processes involving aqueous solutions: Geochimica et Cosmochimica Acta, v. 34, p. 569-592.

Hitchon, B., 1984, Geothermal gradient, hydrodynamics and hydrocarbon occurance, Alberta, Canada: American Association of Petroleum Geologists Bulletin, v. 68, no. 6, p. 713-743.

Hobbs, B. E., Means, W. D., and Williams, P. F., 1976, An Outline of Structural Geology, John Wiley and Sons, Inc, U. S. A., 571 p.

Holland, H. D., and Borcsik, M., 1965, On the solution on depostion of calcite in hydrothermal systems: Symposium on the problems of postmagmatic ore deposition, Prague, no. 2, p. 364-374.

Hower, J., Eslinger, E. V., Hower, M. E., and Perry, E. A., 1976, Mechanism of burial metamorphism of argillaceous sediment: I Mineralogy and chemical evidence: Geological Society of America Bulletin, v. 87, p. 725-737.

Hower, J., 1981, Shale diagenesis, M.A.C. Short Course in Clays and the Resource Geologist, F. J. Longstaff (ed.), p. 60-80.

Hower, J., 1981, X-ray identification of mixed-layer clay minerals: M.A.C. Short Course in Clays and the Resource Geologist, F. J. Longstaff (ed.), p. 39-59.

Hurst, A., and Irwin, H., 1982, Geologic modelling of clay diagenesis in sandstones: Clay Minerals, v. 17, p. 5-22.

Hutcheon, I., Oldershaw, A., and Ghent, E. D., 1980, Diagenesis of the Kootenay Formation at Elk Valley (southeastern British Columbia) and Mount Allan (southwestern Alberta), Geochimica et Cosmochimica Acta, v. 44, p. 1425-1435.

Hutcheon, I., 1981, Application of thermodynamics to clay minerals and authigenic mineral equilibria: M.A.C. Short Course in Clays and the Resource Geologist, F. J. Longstaffe (ed.), p. 169-192.

Hutcheon, I., 1983, Diagenesis 3. Aspects of diagenesis of coarse grained siliciclastic rocks: Geological Association of Canada, v. no. p. 4-14.

Hutton, A. C., and Cook, A. C., 1980, Influence of alginite on the reflectance of vitrinite from Joadja, NSW, and some other coals and oil shales containing alginite: Fuel, v. 59, p. 711-714.

Islam, S., Hesse, R., and Chagnon, A., 1982. Zonation of diagenesis and low-grade metamorphism in Cambro-Orovician flysh of Gaspe peninsula, Quebec Appalacians. Canadian Mineralogist, v. 20, p. 155-167.

Jackson, M. L., 1956. Soil Chemical Analysis- Advanced Course. (fifth printing, 1969). Published by the author, Dept. of Soil Science, University of Wisconsin, Madison, Wis. 53706, 894 p..

Karweil, J., 1956, Die Metamorphose der Kohlen Stand punkt der physikalischen Chemie; Z. Deutsch. Geol. Ges., v. 107, p. 132-139.

Keller, W. D., 1970, Environmental aspects of clay minerals: Journal of Sedimentary Petrology, v. 40, p. 788-854.

Kerr, P. F. (ed.), Optical Mineralogy, Fourth edition, McGraw Hill, Inc., 492 p.

Krumbein, W. C., and Sloss, L. L., 1963, Stratigraphy and Sedimentation, Second Edition, J. Gilluly and A. O. Woodford (eds.), W. H. Freeman and Company, 660 p..

Kubler, B., 1964, Les argiles, indicateurs de métamorphisme. Rev. Inst. Franç. Pétrole, v. 19, p. 1093-1112.

Kubler, B., 1966, La cristallinité de l'illite et les zones tout à fait supérieures du métamorphisme. In: Colloque sur les Etages Tectoniques. A la Baconnière, Neuchâtel, p. 105-122.

Kunze, G. W., 1955, Anomalies in the ethylene glycol solution techniques used in x-ray diffraction: Clays and Clay Minerals, 2, p. 88-93.

Matsumoto, R., and Iijima, A., 1981, Origin and diagenetic evolution of Ca-Mg-Fe carbonates in some coalfields of Japan: Sedimentology, v. 28, p. 239-259.

Menely, R. A., Henao, R. K., and Merritt, R. K., 1975, The north west margin of the Sverdrup Basin, pp.531-544: in Yorath, C. J., Parker, E. R., and Glass, D. J. (eds.), Canadas Continental Margins and Offshore Petroleum Exploration, Canadian Society of Petroleum Geologists Memoir 4, 898 p.

Meddaugh, W. S., and Scott, C. A., 1983. Mineralogy and geochemistry of Green River Formation Oil Shales, C-A Tract, Colorado: In. 16th Oil Shale Symposium Proc., J. H. Gary (ed.), Colorado School of Mines.

Merino, E., 1975a, Diagenisis in the Tertiary sandstone from Kettleman North Dome, California. I. Diagenetic mineralogy: Journal of Sedimentary Petrology, v. 45, no. 1, p. 320-336.

Merino, E., 1975b, Diagenisis in the Tertiary sandstone from Kettleman North Dome, California. II. Interstitial solutions: distribution of aqueous species at 100°C Geochimica et Cosmochimica Acta, v. 39, p. 1629-1645.

Miall, A. D., 1984, Variations in fluvial style in the Lower Cenozoic synorogenic sediments of the Canadian Arctic Islands: Sedimentary Geology, v. 38, p. 499-523.

Miall, A. D., in press, The Eureka Sound Group (Upper Cretaceous-Oligocene), Canadian Arctic Islands: Canadian Society of Petroleum Geologists Bulletin.

Middleton, M. F., 1982, Tectonic history from vitrinite reflectance: Geophysical Journal R.A.S., v. 68, p. 121-132.

Millot, G., 1970, Geology of Clays: Weathering, Sedimentology and Geochemistry: Masson et Cie, Paris.

Moncure, G. K., Lahana, R. W., and Siebert, R. M., 1984, Origin of secondary porosity and cement distribution in a sandstone/shale sequence from the Frio Formation (Oligiocene), In: Clastic Diagenesis, D. A. McDonald and R. C. Surdam (eds.), American Association of Petroleum Geologists Memoir 37, p. 151-162.

Nurkowski, J. R., 1984, Coal quality, coal rank variation and its relation to reconstructed overburden, Upper Cretaceous and Tertiary Plains Coals, Alberta, Canada: American Association of Petroleum Geologists Bulletin, v. 68, no. 3, p. 285-295.

Perry, E., and Hower, J., 1972, Late stage dehydration in deeply buried pelitic sediments. American Association of Petroleum Geologists Bulletin, v. 56, p. 2013-2021.

Perry, C., and Gillot, G. E., 1979, The formation and behavior of montmorillonite during the use of wet forward combustion in the Alberta Oil Sands Deposits: Bulletin of Canadian Petroleum Geologists, v. 27, p. 314-325.

Powel, T. G., Foscolos, A. E., Gunther, P. R., and Srodon, L. R., 1978, Diagenesis of organic matter and fine clay minerals: a comparative study: Geochimica et Cosmochimica Acta, v. 42, p. 1181-1197.

Price, L. C., 1983, Geologic time as a parameter in organic metamorphism and vitrinte refectance as an absolute paleogeothermometer: Journal of Petroleum Geology, v. 6, no. 1, p. 5-38.

Price, L. C., and Barker, C. E., 1985, Suppression of vitrinite reflectance in amorphous rich kerogen- a major unrecognized problem: Journal of Petroleum Geology, v. 8, no. 1, p. 59-84.

Riediger, C., 1985, Sedimentology and Tectonic History of the Tertiary Eureka Sound and Beaufort Formations, Southern Ellesmere Island, Arctic Canada: Unpublished M.Sc. thesis, The University of British Columbia, Vancouver.

Rex, R. W. and Martin, B. D.,1966, Clay mineral formation in sea water by submarine weathering of K-feldspar: Proceed. 14th Conf. Clays and Caly Minerals, Pergamon Press, N.Y., p.235-240.

Reynolds, R. C., Jr., and Hower, J., 1970, The nature of interlayering in mixed-layer illite-montmorillonite: Clays and Clay Minerals, v. 18, p. 25-36.

Rittenhouse, G., 1943, The transportation and deposition of heavy minerals: GSA Bulletin, v. 54, p. 1725-1780.

Robie, R. A., Hemmingway, B. S., and Fisher, J. R., 1978, Thermodynamic properties of minerals and related substances at 298.15°K and 1Bar (10^5 Pascals) pressure and at higher temperatures: USGS Bulletin 1452, 456 p..

Sagon, J. P., and Denoyer de Segonzac, G., 1972. La cristallinite des micas dans les schistes paleozoiques et brioveriens du Bassn de Chateaulin (Massif Ammoricain). C R Academie Sciences ser. D, 275, p. 1023-1026.

Sarkisyan, S. G., 1972, Origin of authigenic clay minerals and their significance in petroleum geology: Sedimentary Geology, v. 7, p. 1-22.

Sedimentology Research Group, 1981, The effects of in situ steam injection on Cold Lake oil sands: Bulletin of Canadian Petroleum Geologists, v. 29, p. 447-478.

Selig, F., and Wallick, G. C., 1966, Temperature distribution in salt domes and surrounding sediments: Geophysics, v. 31, no. 2, p. 346-361.

Shanmugum, G., 1985, Significance of secondary porosity in interpreting sandstone composition: American Association of Petroleum Geologists Bulletin, v. 69, no. 3, p. 378-384.

Siebert, R. M., Moncure, G. K., and Lahanna, R. W., 1984, A theory of framework dissolution in sandstones. In: Clastic Diagenesis, D. A. McDonald and R. C. Surdam (eds.), American Association of Petroleum Geologists Memoir 37, p. 163-176.

Siever, R., 1983, Burial history and diagenetic reaction kinetics: American Association of Petroleum Geologists Bulletin, v. 67, no. 4, p. 684-691.

Smith, J. W., and Young, N. B., 1975, Dawsonite: its geochemistry, thermal behavior, and extraction from Green River Oil SHales: Colorado School of Mines Quarterly, v. 70, p. 69-93.

Sobczak, L. W., Weber, J. R., Goodacre, A. K., and Bisson, J. L., 1963, Preliminary results of gravity surveys in the Queen Elizabeth Islands with maps no. 12-Sverdrup Islands, no.13-Prince Patrick Islands, no. 14-Melville Island, no. 15-Devon Island: Dominion Obsevatory, Ottawa, Gravity Map Series.

Solomon, M., 1963, Counting and sampling errors in modal analysis by point counting: Journal of Petrology, v. 4, part 3, pp. 367-382.

Srodon, J., 1978, Correlation between coal and clay diagenesis in the carboniferous of the upper silesian coal basin, In: Developements in Sedimentology 27, Mortland M. M. and Farmer, V. C. (eds.), Elsevier.

Srodon, J., 1980, Precise identification of illite/smectite interstratification by x-ray powder diffraction: Clays and Clay Minerals, v. 28, p. 401-411.

Srodon, J., and Eberl, D. D., 1984, Illite: Reviews in Mineralogy, v. 13, p. 495-544.

Stott, D. F., 1969, Ellef Ringes Island, Canadian Arctic Archipelago. Geological Survey of Canada, Paper 68-16.

Surdam, R. C., Boese, S. W., and Crossey, L. J., 1984, The chemistry of secondary porosity, In: Clastic Diagenesis, D. A. McDonald and R. C. Surdam (eds.), American Association of Petroleum Geologists Memoir 37, p. 127-149.

—

Thorsteinson, R., 1971, Geology, Strand Fiord, District of Franklin, Geological Survey of Canada., map 1309a

Tozer, E. T., and Thorsteinson, R., 1964, Western Queen Elizabeth Islands, Arctic Archipelago. Geological Survey of Canada, Memoir 332.

Trettin, H. P., 1972, The Innuitian Provence. In Variations in Tectonic Styles in Canada; Price, R. A., and Douglas, R. J. W. (eds.), Geological Association of Canada Special Paper no. 11, p. 83-197.

Waples, D. W., 1980, Time and temperature in petroleum formation: Application of Lopatin's method of petroleum exploration: American Association of

Petroleum Geologists Bulletin, v. 64, no. 6, p. 916-926.

Weaver, C. E., 1960, Possible use of clay minerals in search for oil: American Association of Petroleum Geologists Bulletin, v. 44, p. 1505-1518.

Weaver, C. E., 1961, Clay minerals of the Ouachita structural belt and adjacent foreland. In: The Ouachita System. Bureau Econ. Geol., Austin, Texas, p. 147-160.

Weaver, C. E., 1967, The significance of clay minerals in sediments, In: B. Nagy and U. Columbo (eds.), Fundamental Aspects of Petroleum Geochemistry. Elsevier, Amsterdam, p. 37-75.

Weaver, C. E., and Associates, 1984, Shale slate metamorphism in southern Appalacians, Developements in Petrology, 10, Elsevier.

Wescott, W. A., 1983, Diagenesis of Cotton Valley Sandstones East Texas: Implications for tight gas formation pay recognition: American Association of Petroleum Geologists Bulletin, v. 67, no. 6, p. 1002-1013.

West, R. M., Dawson, M. R., Hickey, and Miall, A. D., Upper Cretaceous and Paleogene sedimentary rocks of eastern Canadian Arctic and related North Atlantic areas. In Geology og the North Atlantic borderlands. Kerr, J. W., and Ferguson, A. J. (eds); Canadian Society of Petroleum Geologists Memoir 7, p 279-298.

White, D. E., 1965, Saline waters of sedimentary rocks: in Fluids in Subsurface Environments, American Association of Petroleum Geologists Memoir 4, p. 342-366.

Williams, H., Turner, F. J. and Gilbert, C. M., 1982, Petrography: an introduction to the study of rocks in thin section, Second Edition, W. H. Freeman and Co., 626 p..

Wilson, M. D., and Pittman, E. D., 1977, Authigenic clays in sandstones: recognition and influence on reservoir properties and paleoenvironmental analysis: Journal of Sedimentary Petrology, v. 47, no. 1, p. 3-31.

Winkler, H. G. F., 1976, Petrogenesis of metamorphic rocks: Fourth edition, Springer-Verlag, 334 P.

Zen, E., 1959, Clay mineral-carbonate relations in sedimentary rocks: American Journal of Science, v. 257, p. 29-43.

APPENDICES

Preparation: K saturated

SAMPLE	7.0- 7.9	8.0- 8.9	9.0- 9.9	10.0-10.9	11.0-11.9	12.0-12.9	13.0-13.9	14.0-14.9	15.0-15.9	16.0-16.9
RAK 9-25	7.19	-	-	10.10	-	-	-	14.02	-	-
RAK 15-25	7.22	-	-	10.04	-	-	-	-	-	-
RAK 20-25	7.25	-	-	10.10	-	-	-	-	-	-
RAK 23-25	7.19	-	-	10.46	-	12.99	-	-	-	-
RAK 30-25	7.15	-	-	10.16	-	-	-	-	-	-
RAK 33-25	7.17	-	-	10.10	-	-	-	14.25	-	-
RAK 38-25	7.22	-	-	10.10	-	-	-	14.25	-	-
RAK 42-25	7.18	-	-	10.11	-	-	-	14.25	-	-
RAK 43-25	7.22	-	-	10.10	-	-	-	14.25	-	-
RAK 45-25	7.18	-	-	10.10	-	-	-	-	-	-
RAK 46-25	7.22	-	-	10.10	-	-	-	14.14	-	-
RAK 50-25	7.22	-	-	10.10	-	-	-	14.25	-	-
RAK 53-25	7.20	-	-	10.10	-	-	-	14.25	-	-
RAK 57-25	7.10	-	-	10.10	-	-	-	14.25	-	-
RAK 60-25	7.19	-	-	10.10	-	-	-	14.48	-	-
RAK 67-25	7.19	-	-	10.10	-	-	-	-	-	-
RAK 68-25	7.22	-	-	10.52	-	-	-	-	-	-
RAK 71-25	7.22	-	-	10.16	-	-	-	-	-	-
RAK 76-25	7.19	-	-	10.10	11.05	-	-	-	-	-
RAK 78-25	7.22	-	-	10.10	-	-	-	-	-	-
RAK 112-25	7.05	-	9.50	-	-	-	-	-	-	-
RAK 125-25	7.19	-	-	10.10	-	-	-	-	-	-

Preparation: K saturated + ethylene glycol

SAMPLE	7.0- 7.9	8.0- 8.9	9.0- 9.9	10.0-10.9	11.0-11.9	12.0-12.9	13.0-13.9	14.0-14.9	15.0-15.9	16.0-16.9
RAK 9-25	7.22	-	-	10.10	-	-	-	-	-	-
RAK 15-25	7.22	-	-	10.04	-	-	-	-	-	-
RAK 20-25	7.25	-	-	10.16	-	-	-	-	15.36	-
RAK 23-25	7.25	-	-	10.22	-	-	-	14.25	-	-
RAK 30-25	7.19	-	-	10.16	-	-	-	-	-	-
RAK 33-25	7.17	-	-	10.10	-	-	-	14.25	-	-
RAK 38-25	7.22	-	-	10.10	-	-	-	14.25	-	-
RAK 42-25	7.19	-	-	10.10	-	-	-	14.25	-	-
RAK 43-25	7.22	-	-	10.10	-	-	-	14.25	-	-
RAK 45-25	7.19	-	-	10.10	-	-	-	14.26	-	-
RAK 46-25	7.22	-	-	10.10	-	-	-	14.25	-	-
RAK 50-25	7.22	-	-	10.10	-	-	-	14.48	-	-
RAK 53-25	7.10	-	-	10.10	-	-	-	14.48	-	-
RAK 57-25	7.22	-	-	10.11	-	-	-	14.37	-	-
RAK 60-25	7.20	-	-	10.10	-	-	-	14.25	-	-
RAK 67-25	7.25	-	-	10.11	-	-	-	-	-	-
RAK 68-25	7.20	-	-	10.10	11.40	-	-	-	-	-
RAK 71-25	7.28	-	-	10.16	-	-	-	14.48	-	-
RAK 76-25	7.20	-	-	10.10	-	-	-	-	-	-
RAK 78-25	7.19	-	-	10.10	-	-	-	-	-	-
RAK 112-25	7.05	-	-	10.10	-	-	-	-	-	-
RAK 125-25	7.25	-	-	10.10	-	-	-	-	-	-

Preparation: Mg saturated

SAMPLE	7.0- 7.9	8.0- 8.9	9.0- 9.9	10.0-10.9	11.0-11.9	12.0-12.9	13.0-13.9	14.0-14.9	15.0-15.9	16.0-16.9	17.0-17.9
RAK 9-25	7.19	-	-	10.11	11.63	-	-	14.25	-	-	-
RAK 15-25	7.19	-	-	10.10	-	12.62	-	14.25	-	-	-
RAK 20-25	7.25	-	-	10.34	-	-	-	14.72	-	-	-
RAK 23-25	n/s	n/s	n/s	n/s	n/s	n/s	n/s	n/s	n/s	n/s	n/s
RAK 30-25	7.19	-	-	10.16	-	-	-	14.72	-	-	-
RAK 33-25	7.19	-	-	10.10	-	-	-	14.25	-	-	-
RAK 38-25	7.22	-	-	10.10	-	-	-	14.25	-	-	-
RAK 42-25	7.19	-	-	10.10	-	12.81	-	14.25	-	-	-
RAK 43-25	n/s	n/s	n/s	n/s	n/s	n/s	n/s	n/s	n/s	n/s	n/s
RAK 45-25	7.21	-	-	10.10	-	12.27	-	14.25	-	-	-
RAK 46-25	7.22	-	-	-	11.78	-	-	14.73	-	-	-
RAK 50-25	7.19	-	-	10.10	11.05	12.62	-	14.48	-	-	-
RAK 53-25	7.20	-	-	10.10	11.78	-	-	14.48	-	-	-
RAK 57-25	7.19	-	-	10.11	-	-	-	14.37	-	-	-
RAK 60-25	7.20	-	-	10.10	-	12.27	-	14.25	-	-	-
RAK 67-25	7.19	-	-	10.10	11.94	12.80	-	14.72	-	-	-
RAK 68-25	7.20	-	-	10.10	11.78	-	-	14.72	-	-	-
RAK 71-25	7.19	-	-	10.10	-	12.27	-	14.25	-	-	-
RAK 76-25	n/s	n/s	n/s	n/s	n/s	n/s	n/s	n/s	n/s	n/s	n/s
RAK 78-25	7.20	-	-	10.04	11.78	-	-	14.25	-	-	-
RAK 112-25	-	-	-	-	-	-	-	-	-	-	-
RAK 125-25	7.22	-	-	10.10	-	12.62	-	14.97	-	-	-

Preparation: Mg saturated + ethylene glycol

SAMPLE	7.0- 7.9	8.0- 8.9	9.0- 9.9	10.0-10.9	11.0-11.9	12.0-12.9	13.0-13.9	14.0-14.9	15.0-15.9	16.0-16.9	17.0-17.9
RAK 9-25	7.19	-	9.40	10.04	-	-	-	14.72	-	-	-
RAK 15-25	7.22	-	-	10.04	-	-	-	-	15.23	16.36	17.67
RAK 20-25	7.25	-	-	10.28	-	-	-	-	-	16.99	17.67
RAK 23-25	n/s	n/s	n/s	n/s	n/s	n/s	n/s	n/s	n/s	n/s	n/s
RAK 30-25	7.20	-	-	10.19	-	-	-	-	15.36	16.99	-
RAK 33-25	7.20	-	-	10.16	-	-	-	14.60	-	16.83	-
RAK 38-25	7.22	-	-	10.10	-	-	-	14.25	-	-	-
RAK 42-25	7.19	-	-	10.04	-	-	-	14.25	15.78	-	-
RAK 43-25	-	-	-	-	-	-	-	-	-	-	-
RAK 45-25	7.19	-	-	10.10	-	-	-	14.22	-	-	-
RAK 46-25	7.23	-	-	10.11	-	-	-	14.48	-	16.99	-
RAK 50-25	7.10	-	-	10.10	-	-	-	14.48	-	16.06	-
RAK 53-25	7.19	-	-	10.10	-	-	-	14.14	-	-	17.67
RAK 57-25	7.22	-	-	10.10	-	-	-	14.48	-	-	-
RAK 60-25	7.19	-	-	10.11	-	-	-	14.72	-	16.99	-
RAK 67-25	7.10	-	-	10.10	-	-	-	14.72	-	16.09	-
RAK 68-25	7.22	-	-	10.10	-	-	-	14.72	15.23	16.99	-
RAK 71-25	7.22	-	-	10.10	-	-	-	14.25	-	-	17.32
RAK 76-25	n/s	n/s	n/s	n/s	n/s	n/s	n/s	n/s	n/s	n/s	n/s
RAK 78-25	7.20	-	-	10.04	-	12.27	-	14.25	-	16.99	-
RAK 112-25	-	-	-	-	-	-	-	-	-	-	-
RAK 125-25	7.18	-	-	10.10	-	-	-	-	-	16.99	-

Preparation: Non-cation saturated

SAMPLE	7.0-7.9	8.0-8.9	9.0-9.9	10.0-10.9	11.0-11.9	12.0-12.9	13.0-13.9	14.0-14.9	15.0-15.9	16.0-16.9	17.0-17.9
RAK 9-25	7.19	8.84	-	10.16	-	-	-	14.14	-	-	-
RAK 15-25	-	-	-	10.28	11.78	-	-	-	-	-	-
RAK 20-25	7.19	-	-	10.10	-	-	-	14.48	-	-	-
RAK 23-25	7.19	-	-	10.16	-	-	-	14.72	-	-	-
RAK 30-25	7.19	-	-	10.16	-	-	-	14.14	-	-	-
RAK 33-25	7.10	-	-	10.10	-	-	-	14.48	-	-	-
RAK 38-25	7.19	-	-	10.10	-	-	-	14.25	-	-	-
RAK 42-25	7.22	-	-	10.10	-	-	-	14.25	-	-	-
RAK 43-25	7.25	-	-	10.11	-	-	-	14.25	-	-	-
RAK 45-25	7.19	-	-	10.04	-	-	-	14.27	-	-	-
RAK 46-25	7.22	-	-	10.11	-	-	-	14.14	-	-	-
RAK 50-25	7.19	-	-	10.10	-	-	-	14.48	-	-	-
RAK 53-25	7.20	-	-	10.10	-	-	-	14.48	-	-	-
RAK 57-25	7.15	-	-	10.10	-	-	-	14.37	-	-	-
RAK 60-25	7.19	-	-	10.10	-	-	-	14.25	-	-	-
RAK 67-25	7.20	-	9.60	10.10	-	-	-	-	-	-	-
RAK 68-25	7.20	-	-	10.10	11.33	-	-	-	-	-	-
RAK 71-25	7.20	-	-	10.10	-	12.27	-	14.25	-	-	-
RAK 76-25	7.20	-	-	10.11	-	-	-	-	-	-	-
RAK 78-25	7.22	-	-	10.10	11.78	-	-	-	-	-	-
RAK 112-25	-	-	-	-	-	-	-	-	-	-	-
RAK 125-25	7.20	-	-	10.10	-	-	-	-	-	-	-

Preparation: Non-cation saturated + ethylene glycol

SAMPLE	7.0-7.9	8.0-8.9	9.0-9.9	10.0-10.9	11.0-11.9	12.0-12.9	13.0-13.9	14.0-14.9	15.0-15.9	16.0-16.9	17.0-17.9
RAK 9-25	7.16	-	-	10.04	-	-	-	-	-	-	-
RAK 15-25	7.22	-	-	10.04	11.05	-	-	14.48	-	-	-
RAK 20-25	7.19	-	-	10.10	-	-	-	14.72	-	16.83	-
RAK 23-25	7.22	-	-	10.10	-	-	-	14.72	-	16.06	-
RAK 30-25	7.19	-	-	10.16	-	-	-	14.02	15.50	-	-
RAK 33-25	7.10	-	-	10.04	-	-	-	14.25	-	-	-
RAK 38-25	7.11	-	-	10.11	-	-	-	14.24	-	-	-
RAK 42-25	7.22	-	-	10.11	11.48	-	-	14.25	-	-	-
RAK 43-25	7.19	-	-	10.10	-	-	-	14.25	-	-	-
RAK 45-25	7.19	-	-	10.10	-	-	-	14.25	-	-	-
RAK 46-25	7.22	-	-	10.09	-	-	-	14.14	-	-	-
RAK 50-25	7.10	-	-	10.11	-	-	-	14.48	-	-	-
RAK 53-25	7.20	-	-	10.10	-	-	-	14.48	-	-	-
RAK 57-25	7.15	-	-	10.10	-	-	-	14.25	-	-	-
RAK 60-25	7.20	-	-	10.10	-	-	-	14.48	-	-	-
RAK 67-25	7.20	-	-	10.11	-	-	13.19	14.72	-	-	-
RAK 68-25	7.22	-	-	10.10	-	12.27	-	-	-	-	-
RAK 71-25	7.20	-	-	10.10	-	-	-	-	-	16.99	-
RAK 76-25	7.25	-	-	10.10	-	-	-	-	-	16.36	-
RAK 78-25	7.22	-	-	10.10	-	12.80	-	-	-	-	-
RAK 112-25	-	-	-	-	-	-	-	-	-	-	-
RAK 125-25	7.20	-	-	10.10	-	-	-	-	-	-	-

Appendix 3:
Non-saturated Clays

Preparation: K saturated + 500 degrees C for two hours

SAMPLE	7.0- 7.9	8.0- 8.9	9.0- 9.9	10.0-10.9	11.0-11.9	12.0-12.9	13.0-13.9	14.0-14.9	15.0-15.9	16.0-16.9	17.0-17.9
RAK 9-25	-	-	-	10.11	-	-	-	14.14	-	-	-
RAK 15-25	-	-	-	10.04	-	-	-	-	-	-	-
RAK 20-25	-	-	-	10.16	-	-	-	-	-	-	-
RAK 23-25	n/s	n/s	n/s	n/s	n/s	n/s	n/s	n/s	n/s	n/s	n/s
RAK 30-25	-	-	-	10.16	-	-	-	-	-	-	-
RAK 33-25	n/s	n/s	n/s	n/s	n/s	n/s	n/s	n/s	n/s	n/s	n/s
RAK 38-25	n/s	n/s	n/s	n/s	n/s	n/s	n/s	n/s	n/s	n/s	n/s
RAK 42-25	-	-	-	10.10	-	-	-	14.25	-	-	-
RAK 43-25	n/s	n/s	n/s	n/s	n/s	n/s	n/s	n/s	n/s	n/s	n/s
RAK 45-25	-	-	-	10.10	-	-	-	14.25	-	-	-
RAK 46-25	-	-	-	10.10	-	-	-	14.15	-	-	-
RAK 50-25	-	-	-	10.10	-	-	-	14.48	-	-	-
RAK 53-25	-	-	-	10.10	-	-	-	14.48	-	-	-
RAK 57-25	n/s	n/s	n/s	n/s	n/s	n/s	n/s	n/s	n/s	n/s	n/s
RAK 60-25	-	-	-	10.10	-	-	-	14.25	-	-	-
RAK 67-25	n/s	n/s	n/s	n/s	n/s	n/s	n/s	n/s	n/s	n/s	n/s
RAK 68-25	n/s	n/s	n/s	n/s	n/s	n/s	n/s	n/s	n/s	n/s	n/s
RAK 71-25	n/s	n/s	n/s	n/s	n/s	n/s	n/s	n/s	n/s	n/s	n/s
RAK 76-25	n/s	n/s	n/s	n/s	n/s	n/s	n/s	n/s	n/s	n/s	n/s
RAK 78-25	n/s	n/s	n/s	n/s	n/s	n/s	n/s	n/s	n/s	n/s	n/s
RAK 112-25	-	-	-	10.10	-	-	-	-	-	-	-
RAK 125-25	-	-	-	-	-	-	-	-	-	-	-

Preparation: K saturated + ethylene glycol + 500 degrees C for two hours

SAMPLE	7.0- 7.9	8.0- 8.9	9.0- 9.9	10.0-10.9	11.0-11.9	12.0-12.9	13.0-13.9	14.0-14.9	15.0-15.9	16.0-16.9	17.0-17.9
RAK 9-25	7.22	-	-	10.10	-	-	-	-	-	-	-
RAK 15-25	-	-	-	10.04	-	-	-	-	-	-	-
RAK 20-25	-	-	9.99	-	-	-	-	-	-	-	-
RAK 23-25	-	-	-	10.04	-	-	-	-	-	-	-
RAK 30-25	n/s	n/s	n/s	n/s	n/s	n/s	n/s	n/s	n/s	n/s	n/s
RAK 33-25	-	-	-	10.10	-	-	-	-	-	-	-
RAK 38-25	7.21	-	-	-	-	-	-	14.02	-	-	-
RAK 42-25	-	-	-	10.10	-	-	-	14.24	-	-	-
RAK 43-25	-	-	-	10.10	-	-	-	14.25	-	-	-
RAK 45-25	-	-	-	10.10	-	-	-	14.25	-	-	-
RAK 46-25	-	-	-	10.10	-	-	-	14.14	-	-	-
RAK 50-25	n/s	n/s	n/s	n/s	n/s	n/s	n/s	n/s	n/s	n/s	n/s
RAK 53-25	-	-	-	10.10	-	-	-	14.48	-	-	-
RAK 57-25	-	-	-	10.12	-	-	-	14.48	-	-	-
RAK 60-25	-	-	-	10.10	-	-	-	14.28	-	-	-
RAK 67-25	-	-	-	10.10	-	-	-	-	-	-	-
RAK 68-25	-	-	-	10.10	-	-	-	-	-	-	-
RAK 71-25	-	-	-	10.10	-	-	-	-	-	-	-
RAK 76-25	-	-	-	10.10	-	-	-	-	-	-	-
RAK 78-25	-	-	-	10.10	-	-	-	-	-	-	-
RAK 112-25	-	-	-	10.10	-	-	-	-	-	-	-
RAK 125-25	-	-	-	10.10	-	-	-	-	-	-	-

Appendix 4:
Heat Treated Clays